The Influence of Mooring Dynamics on the Performance of Self Reacting Point Absorbers

by

Juan Pablo Ortiz
B.Sc. Mechanical , University of Costa Rica, 2006

A Thesis Submitted in Partial Fulfillment
of the Requirements for the Degree of

MASTER OF APPLIED SCIENCE

in the Department of Mechanical Engineering

Supervisory Committee

The Influence of Mooring Dynamics on the Performance of Self Reacting Point Absorbers

by

Juan Pablo Ortiz Garcia
B.Sc. Mechanical, University of Costa Rica, 2006

Supervisory Committee

Dr. Brad Buckham, (Department of Mechanical Engineering)
Co-Supervisor

Dr. Curran Crawford, (Department of Mechanical Engineering)
Co-Supervisor

Abstract

Supervisory Committee

Dr. Brad Buckham, (Department of Mechanical Engineering)
Co-Supervisor

Dr. Curran Crawford, (Department of Mechanical Engineering)
Co-Supervisor

The design of a mooring system for a floating structure is a significant challenge; the choice of line structure and layout determine highly non-linear hydrodynamic behaviors that, in turn, influence the dynamics of the whole system. The difficulty is particularly acute for Self-Reacting Point Absorber Wave Energy Converters (SRPA WEC) as these machines rely on their movements to extract useful power from wave motions and the mooring must constrain the SRPA WEC motion without detracting from power production. In this thesis this topic has been addressed in an innovative way and new ideas on how these devices should be moored were investigated.

As part of the study, an optimization routine was implemented to investigate the optimal mooring design and its characteristics. In this process, different challenges were faced. To evaluate the different mooring configurations, a high fidelity representation of the system hydrodynamics is necessary which captures the non-linearities of the system. Unfortunately, high-fidelity modeling tends to be very computationally expensive, and for this reason previous studies based mooring design largely relies on simplified representations that only reflect part of the mooring design space since some physical and hydrodynamic properties are dropped. In this work, we present how a full hydrodynamic time domain simulation can be utilized within a Metamodel-Based Optimization to better evaluate a wider range of mooring configurations spanning the breadth of the full design space. The method uses a Metamodel, defined in terms of the mooring physical parameters, to cover the majority of the optimization process a high fidelity model is used to establish the Metamodel in a pre-processing stage. The method was applied to a case study of a two-body heaving SRPA WEC. Survivability constrains where introduce into the model using a new statistical approach which reduces the execution time, and allowed the optimization routine.

The analysis results lead to the conclusion that for SRPA WEC the mooring loads have a significant impact on how the body reacts with the waves, affecting both the energy that enter the system as well as the energy that is extracted as power. This implies that, in some cases, the mooring lines need to be

considered in early stages of the designs as opposed to an afterthought, as is typically done. Results indicate that an optimal mooring design can result in a 26% increase in total annual power production. In addition, the mooring lines impact on mitigating parasitic pitch and roll were analyzed. It was established that in regular waves, the mooring lines can reduce the parametric excitations and improve the power extraction up to 56% for a particular sea state. By applying a computationally efficient iterative design approach to a device's mooring, parasitic motions and suboptimal device operation can be reduced, ultimately making WECs a more competitive source of energy.

Table of Contents

List of Tables

List of Figure

Acknowledgments

I would like to thank all those who in one way or another contributed to the completion of this thesis. Thanks to my supervisors for the opportunity to work in such an interesting research area. A very special thanks to Dr. Brad Buckman, a gifted teacher whose patience and support helped me overcome many critical situations. A special thanks to Dr. Curran Crawford who has been always there to listen and give advice. I would also like to thank all of the members of the WCWI research group, who began as my colleagues only but ended being good friends. Thanks for making work fun. Thanks to the Casa Oso crew for being awesome. Lastly, and most importantly, I wish to thank my family, for being always there, as an infinite source of support.

This research would not have been possible without the financial assistance of Natural Resources Canada, the Pacific Institute of Climate Solutions, the Natural Sciences and Research Council of Canada, The Ministry of Sciences and Technology of Costa Rica (MICITT) and CONICIT and the computer resources lent by Ocean Network of Canada.

Dedication

To all the good people that I have encountered in this journey.

Nomenclature

A	Wave Amplitude
Aj,k	Added Mass
A(∞)	Added mass at infinite
ALS	Accidental Limit State
Bj,k	Damping
C	Celerity
ci	Constant coefficients related
CJ	PTO damping constant
CF	Constrain function
DS	Design Space
DVN	Det Norske Veritas
ε	Wave Phase
H3	Best configuration with 3 lines
θ	Direction
F	Total Force
fe	Excitation forces
FLS	Fatigue Limit State
Hs	Significate height
h	Mean surface elevation
GHG	Green House Gas
k	Wave number
kr(t)	Radiation kernels
L3	Configuration that extracts less energy with 3 lines
L4	Configuration that extracts less energy with 4 lines
η	Elevation
NM	No Mooring configuration
M	Total Moments
MARS	Multivariate Adaptive Regression Splines
MBO	Metamodel-Based Optimization
OF	Objective function
OWSC	Oscillating Wave Surge Converter
P	Penalty coefficients
p	Pressure
PTO	Power Take Off
RAO	Response Amplitude Operator
SF	Safety Factor
SRPA	Self-Reacting Point Absorbers
Te	Energy period
ϕ	Velocity potential
ULS	Ultimate Limit State
ω	Angular Frequency
ω_n	Natural Frequency
w_i	Weight

WCWI	West Cost Wave Initiative
WEC	Wave Energy Converters
Z(x)	Local deviation

Chapter 1

Introduction

1.1 Motivation

The global climate is changing. Year by year, symptoms of this change are registered: the severity of storms and droughts is increasing; extreme seasonal temperatures are rising, destructive climatic phenomena (e.g. tornadoes and hurricanes) are more frequent; the diminution of the ice caps and iceberg volumes is accelerating [1][2]. It is known that climate change is symptomatic of the increasing volume of greenhouse gases (GHG) in the atmosphere, and the dominant anthropogenic driver of GHG emissions is the energy system. Large economies such as China, USA, Canada, etc., still depend on energy matrices based on non-renewable sources such as coal, oil and gas, which are main contributors to GHG emissions. It has been forecast that continuation of current behavior could be catastrophic [3], and thus humanity is being forced to find new ways to produce clean energy. Initiatives such as COP21[1] and IEV[2] have seen several nations commit themselves to reducing GHG emissions to ensure that increases in the global average temperature remain below 2°C. To achieve this objective goal renewable energy technologies must be improved and implemented.

---

[1] "Sustainable Innovation Forum." [Online]. Available: http://www.cop21paris.org/ [Accessed: 21-Apr-2016].
[2]"International Energy Agency " [Online]. Available: http://www.iea.org/ [Accessed: 21-Apr-2016].

Investment in research and development across different types of renewable energy generation technologies varies widely. Low carbon energy technologies such as wind turbines and hydroelectric power are mature technologies; while incremental advances continue to be developed for these technologies, they have reached a point where they are economically viable in a wide variety of jurisdictions. For example, according to the European Wind Energy Association, wind energy has reached 15.6% of the total installed power capacity of the EU, overtaking hydroelectric power which provides 15.5% of the installed capacity[3]. Other renewable energy technologies, such as wave energy converters (WECs) are in an earlier stage of development and haven't yet reached the stage where they are attractive to power project developers on an economic basis. The relatively high costs of wave energy can be attributed to the ocean environment producing intense structural requirements, frequent and expensive maintenance, raising operating expenses and the cost of cable connections [4]. Even for a proven conversion technology such as a wind turbine, the demands of the ocean environment drastically alters project economics - offshore wind turbines remain two to three times more expensive than onshore installations[4].

In order to meet the decarbonization goals agreed to at COP21 and IEV, a worldwide restructuring of the energy matrix is required; for this, a full portfolio of renewable energy alternatives is necessary, so as to present feasible options for each region, according to its available renewable resources. As all renewable options are not available in every location, it is imperative to invest in the development of all renewable energy technologies and make them economically feasible as soon as possible. For example, along the West Coast of Canada, which is around 1000 km long and demonstrates one of the most energetic wave climates in the world, the average annual wave energy transport at the continental shelf has been assessed at 40–50 kW/m [5]. Wave energy therefore represents a potentially important resource for western Canada that so far has not been exploited. In addition, this energy source has a particular advantage; as the swell originates far from the coast, the wave climate can be more accurately forecast days in advance, relative to other renewable options such as wind and solar [6]. In addition, wave energy is more consistent than wind, and there is an opportunity to achieve relatively high annual capacity factors

[3] "European Wind Energy Association." [Online]. Available: http://www.ewea.org/statistics/european/. [Accessed: 03-Apr-2016].

[4] "International Renewable Energy Agency." [Online]. Available: http://www.irena.org/ [Accessed: 22-Apr-2016].

with wave energy technologies [7]. Also, wave energy has a seasonal behavior which could be an advantage for certain locations. For example in the northern hemisphere, most of the wave energy is available in the winter, which matches the period of high energy demand.

In order to make wave energy viable, it is desired to find an optimal blend between cost, power production, and durability of the system [8]. The design of a wave energy converter (WEC) is complicated by the fact that these three factors are highly coupled. The cost of the system is directly related to the requirements for strength and abrasion loading for the design life [9], which affects the system mass, inertia, dynamics and, subsequently, its power capture ability. Another dilemma is the choice of the WEC deployment location which significantly impacts system behavior and cost. When the system is onshore, its construction, operation and maintenance is less expensive, but the power capture is limited, due to the attenuation of the available wave energy through the accumulated action of sea bed friction and wave spilling or breaking. If the WEC is moved into the water (whether at shallow waters very near the coast or in deeper waters offshore) the energy capture can be higher as the losses will decrease, but new design challenges arise, as restraining the WEC costs increases and so do those of the energy transmission lines.

Wave energy converters installed in the water must be bottom founded (structurally connected to the seabed) or floating devices that rely on moorings to provide seakeeping. Moored technologies have some advantages over bottom founded devices. For bottom founded devices, construction, operation and maintenance is more difficult since the structures tend to be very large, are always submerged and are thus costlier to repair. In contrast, relatively lightweight mooring line components can be designed with a degree of compliance to reduce structural loads in extreme events, and can be easily replaced to facilitate extended life of the WEC. Finally, moored devices are much easier to license for early stage deployments because the developer can assure complete removal of the WEC system; this feature is a requirement of the “strategic environmental assessment” being championed in Canada and the US.

While moorings present desirable logistical characteristics, they significantly complicate the system dynamics and thus are a challenging addition to the WEC design process. Due to accumulated hydrodynamic drag over the mooring line lengths, moorings have extremely non-linear dynamics – this is particularly true in larger wave heights. Since the mooring must ensure the WEC holds station, it must exert forces (at times) that dominate the complete system dynamics – in these moments the mooring ensures the system survivability. Since all moorings are compliant to some degree, there are other moments where the mooring may exert little force on the floating WEC. Accommodating for these two

extremes, and understanding the litany of operational circumstances that occur in between them and the impact of these circumstances on WEC performance, is a massive design challenge. Despite the significant influence of moorings on system behavior, relatively little study has been put into mooring design for floating WECs. To help fill this gap, this thesis will focus on developing a computational framework for floating WEC mooring design.

1.2 BACKGROUND

In this section, a summary of the different established WEC technologies is provided. Special attention is paid to the Self-Reacting Point Absorber (SRPA) class of WECs, due to the prominent role of this particular WEC class in this study (see §1.2.2). A brief explanation of how WEC dynamics are typically modeled is presented next, with close attention paid to commentary works on how WEC mooring lines can affect a WEC's power production.

1.2.1 WAVE ENERGY CONVERTERS

Unlike wind turbine technology, which has largely converged to a single design concept [10], WECs are not a fully developed technology and there exists a wide variety of concepts in the exploratory stage of development. These concepts differ markedly in the way they extract energy from the waves. These differences can be categorized by deployment location (shoreline, nearshore, offshore) and how the device is positioned and oriented relative to the primary wave direction. In order to provide context for the current work, the different WEC concepts, or classes, are presented. The classes are distinguished by deployment location, orientation with respects to the wave direction and by operating principles.

Classification by Installation Site.

Onshore WECs: are devices where the entire system is located onshore. This kind of device normally has only one degree of freedom. As they are accessible from dry land, onshore WECs have the advantage of lower operational and maintenance costs than other devices. Their major disadvantage is that much of the available wave energy dissipates before it reaches the device. Examples of these systems are fixed oscillating water columns (OWC); and tapered channels. Figure 1 shows an example of a fixed OWC, developed by Wavegen and Queen's University Belfast and installed at Islay in Scotland.

Onshore-nearshore WECs are systems designed to capture energy near the shore, but where the energy conversion mechanism is on shore. This kind of device normally pumps a working fluid to shore, where a turbine converts the energy stored as pressure and flow rate into electricity. Since the powerhouse is located on shore, the operation and maintenance of these systems is easier relative to the nearshore-offshore devices discussed below. Also, these device can be used to pump high pressure sea water to shore, which can be used in desalination processes directly without first converting to electricity. The main problem with onshore-nearshore systems is the head losses that occur as the fluid is pumped from the offshore location to the powerhouse. Carnegie Wave Energy's CETO[5], shown in Figure 1-1, is an example of this kind of device. CETO consists of a submerged buoy that moves in heave and surge and pumps water to shore, using a piston that then can be used for desalinization or to produce electricity.

Nearshore-offshore WECs are devices that are deployed, either nearshore or offshore, without an onshore powerhouse. The energy conversion losses are minimal, as the energy is converted to electricity near to the WEC, normally within the hull of the converter. However, maintenance is challenging as the device is normally deployed in very energetic locations, is frequently moving and the internals may be sealed and difficult to physically access or extract in site. A well-known Nearshore-offshore WEC is the Powerbuoy, of Ocean Power Technologies. The Powerbuoy is a two body self-reacting WEC which has an underwater substation as shown in Figure 1-1

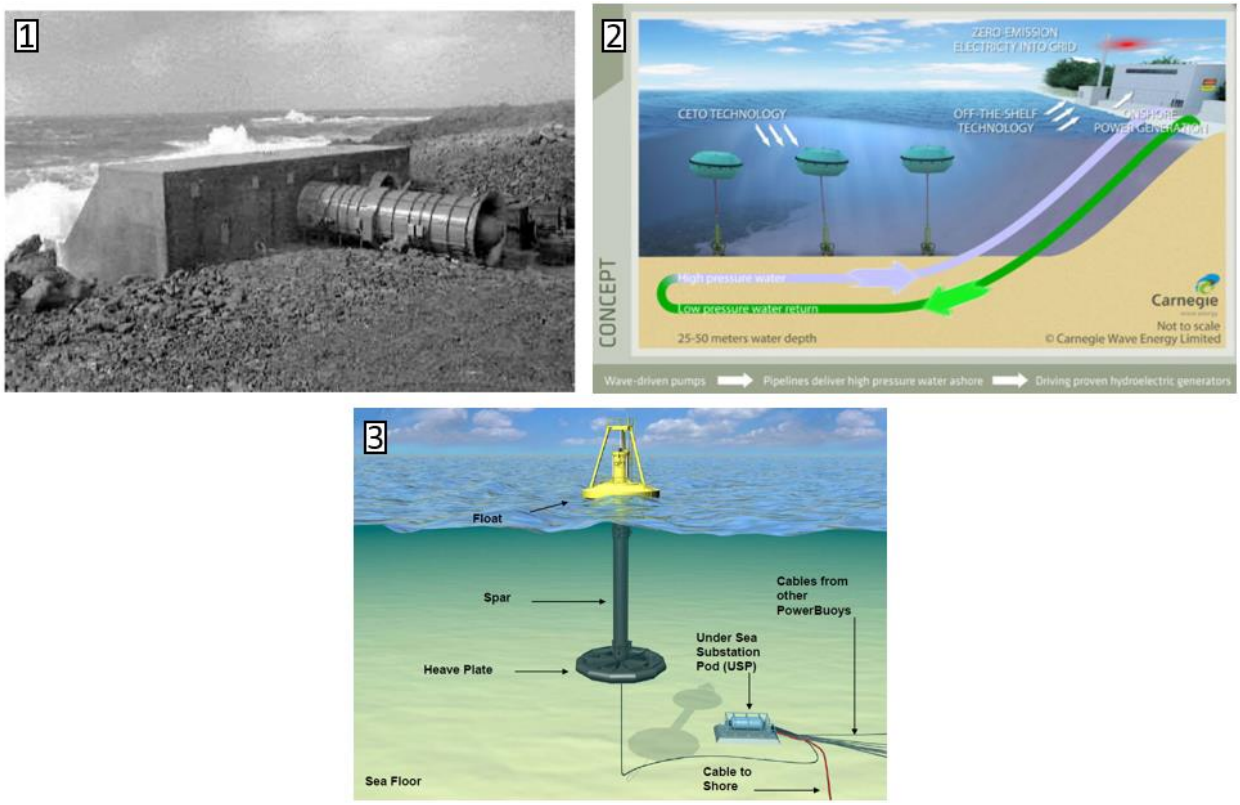

Figure 1-1: Classification by Installation Site.
1- Limpet OWC[11] 2-Ceto, Carnegie Wave Energy[5]
3-Right: Ocean Power Technologies[6]

[5] "Carnegie Wave Energy - General." [Online]. Available: http://www.carnegiewave.com/. [Accessed: 12-Aug-2015].

[6] "Ocean Power Technologies." [Online]. Available: http://www.oceanpowertechnologies.com/. [Accessed: 12-Aug-2015].

Classification by Device Orientation with respects to Wave Direction.

Point absorbers are devices that are small in comparison with typical wavelengths and whose alignment with the predominant direction of the wave is not important. This kind of device can be bottom mounted or a floating structure that extracts energy from the incident wave and pressure differences [12] [13]. The power conversion mechanism for these devices takes advantage of the reaction of the body with the sea bed, or from the relative motion between two parts of the device. The latter system is of particular interest for this research and will be referred to hereafter as a self-reacting point absorber wave energy converter (SRPA WEC). This kind of device consists of floating structures that rely on the incident wave to move and extract power from the relative movement of two floating parts. Some of them rely on pitch and surge movements for extracting energy, such as PS Frog and Frog developed by Lancaster University Renewable Energy Group[14] and Penguin[8] from Wello Oy. Other devises such as Powerbuoy (Figure 1-2) and Wavebob (Figure 1-2) depend on only the heave movements for power generation [15] .

Attenuators are devices that lay parallel to the predominant direction of the wave propagation and extract power as the incident wave travels along the device, inducing phase shifted motion of its component hulls [12][13]. An example of this kind of WEC is Pelamis, developed by Ocean Power Delivery Ltd shown in Figure 1-2.

Terminators are devices that physically intercept waves by lying perpendicular to the predominant wave direction[12][13]. Arguably the most recognized device of this type is the Salter Duck, which was developed by Dr. Stephen Salter at the University of Edinburgh in 1978[7].

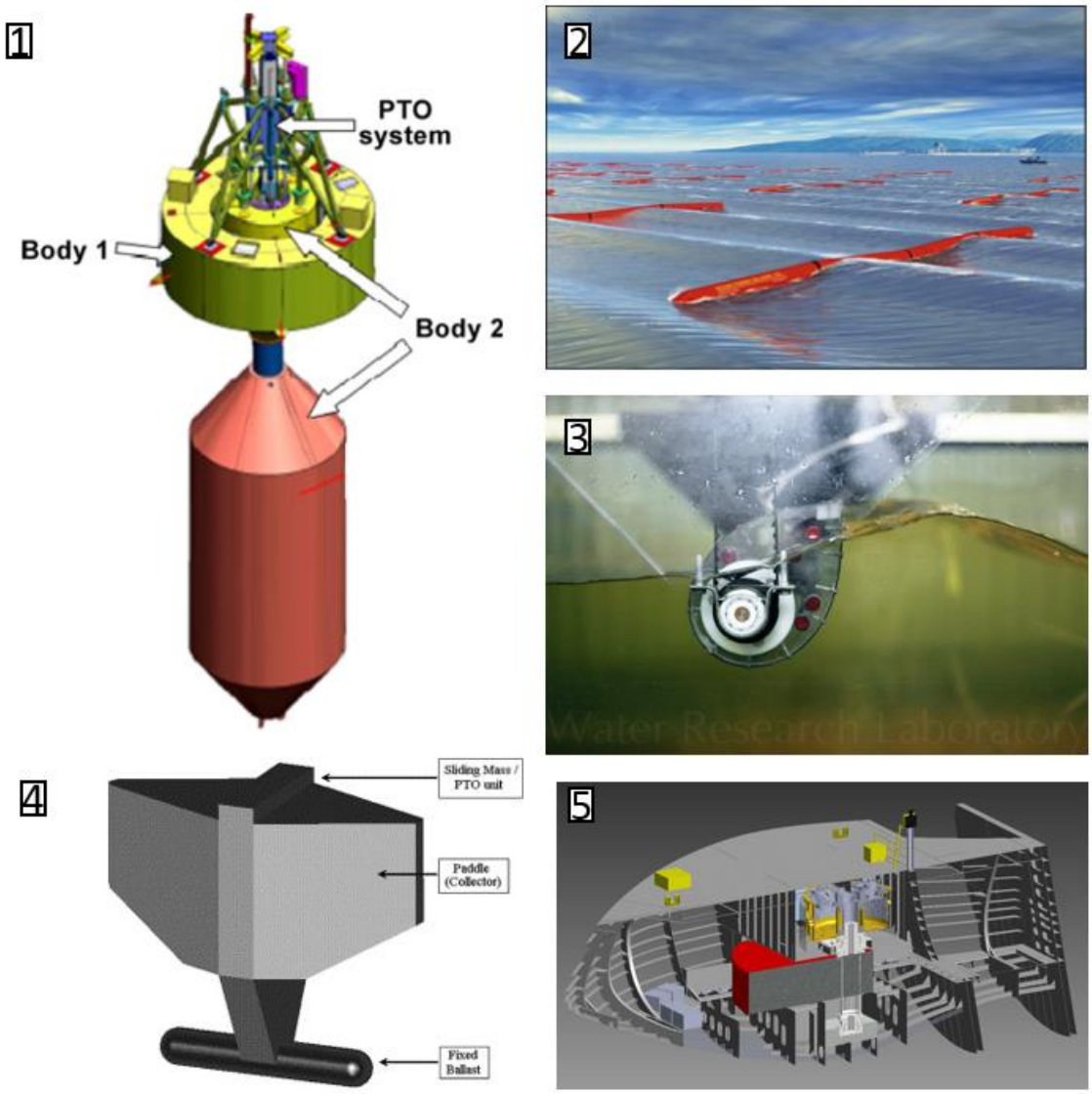

Figure 1-2: WEC classification by Device Orientation with respects to Wave Direction.
1-WaveBob [15] 2-Pelamis [16] 3- Salter Duck[7] 4- PS Frog[14] 5- Penguin[8]

[7] "2D Physical Modelling of the Salter's Duck | Water Research Laboratory (WRL)." [Online]. Available: http://www.wrl.unsw.edu.au/news/2d-physical-modelling-of-the-salter%E2%80%99s-duck. [Accessed: 12-Aug-2015].

[8] Penguin WEC| Wello Oy [Online]. Available: http://www.wello.eu/en/.[Accessed: 05-Apr-2015].

Classification by Principle of Operation

Overtopping devices capture sea water of incident waves in a raised reservoir by two large curved reflectors that gather waves into a central receiving part where they flow up a ramp and over the top into the reservoir. The water is then allowed to return to the sea via a number of low-head turbines. An example of this kind of device is Wave Dragon shown in Figure 1-3.

Wave activated WECs are devices that capture energy as the body oscillates with the passing of each wave. The oscillatory movement can be vertical, horizontal, pitch or a combination, and is induced by the motion between the body and an external fixed reference. An example of this kind of device is Seabase developed by Seabase AB (Figure 1-3) or any other floating body (as shown in Figure 1-1 and Figure 1-2) [13].

Oscillating Wave Surge Converter (OWSC) WECs are a concept where articulated or flexible structures would be positioned perpendicular to the wave direction. The idea is that the pressure of the wave pushes a flap back and forth, which in turn drives a hydraulic mechanism that pumps fluid that can be used in a desalinization process or to produce electricity [13]. An example of this kind of device is Oyster, developed by Aquamarine Power[9], as shown in Figure 1-3.

Oscillating Water Columns (OWCs) consist of a chamber with an opening to the sea below the waterline. They rely on the oscillating movement of the waves to pressurize the air chamber and produce electricity by pushing air through a bidirectional turbine [13].

Pressure difference (or Archimedes effect) WECs (as with OWCs) rely on the difference in pressure generated by wave crests and troughs, but are bottom-mounted on the seabed and the waves pass over the device. As the crest of the wave passes over the device, the water pressure compresses the air (or other working fluid) that is inside of it and moves the device down. Then, as the trough of the wave passes over the device, the pressure is reduced and the device rises [13]. An example of this kind of device is CETO, from Carnegie. This kind of device has the advantage that because it is underwater it isn't required to be designed for wave breaking loads which lower the costs. Also, as they are underwater and will not

[9] "Aquamarine Power - Wave energy company, developer of Oyster wave power." [Online]. Available: http://www.aquamarinepower.com/. [Accessed: 07-Sep-2015].

change the landscape, the permitting and licensing process for projects using this type of technology may encounter less public opposition.

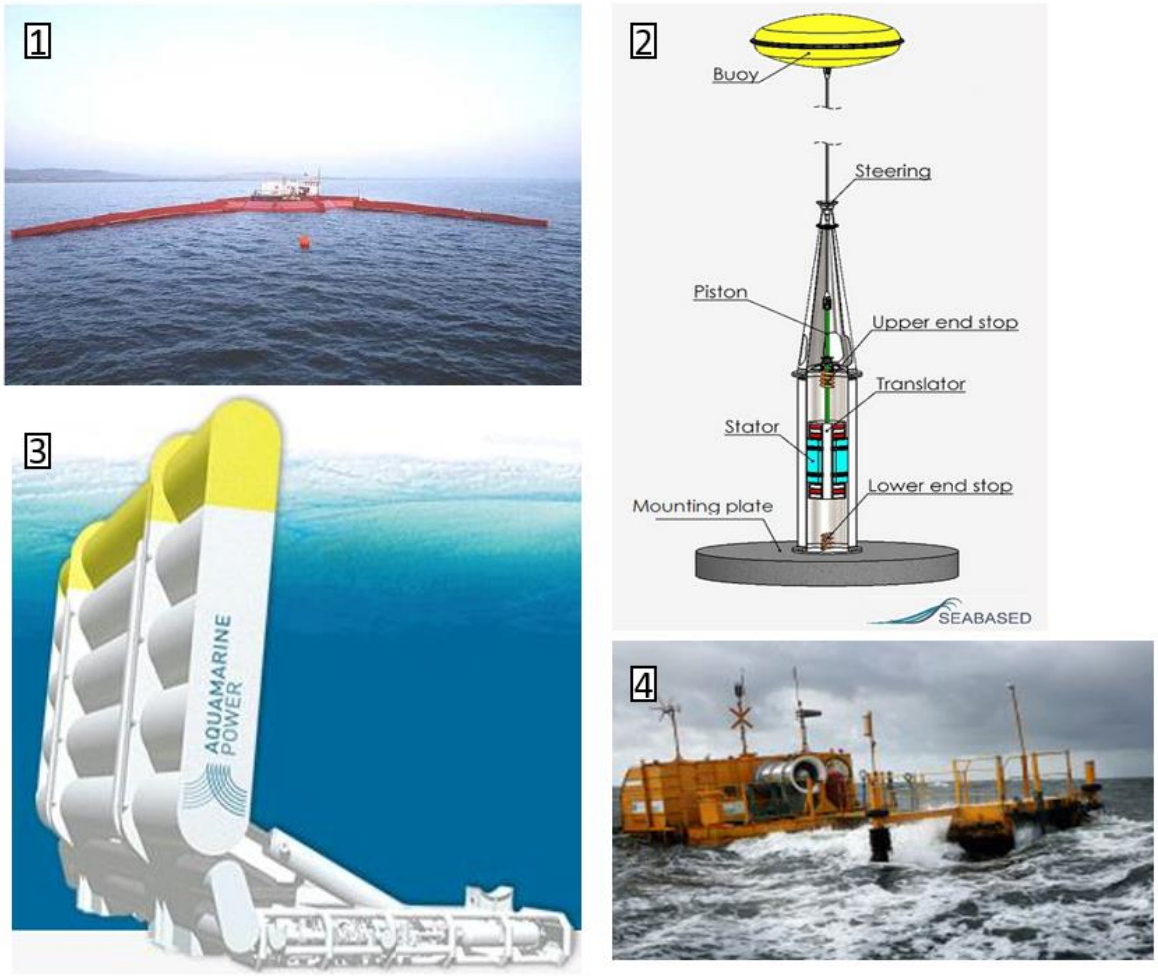

Figure 1-3: WEC Classification by Principle of Operation
1-Wave Dragon[10], 2- Seabased[11], 3- Oyter[12] , 4-Ocean Energy OWC[13]

[10] "Energy and the Environment-A Coastal Perspective - Overtopping Terminator." [Online]. Available: http://coastalenergyandenvironment.web.unc.edu/ocean-energy-generating-technologies/wave-energy/overtopping-terminator/. [Accessed: 12-Aug-2015].

[11] "Seabased wave energy." [Online]. Available: http://www.seabased.com/en/technology/seabased-wave-energy. [Accessed: 12-Aug-2015]

[12] "Aquamarine"[Online]. Availed: http://www.aquamarinepower.com/technology.aspx. [Accessed: 12-Aug-2015].

[13] "Ocean Energy." [Online]. Available: http://oceanenergy.ie/. [Accessed: 12-Aug-2015].

1.2.2 Self-Reacting Point Absorber Wave Energy Converters (SRPA WEC) Hydrodynamics

SRPA WECs are good candidates for being deployed on the West Coast of Canada. The West Coast has the particular condition that the water reaches about 40 to 50m depth just a few kilometers offshore, allowing moored WECs to be easy to install offshore, where there is more energy available as the sea bed has less impacted on the energy transported, and the line transmission cost is still reasonably low. Moreover, these devices, as can be seen in the following figure, exhibit all the logistical advantages mentioned in § 1.1 and can be easily removed and accessed, which makes the maintenance and retrieving operations easier, and they have been shown to have a good potential. For these reasons it is considered justifiable to perform more research on SRPAs.

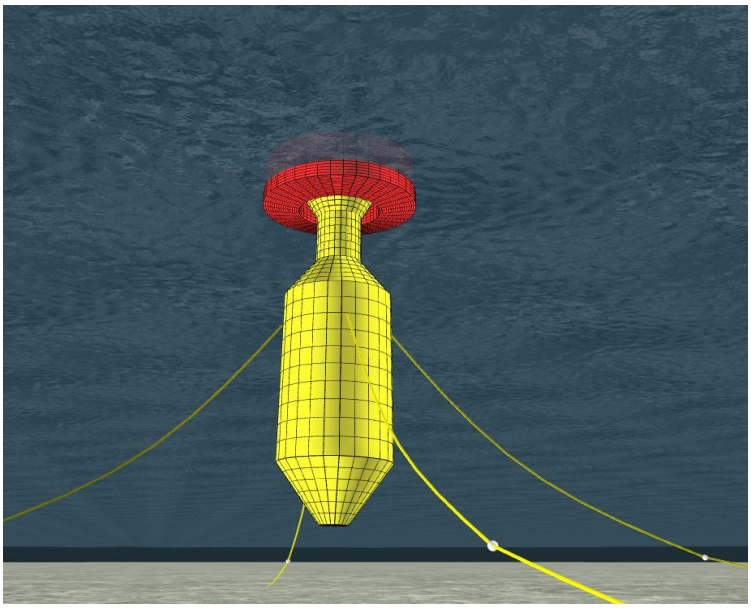

Figure 1-4: SRPA WEC
A two body heave SRPA WEC
composed by the spar(yellow) and float(red).

Economic and robust design of moored SRPA WECs depends on numerical modeling: it is not feasible to depend on iterative prototype development since the time required on each iteration beyond the scope of the funding cycles that most WEC developers are subject to. Even if the costs of prototype development could be reduced, the time required to wait for nature to provide the full range of desired test conditions

would be excessive. A field test of a moored system in a 50 year wave condition would require waiting for that condition to occur.

Unfortunately, computational modeling a SRPA WEC is a complicated task as it must capture the complete spatial motion of the SRPA's articulated hulls as driven by irregular ocean waves. An irregular wave field is a superposition of regular waves (simple sinusoids) at the WEC's specific location. While a collection of sinusoid amplitudes (a "sea state") can be forecast in advance using physics based models [6] or statistical tools [5], these forecasts cannot predict the phases of these sinusoid constituents and thus the specific temporal fluctuation of the free surface at the location is unknown. To accommodate this, multiple simulations need to be run for any single sea state that considers random changes in wave phases. As such, computational techniques for simulating WEC motion need to be reasonably fast to allow for numerous cases to be considered (i.e. many instances of many sea states).

In each simulation, there are several physical sources of non-linearity in the SRPA WEC dynamics that need to be captured. This is a complex task and usually requires simplifications to represent the reactions that are relevant to study. The predominant approach consists in choosing a parametric representation of the individual phenomena and superposing the resulting forces. In this way, the hydrodynamic forces can be modeled by the summation of buoyancy, inviscid wave radiation and diffraction loads, and drag forces. This is a common approach which has been wildly reviewed in the literature [17]–[19]. Buoyancy arises from the integration of the pressure over the changing wet area, as the body and the waves interact over time. The inviscid wave radiation refers to the loads due to the moving body generating waves. The diffraction loads are calculated as the reaction forces when the waves encounter an obstacle as they spread. The drag force is associated to the separation of the fluid as it moves around the body [19].

Additionally, other external forces, such as the power take off (PTO), should also be included in the modeling and analyzing of a SRPA. The PTO is the mechanism used to convert the tendency to make relative movements of the WEC components into usable energy. The PTO can be tuned to optimize the power extraction [20]. Additionally, mooring line forces need to be included in any study of SRPA WECs. The mooring lines forces can be highly non-linear and, as will be shown later in this document, they have an important effect on the dynamics of the system and therefore in the power production.

All this wide variety of dynamic factors needs to be included in the analysis of a SRPA WECs, besides the non-linear effects that arise from the interaction of the bodies and waves. It has been shown [21]–[24], that when large spar platforms are excited by waves and they begin to move in the heave direction,

the restoration pitch coefficient changes as it depends on the metacenter of the structure and the displaced water volume. This can lead to pitch and roll instability, and the tendency for the pitch and roll generation is frequency dependent. This phenomenon, known as parametric resonance, can result in large roll motions when the excitation force of the system is close to twice the pitch natural frequency. As SRPA WECs extract energy from one of the degrees of freedom and all the energy is dissipated in different degrees of freedom, and is energy that cannot be harnessed, this effect has particular importance for this class of devices. Beatty et al. [21] showed that by reducing the parametric roll a SRPA WEC can extract over 190% more energy.

As it will be explained in 0, for this analysis a comprehensive software tool was selected that allowed modeling this complex system in the time domain. This software is capable of handling articulated hulls, custom PTO models as well as model complex mooring lines interactions.

1.2.3 Simulation Based WEC Mooring design

So far there are few studies that consider mooring lines concurrent with the conceptual design of the WEC, as the mooring lines are usually included after the main design variables have already been defined. On the other hand, almost none of these studies are based on SRPAs and it is rare that both the mooring and converter are considered using realistic physics. Given the litany of non-linear dynamics that occur in the real world (see previous section) it raises questions if past conclusions can be trusted.

Mooring systems for traditional floating structures, such as oil platforms and ships, are typically designed to keep the structure stationary. In order to reduce the tension loads on the mooring lines it is common practice to ensure that the natural period of the entire structure's motion is at least one order of magnitude larger that the natural period of the waves [25]. This is typically accomplished by shaping the hull to produce desired inertial loads (i.e. hydrodynamic added mass). In contrast, SRPAs are designed to move in reaction to the waves, not remain stationary, and hence WECs have significantly different dynamic characteristics. Since WEC hull motion drives the energy conversion process, a SRPA WEC mooring system must to be designed to maximize the movement in the degrees of freedom where power is extracted. Meanwhile, in the other degrees of freedom movement should limited, since the transfer of wave supplied energy into kinetic energy that does not subsequently transfer to the PTO decreases the overall system efficiency [26].

As it will be shown later in this document, the mooring lines for a SRPA WEC need to be designed to reduce its impact in the power producing mode while mitigating other undesirable motions. For this, consideration should be given to all the different variables involved in the design, as well as possible combinations to thereby define the Design Space (DS). To date, studies of the impact of the mooring lines on the WEC system dynamics and power conversion have been completed by simplified models and sensitivity studies that can only describe part of the DS but do not include all the possible mooring configurations.

One simplified modeling approach was presented by Fitzgerald & Bergdahl [27], who included the mooring line effects in the frequency domain by calculating an equivalent linear impedance from the output of a non-linear time domain model. In that work, four different mooring lines configurations were evaluated for a simplified WEC that extracts power from surge, heave and pitch motions. The linear model they applied had favorable run times, but it neglected non-linear effects created by line drag and non-linear stiffness resulting from large transient motions of the mooring and corresponding changes in the mooring geometry. The authors concluded that the mooring loads can have significant effects on the WEC dynamics and therefore on energy harvesting. Muliawan et al. [28] presented a sensitivity study based on 6 different mooring system configurations; the study was carried out in the time domain using a commercial software that considers the linear hydrodynamics (drag and added mass), PTO and mooring loads. The mooring loads were simulated as non-linear springs and no hydrodynamic drag or added inertia were included. Muliawan et al. concluded that, subject to the mechanics of the mooring model, the impact of the mooring lines on the device in regular waves could vary the total power absorption between +4% to -8%, when compared to a case with no moorings. In irregular waves, the difference between the moored and unmoored cases was found to be smaller, around 1.1%.

Another study was presented by Cerveira et al. [29] who considered an arbitrary sphere-shaped SRPA WEC, in both the time and the frequency domains. To facilitate the frequency domain analysis, the mooring lines were included in the model as forces proportional to the displacements and the velocity, and the PTO extracted power from the heaving and surging motion of a single buoy. Two mooring configurations were considered and compared to the unmoored system; it was found that the influence of the mooring on power production was small. In individual sea states the WEC showed a decrease in the power capture between 0.5% and 1.5% for a slack mooring configuration and around 1% on the total annual energy capture. The author commented that the results were valid for the hypothetical WEC and further investigation was required for a more realistic device.

Use of formal optimization in WEC mooring design was executed by Vicente et al. [30] for a single hemispherical floating WEC subject to regular waves. Two mooring line configurations were considered and the power was extracted by a linear PTO proportional to the absolute heave displacement. Vicente et al.'s study focused on the influence of the slack in the line mooring lines with or without additional sinkers or floaters, on the power absorption and the horizontal displacement. It revealed that the single body WEC considered was in fact influenced by the mooring lines; power conversion could be changed around 2% through the selection of the mooring design variables .

It can be seen that even though some studies that characterize the mooring line's effects on WECs exist, more research is required for two-body SRPA WECs mooring line configurations. There is a great opportunity for optimizing the overall power conversion efficiency, since these devices rely on relative motions that can easily be affected by the mooring system. Moreover, it is believed that the mooring lines can have a positive effect on the reduction of parametric roll. Tarrant, et al. [22] and Villegas, et al. [23] study the effects of the parametric roll on SRPA WECs. They apply a PTO control strategy to reduce the parametric roll and extract more power. Tarrant et al.[22] state that even though if a simplified model of the mooring system, it can change the stiffness of the system which can result in roll instability. A different study was presented by Koo et al.[24], who studied the effects of the mooring lines in oil spar platforms. He concluded that the moorings can help to reduce the effects of the parametric roll as the system becomes more stable.

1.3 OBJECTIVES AND CONTRIBUTIONS

The aim of this thesis is to gain a better understanding of how the mooring systems affect the power production of a SRPA WEC. To that end, a full hydrodynamic time domain simulation was designed within an optimization scheme to evaluate a wider range of mooring configurations spanning the breadth of the full Design Space (DS). This research intended to answer the following outstanding questions regarding SRPA WEC mooring systems:

1. What are the effects of mooring lines on the power production for a SRPA WEC?
2. Is it important to study the whole design space in order to design a mooring system of a SRPA WEC?
3. What defines a "good" mooring system for a SRPA WEC?

4. How can the mooring system help to minimize the parametric resonance problems that the SRPA WEC tends to present?

On the path to answering these questions, several technical challenges had to be overcome. The research contributions made in the course of the research include:

1. Procedures were developed to design the mooring line system for a SRPA WEC based on the power extraction efficiencies and survivability of the system.

2. A qualitative study on the whole DS for a SRPA WEC was carried out considering the survivability of the system and the power production.

3. Propose a mooring line design method that minimizes the parametric roll of a SRPA WEC.

4. Calculated the total yearly energy production of the SRPA WEC.

1.4 THESIS OUTLINE

This document is divided into six chapters. Chapter 2 explains in more detail how the SRPA WEC systems were modeled. On the basis of fluid potential theory, frequency domain and time domain simulations are given. A brief explanation of the PTO and mooring forces is also presented. The objective of this chapter is to introduce to the reader how the SRPA WECs was modeled, including all the techniques and assumptions used.

Chapter 3 addresses the first contribution of this research, by presenting the procedure for designing a mooring system based on the power extraction efficiencies and the survivability of the system. This chapter begins by introducing basic principles for the design of the mooring system, and explaining the limit states that have been defined by the literature and the standards for floating structures. Then in order to explain the optimization technique that was used, the mooring line design parameters for the SRPA WEC presented in Chapter 2 are explained. This chapter ends by introducing the procedure used for designing the mooring system.

Chapter 4 presents the results that were obtained from the SRPA WECs . The proposed mooring system are compared to a case were the device floated freely and also to the mooring system configuration that extracted less power. This chapter address the research contributions number two.

Chapter 5 a study on the mitigation of parasitic pitch and roll excitations is presented as well as the results of the total annual production of the SRPA WEC. This chapter address contributions number 3 and 4.

The last chapter, Chapter 6, is organized to answer the questions that where formulated in § 1.3 . This chapter is organize in other that each of the section of the chapter address one of the questions that have been proposed.

Chapter 2

Wave Energy Converter Dynamics

Many problems in ocean and coastal engineering are solved using a simplified representation of the fluid interaction. This is because solving the full hydrodynamic model can be very computationally expensive and, in most situations, not necessary for the required accuracy. A powerful and versatile technique that has been used in the past and will be used in this thesis is potential flow theory, which, in combination with the proper boundary conditions, can be used to simulate objects under the influence of wave forces.

Current available modeling tools cannot accurately capture all of the relevant phenomena that drive device motion and execute these calculations fast enough to facilitate reasonable run times. For this reason, one of the predominant computational approaches consists of a parametric representation of the individual phenomena and superposition of the individual force components. As shown in Figure 2-2 this approach was considered for this thesis as implemented within the software package ProteusDS[14], a finite element, non-linear, time domain solver used for dynamic analysis of WEC and wave interactions. In this chapter, the specific physical parameters of the SRPA WEC being studied are provided, and the elements of the ProteusDS simulation of this device are described. In the discussion of the ProteusDS model,

[14] Dynamic Systems Analysis Ltd.ProteusDS, 2015.

emphasis is placed on identifying the real world phenomena that are being modeled and qualitatively describing the associated calculations. Detailed derivation of these calculations is beyond the scope of this work. Rather, a discussion of the hydrodynamic calculations is based on describing how the ProteusDS model coefficients were selected and applied.

2.1 WAVE ENERGY CONVERTOR

An SRPA based on the geometry of the WaveBob device is the focus of the current work. As shown in Figure 2-1 the SRPA is an axisymmetric design formed by two coaxial bodies, the toroidal float and the central spar. A PTO connects these two bodies and is driven by relative heaving motion between the two bodies. As explained in § 1.2.2, the PTO produces a force proportional to the relative heave velocity with the constant of proportionality adjusted to match the real part of the radiation impedance of the system, in order to absorb the largest amount of energy [20]. This SRPA is a full-scale version of the physical scale model studied by Beatty et al.[31] .

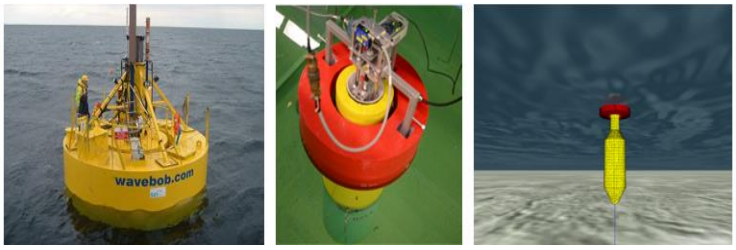

Parameter	Units	Values
Spar Mass	Kg	1.65E+06
Spar Moments of Inertia (I_{XXGg_S}, I_{YYGg_S}, I_{ZZGg_S})	Kgm^2	[5.66E+5.66E+6,6.48E+5]
Float Mass	Kg	2.01E+05
Float Moments of Inertia (I_{XXGg_f}, I_{YYGg_f}, I_{ZZGg_f})	Kgm^2	[5.79E+5,79E+6,1.45E+6]

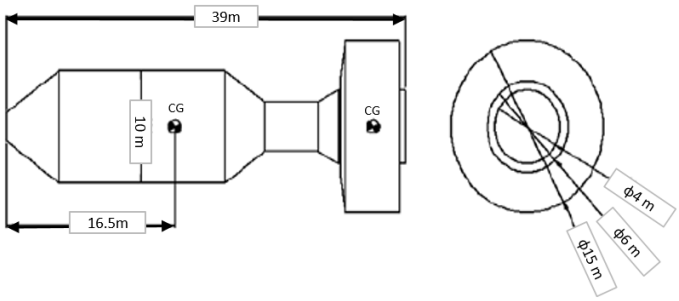

Figure 2-1: Physical scale model and simulated model versions of the SRPA WEC.
The differences between the actual model, the Beatty experiment and the geometry considered for this analysis. Top left corner: Wave Bob device. Top center: the physical scale model described by Beatty et al. in [31] Top Right corner: simulated full scale WEC in ProteusDS. Bottom: Dimensions of the WEC considered in the mooring design study [32] [33]

The ProteusDS software is capable of capturing all of the major components of a complete SRPA system simulation. Specifically, the non-linear dynamics of the mooring lines, the kinematic coupling of the spar and float dynamics (the spar and float form an articulated hull), the kinematic coupling of the spar and mooring lines, the PTO dynamics, and the individual hydrodynamics of the spar and float are all represented. The environmental loads that drive the system simulation are derived from the specification of directional wave spectra which define how the overall free surface oscillation is formed from sinusoidal constituents that have a specific frequency and direction. Figure 2-2 below gives a schematic of the elements of a ProteusDS SRPA simulation, and the environmental, hydrodynamic, PTO and mooring calculations are further discussed in §2.2 to § 2.5 . Just as there are various physical components in a SRPA system simulation, there are a series of components that comprise the hydrodynamic forces calculated on the spar and the float. These include buoyancy, inviscid wave radiation and diffraction loads, drag forces and low frequency wave drift. These individual elements of the hydrodynamics calculations are described in § 2.3 .

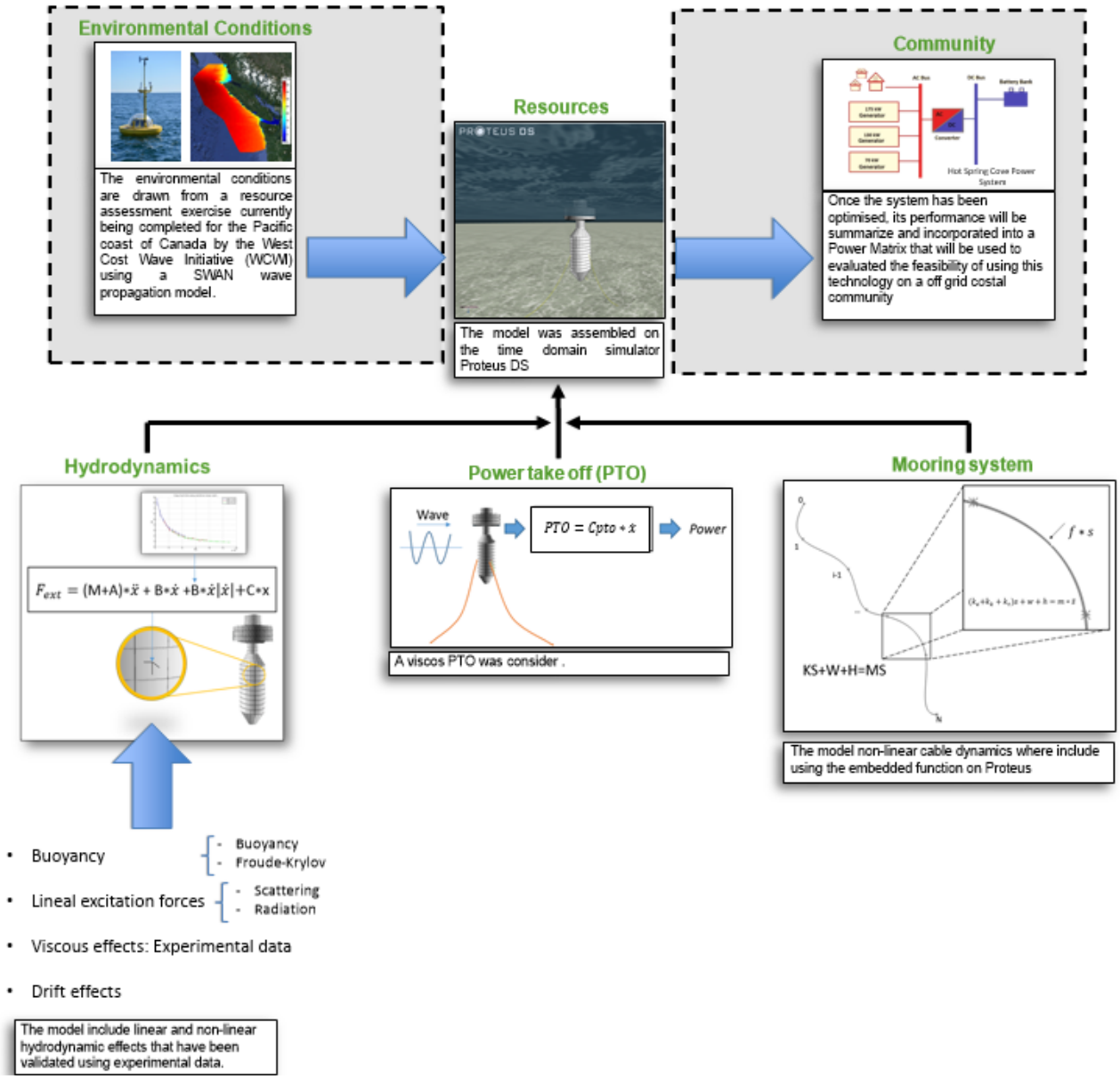

Figure 2-2: Model

Esquematic of the simulation. The environmental conditions are input into the solver, where the loads are simulated. Using the simulation output, the power for each sea state can be calculated and a power matrix build.

2.2 Environmental Conditions

This section provides the description of the environmental conditions used for the analysis of the SRPA mooring system. The wave climate for this analysis is based on observations made from a wave monitoring buoy deployed by West Coast Wave Initiative (WCWI) on Amphitrite Bank in approximately 40 m of

water [33]. As it will be explained, the wave environmental conditions are communicated to ProteusDs as a spectrum. To help the reader interpret the spectrum and understand the wave kinematics that ProteusDS applies, a review of Airy wave theory is given.

2.2.1 AIRY (LINEAR) WAVE THEORY

Airy wave theory is based on using the velocity potential (ϕ) as the basis of a solution to the momentum equation ($\rho\frac{dV}{dt} = \rho g - \nabla p + \mu\nabla^2 V$) and the continuity equation ($\frac{\partial\rho}{\partial t} + \nabla(\rho V) = 0$). The velocity potential is a mathematical expression, which describes the velocity (u, v, w) of a water particle by the derivate of the potential function (ϕ) with respect to its position (x, y, z).

$$\nabla\phi = \left[u = \frac{\partial\phi}{\partial x}, v = \frac{\partial\phi}{\partial y}, w = \frac{\partial\phi}{\partial z} \right] \tag{0.1}$$

If the fluid is idealized as incompressible, inviscid and irrotational, the continuity equation can be re-written as the Laplace equation of the potential ($\nabla^2\phi = 0$). Also, the following boundary conditions can be applied to the fluid domain (also shown in Figure 2-3):

- Impermeable sea bed (no flow the sea bed $w = \frac{\partial\phi}{\partial z} = 0$; z = 40),
- free surface kinematic condition ($\frac{\partial\phi}{\partial z} = \frac{\partial\eta}{\partial t}$ at the water line) and
- the free surface dynamic boundary condition ($\frac{\partial\phi}{\partial t} + g\eta = 0$ pressure above the free surface) [34].

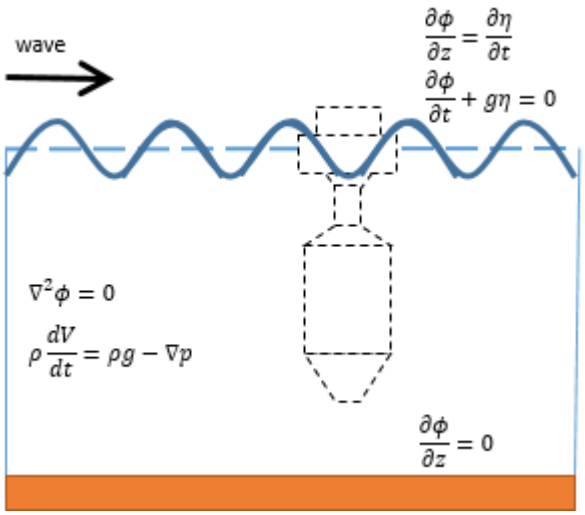

Figure 2-3: Boundary conditions.
The free surface boundary conditions and the sea bed boundary conditions are shown. The WEC is shown as a dashed line to suggest that it is invisible to the incoming waves.

where η is the water surface height and is derived from the Laplace equation and is described by the mean surface elevation (h), the wave amplitude (A), the angular frequency(ω), the wave phase(ε) and the direction(θ) and the wave number(k), as [34]:

$$\eta(x,y,t) = \Re\left\{A\exp\left(-ikx\cos\theta - iky\sin\theta + i\omega t + \varepsilon\right)\right\} \tag{0.2}$$

The wave number (k) is found by iteration using the dispersion relation $\omega^2 = gk\tanh(kh)$. According to this theory, the wave group has a dispersion velocity defined as the velocity with which the overall shape of the wave's amplitudes propagates. This concept is also known as celerity and is defined by the following relation:

$$C = \frac{\omega}{k} = \frac{gT}{2\pi}\tanh\left(\frac{2\pi d}{L}\right) \tag{0.3}$$

These equations are used by ProteusDs to solve the motion of the water particles around the floating body and in this way, model the ocean waves. It can be seen that the only parameters needed to solve this equations are the amplitude, angular frequency and the mean surface elevation, as the phase is random and specified by the user. In the following section, it will be shown that by superimposing different waves at different phases irregular sea states can be model.

2.2.2 DEFINING THE SRPA'S OPERATIONAL CONDITION

The irregular behavior of the waves in the ocean are characterized by sea states, which are time intervals in which the conditions are more or less constant and can be statistically defined. A statistical representation is required, as real sea states cannot be defined by a single wave pattern moving in a singular direction. More likely, they are defined by different waves with different headings, amplitudes, frequencies and phases, which are superimposed as they travel across the ocean surface, in a stochastic process. A wave spectrum S(ω) analysis is required to define the spectral spread, where the time domain surface displacement is decomposed into regular waves using a Fourier transformation [34], which can then be quantified, organized and fitted into a spectrum.

To have a good quality spectrum, different surface displacement time series are required, which are treated as realizations of the same stochastic process, as the spectrum approach describes all the possible observations and not only a specific wave surface series. The spectrum can be described using statistical information, such as significant wave height (Hs), which is defined by average of the highest 1/3 of the waves on the record, and peak period defined as wave period with the highest energy [34]. For this thesis a JONSWAP spectrum will be used as shown in the following figure.

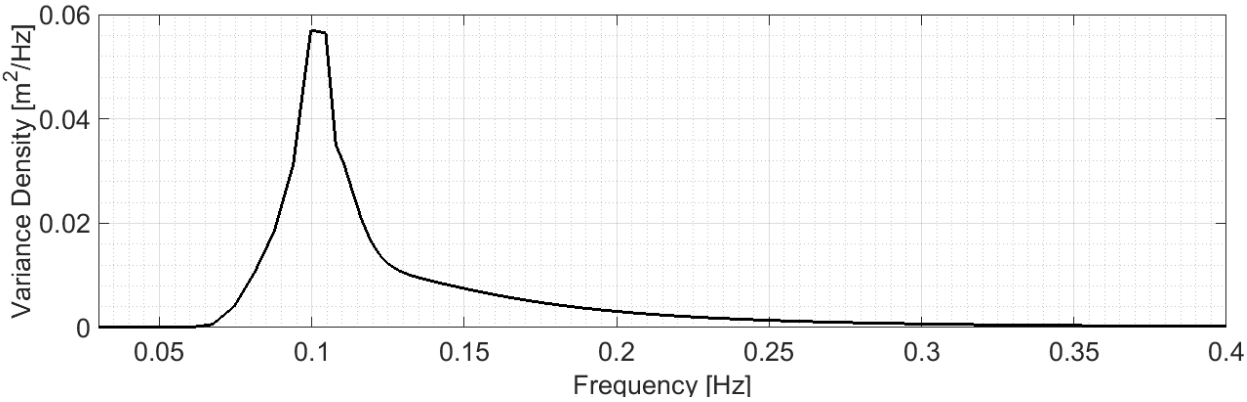

Figure 2-4: JONSWAP Spectrum

JONSWAP spectrum for Hs = 2.75m and Tp=9.5s

The wave environment conditions for this analysis are based on observations made from a wave monitoring buoy deployed by West Coast Wave Initiative (WCWI) on Amphitrite Bank, in approximately 40 m of water depth [33]. As shown in Figure 2-5, this location is close to the shore and features significant annual wave energy transport (~ 40 kW/m), which makes it a possible candidate for future WEC deployments.

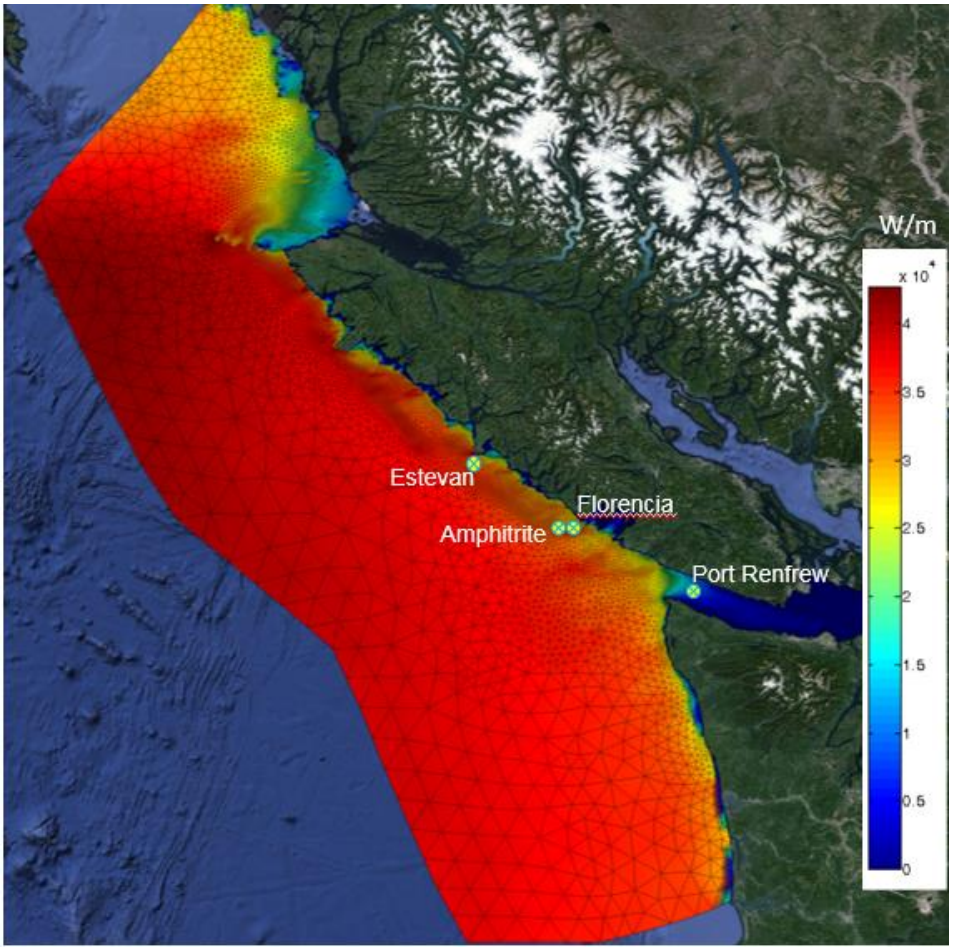

Figure 2-5: Amphitrite buoy location.

The sea state is re-constructed using a JONSWAP spectrum with an average direction aligned with one of the moorings lines. The spectrum has a cos squared directional spread, with a spread parameter of 15[35]. The amplitudes of the regular waves are multiplied by a directionally dependent parameter that preserves the spectral variance density, as presented in Figure 2-6:Figure 2-6. Therefore the primary direction has the most wave power with the directions ±90 degrees having decreasing wave power. The sea states tested had seven different wave directional headings, with each direction having sixty different wave frequencies, making 420 individual regular wave components.

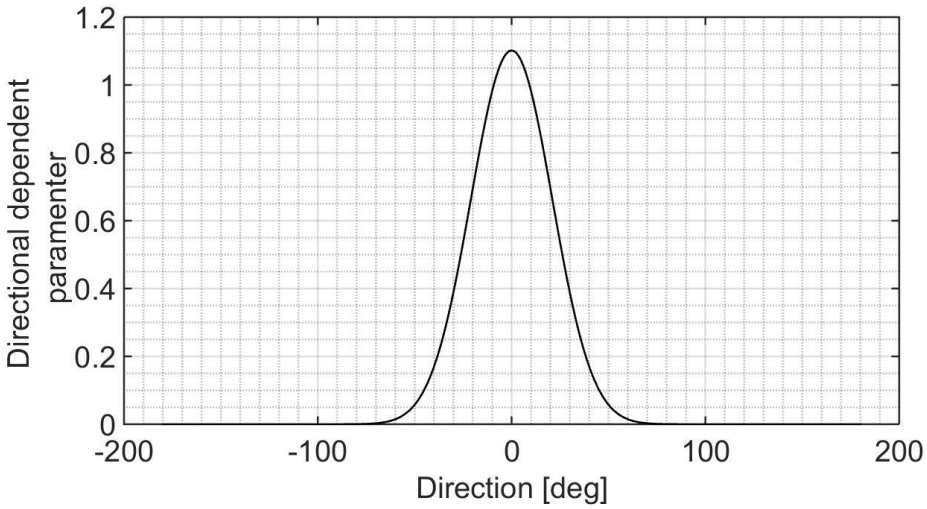

Figure 2-6: Directionally dependent parameter

As shown in Figure 2-7, the complete wave climate of a particular location can be represented by a wave histogram where each of the bins contains all the sea states of a given year which can be represented by a spectrum defined Te and Hs.

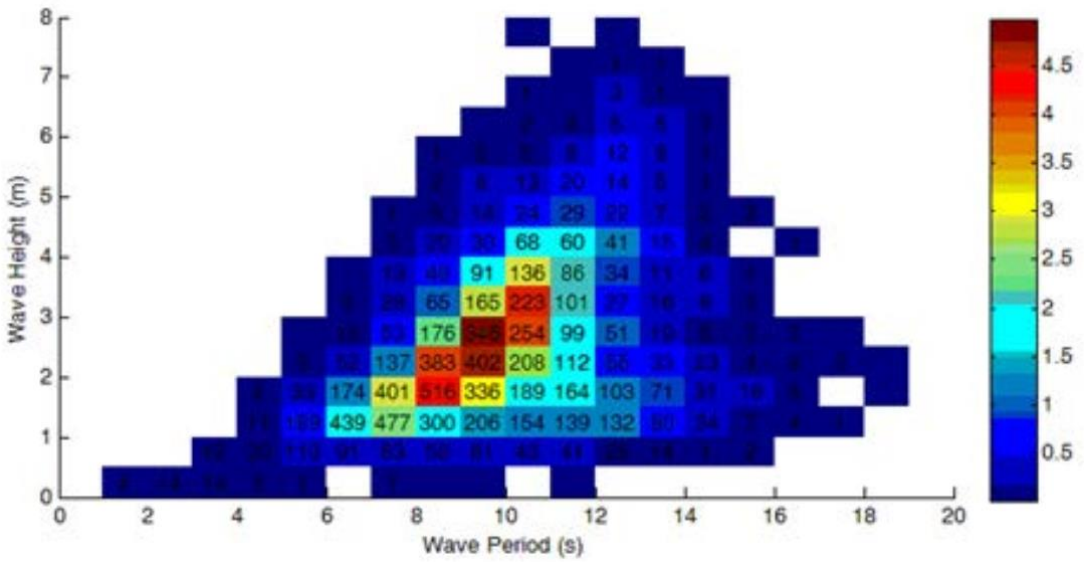

Figure 2-7: Wave conditions Histogram.
The histogram shows the occurrence frequency and energy distribution at the Amphitrite buoy location. The numbers indicate the occurrences per year (hrs), while the contour colours indicate the percentage of total energy within that sea state (%). [33]

2.3 SPAR AND FLOAT HYDRODYNAMICS

Since wave forces are created through complex fluid structure interactions, they usually require drastic simplifications in order to facilitate reasonable calculation times. Furthermore, the overall wave forces

are assembled from simple constituents, each piece being formed from a simplified view of the overall fluid structure interaction. For instance, the first order inviscid wave forces are approximated using a Taylor expansion of the Bernoulli equation up to the constituent proportional to the wave amplitude. As this is a linear problem, it can be solved by dividing it into two forces that can be superimposed [17]: the linear buoyancy and linear excitation forces. This approach can be extended to other non-linear forces as viscous forces, second order wave effects, power take off forces and mooring line loads. The resultant force on the body can then be used in Newton's second law, balancing the product of the mass (m) and body acceleration with the net external forces (F_{ext}).

$$\begin{aligned} m\dot{u} &= F_{ext} \\ &\approx f_{NB} + f_e + f_{nd} + f_s + f_{PTO} + f_m \end{aligned} \tag{0.4}$$

For this analysis, the external forces considered correspond to the buoyancy (f_{NB}), excitation forces (f_e), radiation force (f_r), non-linear viscous drag (f_{nd}), second order wave effects (f_s), power take off forces (f_{PTO}) and mooring line loads (f_m).

In time domain simulations this process is repeated for each time step by integrating the forces over time and calculating the acceleration of the body. Time domain simulations are required when modeling transient behavior and irregular sea states. Depending on the effect that needs to be captured, the complexity of the model technique will vary. A simple but powerful tool for modeling time domain problems is *Time-Domain Linear Hydrodynamics.* This technique relies on the superposition of any number of regular monochromatic waves to model irregular waves environments. In the same way, the linear force equation can be calculated for each regular wave in the frequency domain, which requires less computational power before bringing it into the time domain. In this case, time domain solvers, such as ProteusDs, are used to scale and link the phases of each individual wave to the discrete realization of the wave spectrum that is being simulated [17]. Additionally, some non-linear effects that could be important for simulating the behaviour of a floating body can also be included in the calculation by a simple alteration of the basic *Time-Domain Linear Hydrodynamics* formulation. Within ProteusDs this

process is carried out in the time domain by an adaptive 4th /5th Runge-Kutta integrator, which varies the length of time step to avoid instability[15].

2.3.1 BUOYANCY

As explained by Faltinsen [17], when considering linear wave theory, the response of a body in regular waves can be used to approximate the response of a body in irregular waves by super-imposing the regular wave results. For calculating the buoyancy force, the linear version of the Bernoulli[16] equation is used to define the pressure over the surface of the structure which is defined by balancing the momentum equation for an unsteady flow over the body:

$$p = p - p_0 = -\rho g X_3 - \rho \frac{d\phi}{dt} \tag{0.5}$$

The reaction of the device can then be calculated by integrating the normal pressure ($p\overrightarrow{N}$) over the instantaneous wetted water surface of the body (S). The moments are calculated in the same way, by considering the perpendicular distance to the center of gravity $\overrightarrow{X}$'.

---

[15] "ProteusDS Manual" [Online]. Available: http://www.dsa-ltd.ca/proteusds_downloads/documentation/ [Accessed: 24-Apr-2015].

[16] The complete, non-linear Bernoulli equation is defined as $p = p - p_0 = -\rho g X_3 - \rho \frac{d\Phi}{dt} - \frac{\rho}{2}\left|\nabla\Phi\right|^2$. For the linear version, the non-linear terms are not considered as shown in Eq. (0.5)

$$\overrightarrow{F} = \iint_S p \cdot \overrightarrow{N} \cdot ds$$
$$\overrightarrow{M} = -\iint_S p \cdot \left(\overrightarrow{X}' \times \overrightarrow{N} \right) \cdot ds \quad (0.6)$$

The wetted surface is defined as shown in Figure 2-8, by the constant part of the wet surface $(S_0(S_0)$ and the splash zone(s), which is defined by the area between the static hull waterline and the wave profile along the body.

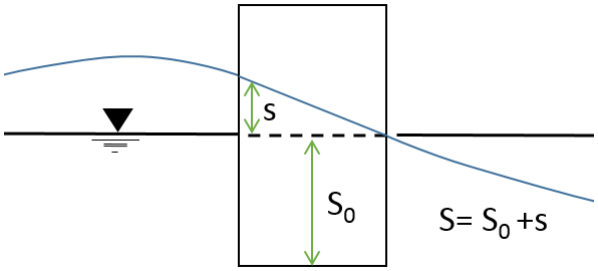

Figure 2-8: Wetted surface free surface calculation

As shown in Figure 2-9 ProteusDS requires that the surfaces of the bodies are discretized into panels to calculate the wetted area based on the current position and orientation. The idea is to account for the changes in the water line due to the combined effects of the first order wave, and the movement of the object.

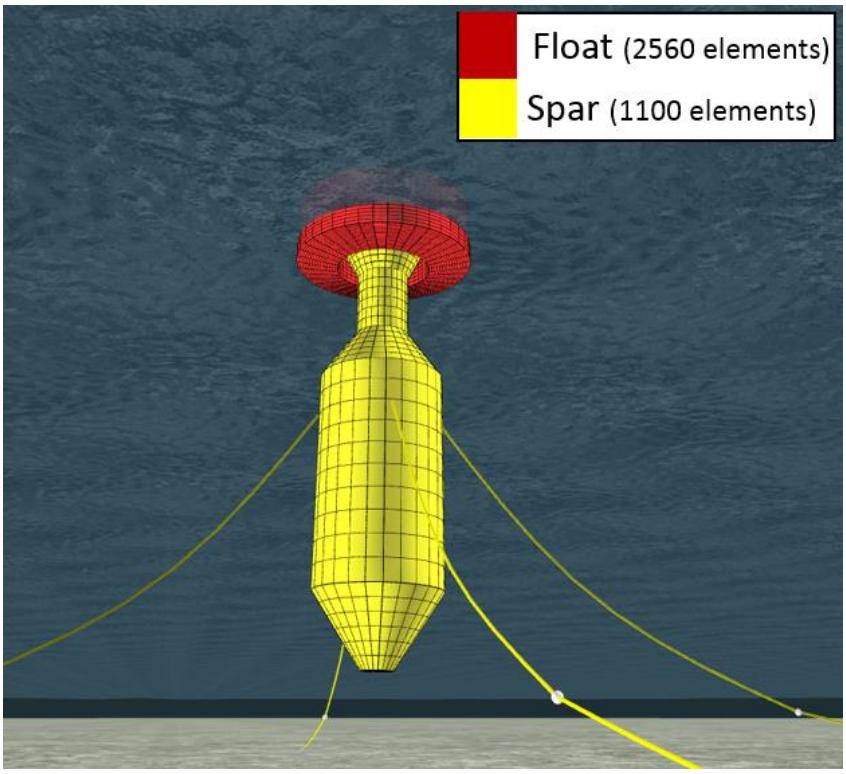

Figure 2-9: The surface panel meshes for the SRPA spar and float hulls.

The buoyancy force is then calculated by integrating the pressure at each time step over the wetted surface(S) defined in Figure 2-8. The buoyancy force is comprised of two forces: the hydrostatic forces and the Froude-Krylov force. The hydrostatic force is the static restoring forces that results from the volume of water being displaces. When a body is moved along one of its degrees of freedom from its equilibrium position a reaction force proportional to the displaced volume of water is experienced which can be calculated by finding the quantity and the centroid of the water volume displaced by the platform [36]. The Froude- Krylov force is defined by the pressure effect due to the undisturbed wave when the body is considered hydrodynamically inviscid. ProteusDS also employs a stretching algorithm to account for the body presence in the water. The stretching algorithm approximates the change in hydrostatic pressure due to the standing wave created as an incident wave encounters the body. The pressure on the splash zone(s) is account by the Wheeler stretching method[37] which extrapolated the vertical limit of the water wetted area for each time step according to:

$$z = \frac{z_s - \eta}{1 + \eta / d}; \qquad -d < z; -d < z_s < \eta \tag{0.7}$$

where η is the free surface elevation, z_s is the distance from the mean elevation and d is the water depth. This method is based on the observation that the fluid velocity at the water surface is reduced compared with linear theory. As, will be shown later, this accounts for part of the second order wave effects.

2.3.2 INVISCID EXCITATION (RADIATION AND SCATTERING)

The excitation forces arise from the wave propagating around the body. This force is defined by the fluid potential solution embedded in the linearized Bernoulli equation, which is solved by considering the boundary value problem for the Laplace equation $\nabla^2(\phi_I + \phi_D) = 0$, with boundary conditions of no flow though the surface of the body:

$$\frac{\partial \phi_I}{\partial \hat{n}} + \frac{\partial \phi_D}{\partial \hat{n}} = 0 \tag{0.8}$$

where $\hat{n}$ is the normal vector to the body surface (S).

Such problems are normally solved by applying a frequency domain panel method approach in which the surface of the submerged body is discretized into panels with a potential source strength. Then the solution of each of these panels source strengths is summed and used to calculate the force due to the pressure on the wetted surface, using Bernoulli's equation.

According to equation (0.8) the fluid potential is composed of two constituents: the scattering potential (ϕ_D), which refers to the fluid potential required to represent the waves scattering around the body, and the incident wave fluid potential (ϕ_I), due to unsteady undisturbed waves when the body is consider invisible to the wave. The outcome resultant force from the integration of the incident potential over the wet area (S) is known the Froude-Krylov force.

The third part of the linear hydrodynamic problem is the radiation force. The radiation problem captures the forces generated when the body moves in still water. When the body moves, it creates waves over the water surface that keep propagating even when the body has stopped moving. This changes the pressure field in its wake and therefore impacts the body's motion. This is known as the memory effect, as it makes the instantaneous motion of the body dependent on its past motion.

Similar to the excitation forces, the radiation forces are calculated by solving a boundary value problem by considering the Laplace equation $\nabla^2\phi_R = 0$, where ϕ_R refers to the radiation potential. For this problem, the change in the water pressure is calculated by considering the normal relative velocity between the body and the still water.

$$\frac{\partial\phi_R}{\partial\hat{n}} = v_R\hat{n} \tag{0.9}$$

Similar to the excitation forces problem, the solution of the radiation force problem involves solving the boundary value problem using a frequency domain panel method for calculating the pressure due to the radiation potential solution. The net force is calculated by integrating the pressure over the wetted area of the body, according to Figure 2-8. In order to characterize the hydrodynamic forces, a different analysis is required for each DOF and frequency. Also, it is important to notice that period dependent forces can be decomposed into two components: one in phase with the body velocity, known as the damping (B), and one in phase with the acceleration, known as the added mass (A).

$$(B_{j,k} + i\omega A_{j,k})U(\omega) = -\rho\iint_{S_{body}} \frac{\partial\phi_{Rj}}{\partial t}\hat{k}\hat{n}\,dS \tag{0.10}$$

Occasionally, this equation is presented by subtracting the added mass at infinitive frequency A(∞) from the frequency dependent added mass. In this way, the radiation forces in the frequency domain are represented as a constant infinite added mass $A(\infty)$ proportional to the acceleration, and a fluctuating term, proportional to the velocity, known as impedance (K) [36].

$$i\omega A(\infty)U(\omega) + \underbrace{(B_{j,k} + i\omega[A_{j,k} - A(\infty)])}_{K}U(\omega) \tag{0.11}$$

This interpretation gains particular importance when the frequency domain results are used to represent irregular wave responses.

For the frequency domain calculations WAMIT (WaveAnalysisMIT) was used. WAMIT is a linear hydrodynamics solver that is used to provide the input hydrodynamic coefficients for the time domain simulation. WAMIT discretizes the surface of the bodies into panels which are then used to find the

harmonic solutions of the excitation and radiation boundary value problems for rigid bodies in water, by considering fluid potential theory.

For the frequency domain calculations a three-body analysis was performed, where the spar, the float and a numerical moon-pool lid were included. The numerical moon-pool lid is required to eliminate the error in the numerical solutions that leads to negative added mass and unrealistically high radiation damping which happen due to resonant oscillations at the enclosed volume [38]. The bodies were discretized as shown in Figure 2-10.

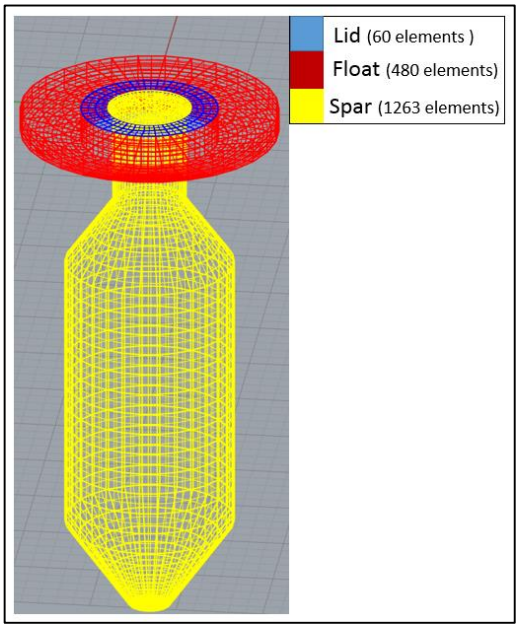

Figure 2-10: Mesh
Mesh for calculating the hydrodimamic coefficients in WAMIT.

The excitation and radiation forces were calculated for all DOFs considering enough frequencies for accurately representing a complete wave spectrum. Also, the infinite added mass was included by calculating the zero period value. The following figure shows the results for these calculations.

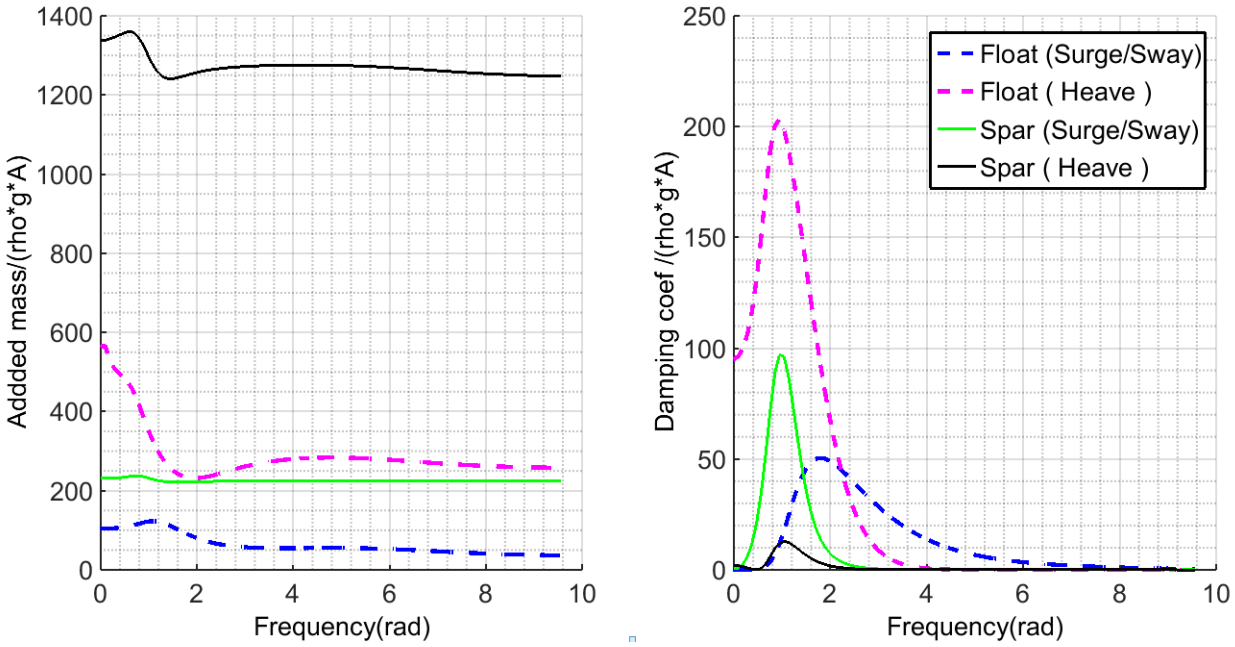

Figure 2-11: Normalized Added mass and Damping Coefficient

For linear systems, the net response of a specific location subject to alternating forces, defined by an irregular sea state, can be calculated by the sum of the responses which would have been caused by each regular wave individually. In this way the results from the frequency domain from can be brought into the time domain by utilizing the superposition principle.

As explained by Price et al. [36], the radiation impedance (K) (that was introduced in the last section and is defined by the linear damping and the fluctuating added mass), can be used to calculate the wave radiation retraining kernel function. The kernel function (k_r), is a Dirac delta function that represents the transient response of the body to a unit impose in body velocity. It is calculated by applying the inverse Fourier transform to either the linear added mass or the linear damping coefficients. For the system used in this thesis, a sensitivity study showed that the linear damping radiation kernels produce better results as they are more stable.

$$k_r(t) = \frac{2}{\pi}\int_0^\infty B\cos(\omega t)d\omega \tag{0.12}$$

Here $k_r(t)$ and $B(\omega)$ are six-by-six matrices, with each cell related to a reaction of one DOF due to a movement in another DOF. For example, the first cell represents the response on the first DOF of the system to a movement in the first DOF. The radiation force is then formulated in the time domain by considering the convolution integration of the kernel function (k_r) and body velocity vector:

$$f_r = \int_0^t \dot{\eta}(\tau) k_r(t-\tau) d\tau \tag{0.13}$$

In Figure 2-12, the kernel function for the diagonal terms of the spar and float are presented. As can be seen, the memory effects are captured in the kernel function since they represent how an impulse in initial displacement would decay over time in an underdamped manner.

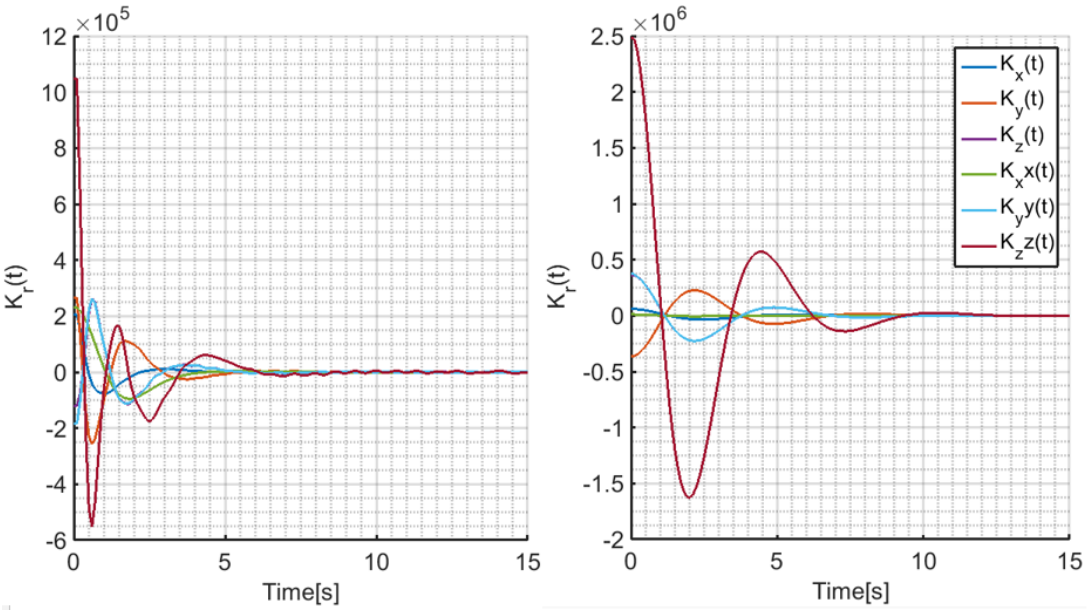

Figure 2-12: Kernel function.
Left figure: Spar, Right figure: Spar

2.3.3 VISCOUS EFFECTS

The non-linear viscous drag effects were included in the model according to Morison's equation. The drag coefficients were obtained from experimental data presented by Beatty et al. [38].

When non-linear viscous drag effects are important in comparison to the inviscid forces, the hydrodynamic load calculation can be completed according to Morison's equation. This equation is a semi-empirical equation which defines the horizontal force (f) on an axisymmetric body in a wave field as function of the relative velocity by considering the sum of the inertial force, the added mass and the non-linear drag forces [26 pg.231-269].

$$f = \underbrace{\rho \frac{\pi}{4} D\dot{u}A}_{inertia} + \underbrace{\rho \frac{\pi}{4} DC_A(\dot{u}-\dot{v})A}_{added\ mass} + \underbrace{\frac{1}{2}\rho C_D(u-v)\,|u-v|\,A_j}_{nonlinear\ drag\ force} \tag{0.14}$$

where f is the hydrodynamic force, D is the cylinder`s diameter, Aj the projected area, C_A and C_D are the empirical added mass and the drag coefficients, found by experiment or more detailed computation, for a single geometry and flow direction.

In order to work with rotating degrees of freedom and non-uniform water kinematics, the non-linear drag force of Morison's equation can be approximated using a panel method, where the body surface is discretized into panels. The drag force is calculated individually for each panel, using its projected area and considering the definition of absolute velocity.

$$(Cp,i) = v_{body} + \omega_{body} \times C_{p,i} \tag{0.15}$$

where v_{body} and ω_{body} are the absolute velocity, the angular velocity, and $C_{p,I}$ the distance from the polygon centroid to the body centroid.

To quantify the relative importance of the viscous effects versus inviscid forces on a submerged body subject to oscillatory motion, the Keulegan-Carpenter (KC) number is used. The KC number is defined using the ratio of the product of flow velocity (V) and period (T) of oscillation, divided by the characteristic length (L) of the structure. For small KC numbers, the wave inertia forces dominate and the added mass and damping calculated based on wave radiation provide a good approximation. For large KC numbers, the viscous effects dominated and the drag force needs to be included in the simulation. When the KC number is intermediate or the structure is complex, both effects needs to be modelled [19].

For this study, the structure has been classified in the third group and both effects will be included. The radiation forces and external forces were included according to linear hydrodynamic theory and non-linear drag was superimposed as a correction factor. The drag coefficient has been taken according to Beatty et al [31] and is summarized in Table 2-1.

Table 2-1: Spar drag coefficients

Vertical	3.5
Lateral	1

2.3.4 WAVE DRIFT

If the fluid potential approach is used to represent the response of a structure under wave forces, a first order approximation could be sufficient for the analysis. First order wave forces are approximated

using a linear expression of the Bernoulli equation with the constituents proportional to the order of the wave amplitude. Using the first order fluid solution, the pressure and velocity of the fluid particles are linearized and the free surface and impermeable body conditions are satisfied at the mean water line and at the submerged hull surface respectively. In some cases, additional constituents need to be included in the calculation, in order to consider other important effects. For example, the structure's response due to the *second order wave forces* has been shown to be important for designing moored structures [16], [39]–[41]. If the pressure field is approximated by preserving the first order terms, as well as those proportional to the square of the amplitude, this results in the inclusion of second order wave forces in the model [14 pg. 131-169]. For the second order fluid solution, the zero normal flow condition is accounted for more accurately by including the reflected waves with the original incident waves in the application of the impermeable wall condition. As explained in [17] and [42], second order wave effects are a consequence of the waves generated by the fluid interacting with the structure, in contrast to first order wave effects which treat the body as transparent to the incoming waves.

For this analysis, the second order effects were considered approximately, in the form of viscous drift forces and the interaction of first order effects. Faltinsen describes the process for calculating the *viscous mean drift force* as a two part integration [17]. Considering Figure 2-8, the first stage consists of the integration of only the viscous drag forces over constant area S_0. The second term corresponds to the integration from the mean water line to the actual location of the free surface, which corresponds to the splash zone s, according to Figure 2-8. The second term can be seen as a correction factor as it compensates for the change of the water surface elevation. Over a sustained period of time, the mean of the first part of the surface integration is zero, while the mean of the second contribution is non-zero and can be estimated considering the relative velocity of the body and the water.

The second order forces due to combinations of first order effects are also included in this analysis. As shown in Table 2-2, even though the inertia forces are linear and proportional to the relative acceleration between the centroid of the panel and the water, the way that the forces on the panels are integrated (using the stretching algorithm) can lead to non-linear results, which could excite the body so that it will oscillate in different modes.

Table 2-2: "Second order wave effect" contributions

#1 *Contribution of the vector product of angular motion and inertia forces.*	$\vec{F}_A^{(2)} = -\iint_{S_0} \left(p^{(1)} \cdot \vec{N}^{(1)}\right) \cdot dS$	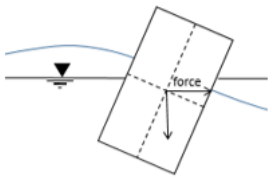
Contribution of the pressure change due to the body rotation.		
#2 *First order kinematic pressure*	$\overrightarrow{F_B^{(2)}}_1 = \iint_{S_0} \frac{1}{2}\rho\left(\vec{\nabla}\Phi^{(1)}\right)^2 \vec{n} dS$	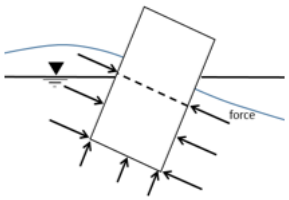
Contribution of the pressure due to the fluid changing its first order velocity($\nabla\Phi$) as it goes around the body.		
#3 *Second order fluid potential pressure gradient.*	$\overrightarrow{F_B^{(2)}}_2 = \iint_{S_0} \rho \frac{\partial \Phi^{(2)}}{\partial t} \vec{n} dS$	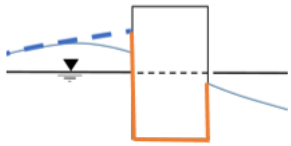
Contribution of the pressure gradient due to the free surface boundary condition defined by the second order fluid potential ($\frac{\partial \Phi^{(2)}}{\partial t}$). In this term the change of the free surface due to the interaction of different waves is considered.		
#4 *Pressure difference in the respective body position.*	$\overrightarrow{F_B^{(2)}}_3 = \iint_{S_0} \rho \overrightarrow{X^{(1)}} \nabla\left(\frac{\partial \Phi^{(1)}}{\partial t}\right) \vec{n} dS$	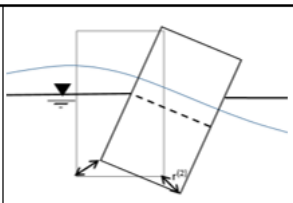
Contribution of the product of the pressure gradient ($\frac{\partial \Phi^{(1)}}{\partial t}$) and the motion amplitude(X).		
#5 *Change in the zero order pressure over the splash zone*	$\vec{F}_C^{(2)} = -\iint_s \left(p^{(0)} \cdot \vec{N}^{(1)}\right) \cdot dS$ $\overrightarrow{F_C^{(2)}} = 0$	
There is no contribution of $p^{(0)}$ on the splash zone(s), as p(0) do not varied.		
#6 *Change in the first order wave elevation*	$\vec{F}_D^{(2)} = -\iint_s \left(p^{(1)} \cdot \vec{n}\right) \cdot dS$	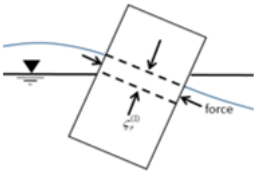
Contribution due to the change of relative wave elevation (ζ).		

The contributions 1, 2, 4 and 6 depend on first order forces and the relative movement of the body and therefore the models used in the current work are expected to capture part of the effects.

2.4 POWER TAKE OFF

The power take off (PTO) is the mechanism used to extract power from the waves. For a SRWEC, the PTO connects the float and the spar and produces a force proportional to the relative velocity of the two bodies. It is adjusted to match the real part of the radiation impedance of the system in order to absorb the largest amount of energy [20]. This kind of system is known as viscous PTO because it acts as a damping force. For the particular case of a WEC that extracts energy by the relative motion of two bodies, the damping constant (Cj) is defined for a regular sea state by Falnes [20] as:

$$\mathrm{Cj}=\left|\frac{(\mathrm{Z}_{spar} * \mathrm{Z}_{\mathrm{float}})}{(\mathrm{Z}_{spar} + \mathrm{Z}_{\mathrm{float}})}\right| \tag{0.16}$$

where Z_{spar} and Z_{float} are the impedance of each body defined by:

$$Z_i = B_i + i\omega(M_i + m_i - \frac{C_i}{\omega}); \tag{0.17}$$

where B_i is the damping of the body, M_i the mass of the body, m_i the added mass, C_i the stiffness and ω frequency where the damping constant is calculated. Equation (0.16) is used for tuning the PTO damping constant for one particular frequency at the time by only considering fiscal properties of the device itself, and no other external forces as the mooring lines.

2.5 MOORING LINE DYNAMICS

Mooring systems serve a station-keeping function by preventing the WEC from drifting in the water under current, wave, and wind loads. It also contributes to the WEC dynamics as the mass and hydrodynamic drag forces affect the WEC motion.

The mooring line dynamics are modeled in ProteusDS using a finite-element method based on cubic-spline element geometry. The cable model, as explain by Buckham et al. [43]., employs a lumped mass approximation to the cable continuum and calculates the hydrodynamic drag, added mass terms, weight and seabed friction forces at the node points. Cable node accelerations are calculated explicitly and the cable state is evolved with the WEC position and orientation using an adaptive Runge-Kutta integration

scheme. The cable element tensions, including at the boundary node at the fairlead location on the spar, are recovered from the current values of the cable node positions using constitutive relations.

Chapter 3

Mooring Line Optimization

The design of a mooring system for a floating structure is a significant challenge: the choice of line structure and layout determine highly complex hydrodynamic behaviors that, in turn, influence the dynamics of the whole system. The difficulty is particularly acute for floating SRPAs as these machines rely on internal movements to extract useful power from wave motions – the mooring must constrain the low frequency SRPA drift motions without detracting from power production. To evaluate candidate mooring layouts, a good representation of the mooring hydrodynamics is necessary to capture the salient hydrodynamic properties in a time domain simulation. Unfortunately, this kind of modeling tends to be very computationally expensive, and for this reason previous simulation based mooring design largely relies on simplified representations that only reflect part of the mooring design space since some physical and hydrodynamic properties are dropped. In this chapter, we present how a full hydrodynamic time domain simulation can be utilized within a Metamodel-Based Optimization to evaluate a wide range of SRPA mooring configurations – a range that spans the breadth of the design space. The method uses a metamodel, defined in terms of key mooring physical parameters, to cover the majority of the optimization process; the high fidelity ProteusDS SRPA simulation discussed in Chapter 2 is used to establish the metamodel in a pre-processing stage.

3.1 MOORING LINE DESIGN

The primary function of traditional mooring systems is to keep the WEC on-station even in the most severe storm conditions. The cost of the system is directly related to meeting this requirement and is thus proportional to sea conditions (heights of waves, strength of winds, magnitude of currents, etc). For SRPAs it is also of great importance that the mooring system doesn't have a negative impact on power production. Thus, while the design of this type of anchoring system can be partially based on other industry standards, such as oil and gas platforms, the design process must be altered to ensure performance is not sacrificed.

In the following sections, the class of mooring that is considered, the parameterization of this mooring class using design variables and the environmental conditions for operational and survival (i.e. extreme) circumstances are presented. These elements are applied in the optimization algorithm described in §3.2

3.1.1 MOORING TYPE

As SRPA WECs rely on relative movement between bodies for power extraction, a catenary anchor leg mooring system is preferable over any other taut mooring configuration. Even more, the specific SRPA that was considered for this thesis requires that the both the spar and the float are able to move in a way that is impossible for a taut mooring configuration. A Catenary Anchor Leg Mooring system normally consists of a wire-chain system, with or without line floats, and drag-embedded anchors. Catenary Anchor Leg Mooring systems rely on the line weight to keep the structure in place and not on the reaction of the line with the sea floor. In this way, the basic concept of the design can be preserved because the reaction forces are less intense [44].

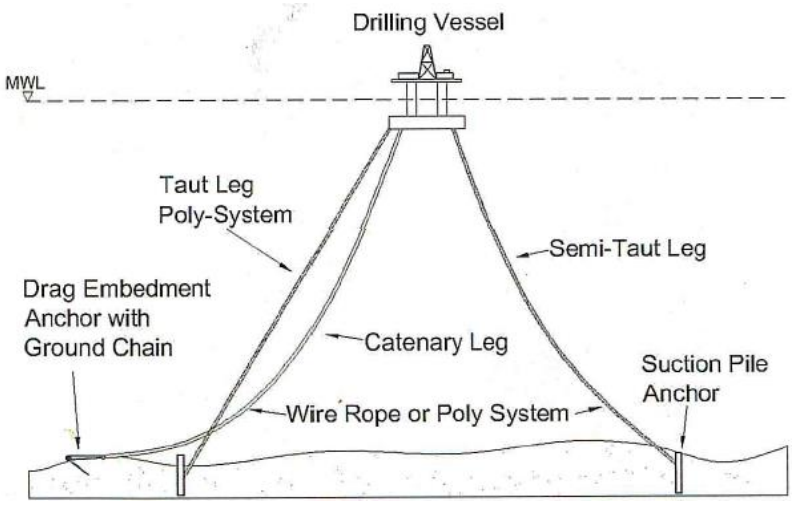

Figure 3-1: Schematic of catenary and taut leg mooring line [44]**.**

3.1.2 DESIGN VARIABLE SELECTION

Any single mooring configuration must be completely described by the design variables used in the optimization; these include line material composition, line diameter, number of mooring lines, size and location of subsurface floats, maximum slack allowed in the line, etc. For this analysis, nine design variables were chosen. These were selected by surveying what mooring components have been considered by different authors in previous works [28]–[30] as well as recommendations for Catenary Anchor Leg Mooring construction from the Det Norske Veritas(DNV) standard [37]. The design variables are believed to yield a broad design space that extends beyond conventional mooring configurations, and this nine parameter set should provide opportunity to uncover innovative mooring configurations. Table 3-1 summarizes the nine design variables:

Table 3-1: The nine design variable used to parameterize the SRPA Catenary Anchor Leg Mooring.

Parameter	Minimum	Maximum
Number of Lines	3	4
Float Mass (Percentage of total line weight)	0	100%
Line Slope (b/a according to Figure 3-2)	1:4	8:1
Connection Point on the Spar (distance e according to Figure 3-2)	11.19 m	25 m
Line Diameter chain	54 mm	180 mm
Line Diameter wire	54 mm	180 mm
Float location (distance along line from spar to anchor)	2%	20%
Slack in line (Percentage b according to Figure 3-2)	5%	20%
Relationship between chain and wire length	30%	100%

The first design variable considered was the number of lines; only values of 3 and 4 lines were allowed as existing literature shows these arrangements to be necessary to moor a device in storm conditions [28], [29]. The lines were always arranged axisymmetrically; 120 degree separation when the mooring system had 3 lines and 90 degree separation when 4 were used. As it will explained in section 3.1.3 a unidirectional sea state aligned with one of the mooring lines was considered in the analysis.

The in-line floats were defined as spheres and their mass was defined by considering a percentage of the minimum flotation needed to lift the entire weight of the mooring line assuming a float density of 384 kg/m3 (i.e. “Syntactic Foam” as per [44]). The location of the float on the line is determined as a percentage of the total length of the line, and is measured from the spar to the anchor.

To define the mechanical properties of the mooring lines two materials were considered, 'spiral stand' steel wire and chain grade 'R4'. The use of these two materials is in compliance with the DNV standard [37] and recommendations given in [45]. The slope of the lines was defined as shown in Figure 3-2, where "a" corresponds to the elevation of the connection point of the mooring line when the WEC is at its still water position and "b" is the horizontal distance from the WEC to the anchor point. The slack in the line was varied by adding extra length to the lines of between 5% and 20% of the length of the imaginary hypotenuse of the triangle constituted by sides "a" and "b". The pretension of the line was controlled indirectly by considering different combinations of mooring diameter, slope and connection height. A sample realization for a single design variable set is presented in Figure 3-2.

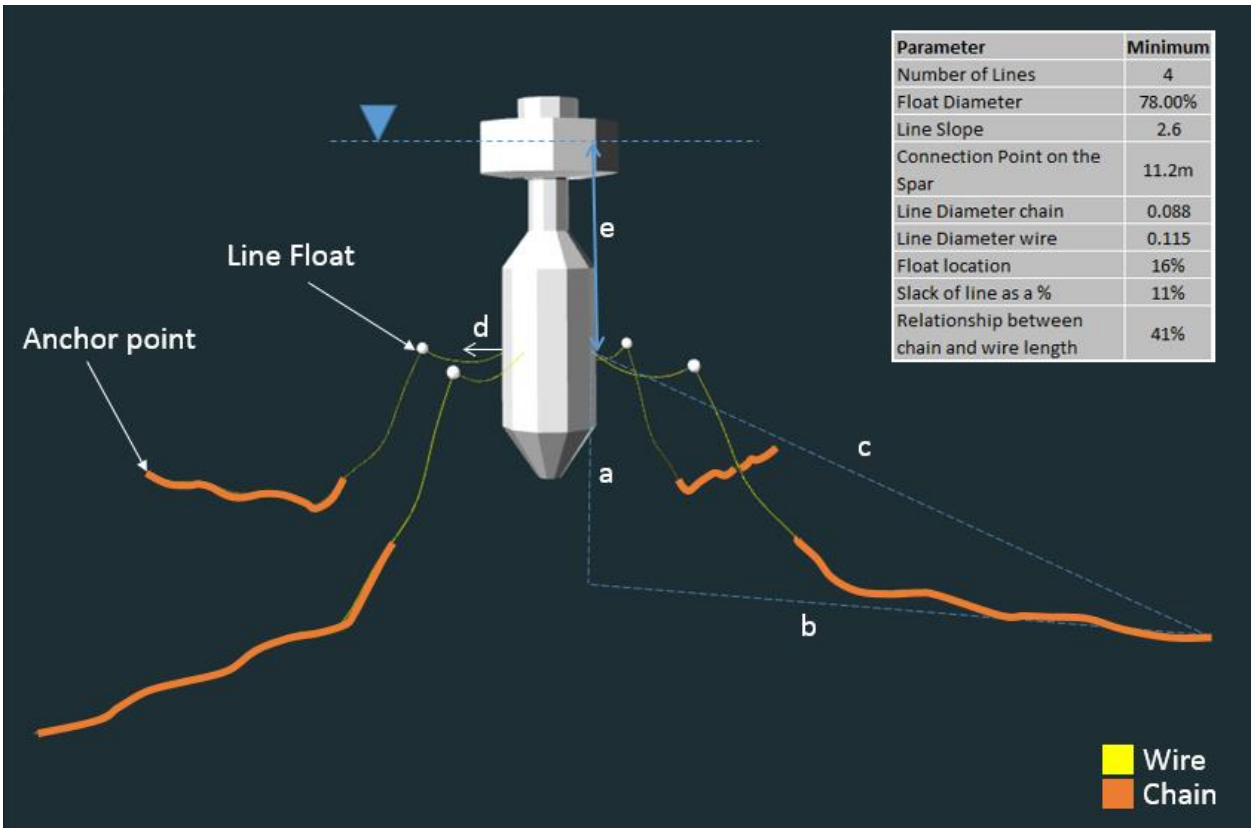

Figure 3-2: Mooring configuration example.

As the main interest of this paper is to study how the mooring lines affect the power extraction, the objective function was defined as the inverse of the mean power extracted by the WEC at the sea state defined in §2.2 .The best configuration was found by minimizing the objective function.

3.1.3 DESIGN CONDITION

The sea state used for the optimization was carefully selected in order to embrace the specific qualities of the SRPA. A 2.75 m wave height and a 9.5 second peak period were selected, as this sea state is close to the natural frequency of the device. As was show in section 3.1.3, this corresponds to the sea state with the most energy at Amphitrite bank, a high wave energy location [5]. For this particular study, a water depth of 40m was considered with no variation due to tides. The current and wind loads were ignored and a JONSWAP wave spectrum aligned with one of the mooring lines was considered to represent the sea state. The sea state was reconstructed from the specified JONSWAP spectrum using 119 regular waves, which gives a good balance between solution time and sea state resolution. The spectrum is shown in Figure 2-4.

3.1.4 ENVIRONMENTAL CONDITIONS – WEC SURVIVABILITY

Since there is no specific standard for WEC mooring line design, the practices from offshore wind and the oil and gas industry are referred to in this thesis. In particular, the DNV standard was used for defining the limit states for the design [37]. The limit state is a set of conditions beyond which the design criteria is not valid. The conditions are selected using probability theory, in order to forecast the worst combination of conditions that can occur during the design life of the system. In the DNV standard, three limit states are defined for mooring line systems. The ultimate limit state (ULS) ensures that the individual mooring lines have adequate strength to withstand the load effects imposed by extreme environmental actions. The accidental limit state (ALS) confirms that the mooring system has adequate capacity to withstand the failure of one mooring line. The fatigue limit state (FLS) investigates whether each mooring line has adequate capacity to withstand cyclic loads.

For this analysis only the ULS was considered. The wave incident direction was defined to be in alignment with one of the mooring lines, in order to cause the maximum tension in this mooring line, while the tension in the other lines is considered small. This is a more restrictive case than what the ALS requests. According to the DNV standard [46], the maximum cable tensions for the ULS should be estimated based on a storm with a return period of 50 years according to the contour line method. The contour line method is used to estimate long term extreme conditions by extrapolating the sea states within return period of 50 years using buoy observations. For this study, data from Amphitrite bank was used to constructed the following contour line for a return period of 50 years (Figure 3-3.)

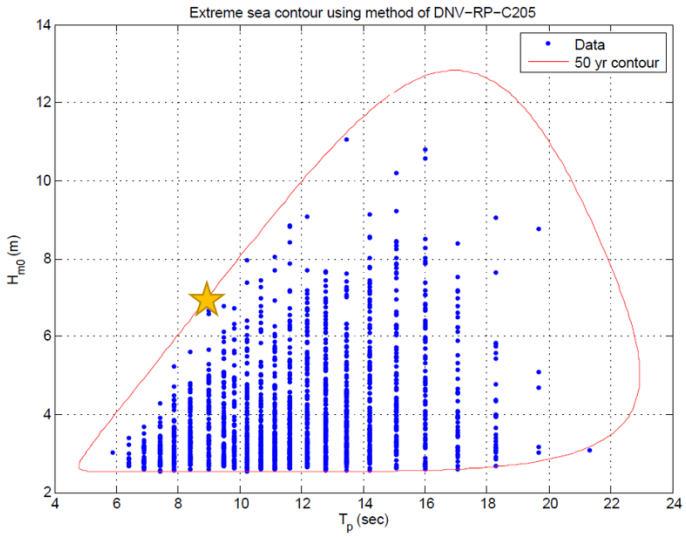

Figure 3-3: 50 year Amphitrite bank Contour plot.

Since the reaction of the mooring line system is controlled by the reaction of the floating structure under the incident waves of a particular sea state, and the sea state is defined as a stochastic process. The DNV standard recommends considering different realizations for different sea states defined along the contour line. The realizations are different wave combinations, defined by different wave heights, direction, frequency and phase, for the same sea state, which are generated randomly. The following figure shows part of the two time series of two different realizations.

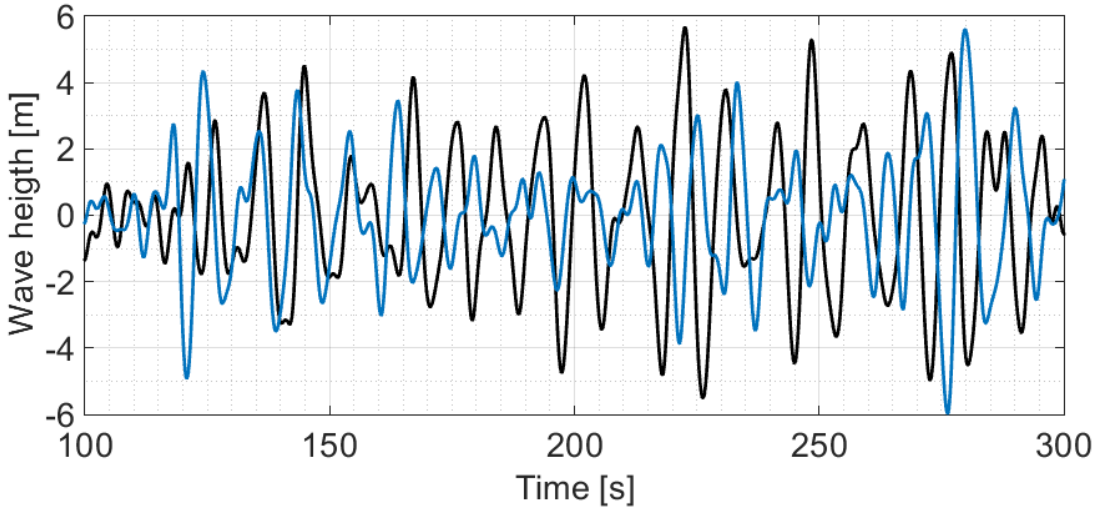

Figure 3-4: Wave realization Hs = 7.85m Te= 9.5 s.
To realizations of the the same sea state is shown in this figure.

As shown in Figure 3-5, the DNV standard recommends calculate the maximum stress using several sea states and between 10 to 20 realization for each one. Each realization should be simulated at least for 3 hours of operation. This is very computationally expensive and would be impossible to consider inside an

optimization algorithm. Recognizing the importance of computational constraints, in this thesis a simplified statistical approach had to be considered which is summarized below.

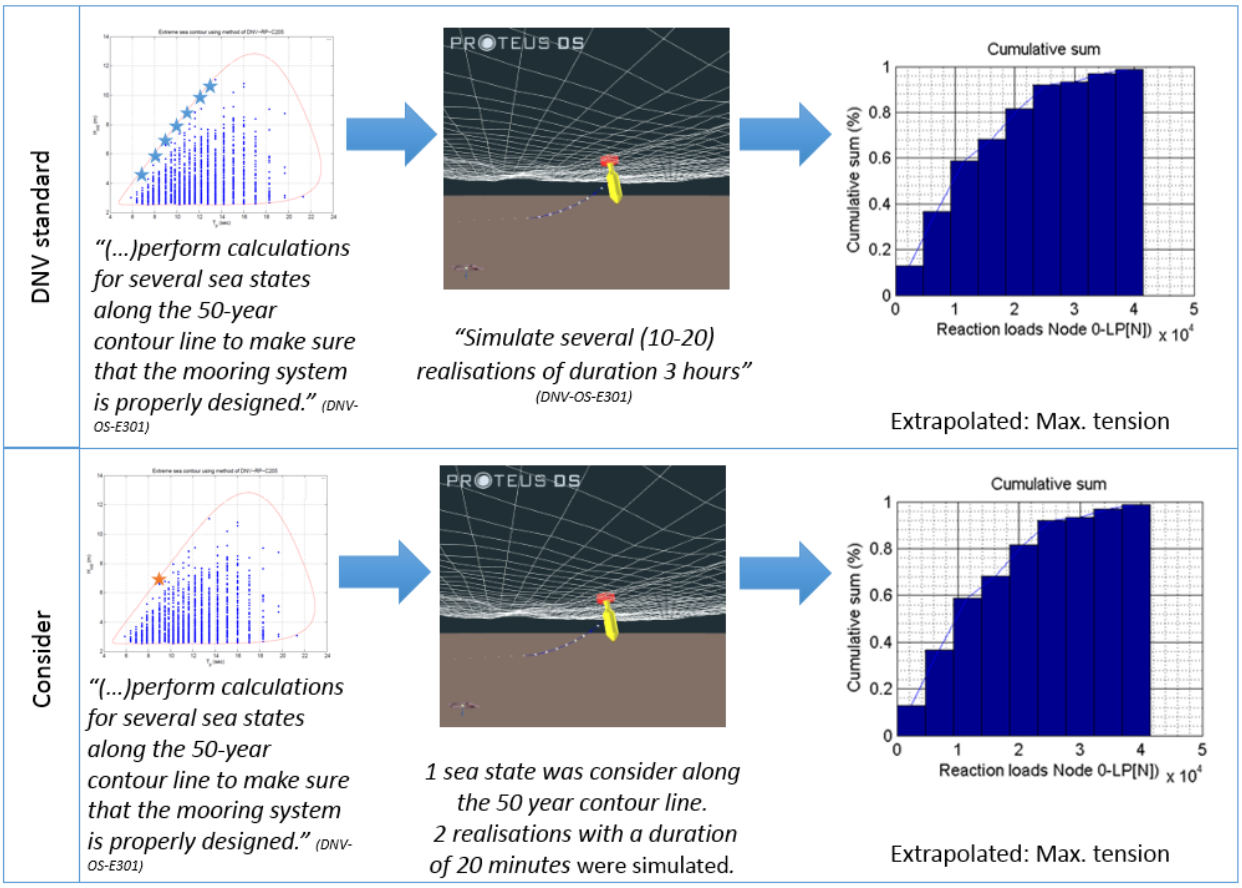

Figure 3-5: Limit state

This figures presents the differences between the requirements of the DNV Standard and what was considered in this analysis. The main differences are the number of sea states that were considered and the time of the simulation.

First, a sea state with a period of 9.75s and a significant wave height of 7.8m was selected, as it is near the natural frequency of the device and in the middle of the 50 year contour line. Then, the system was simplified, by considering only one line, which was aligned with the incident waves. By reducing the multi-line mooring to a single line, a conservative estimate of the maximum line load should be realized, while simultaneously reducing the required computational time. Also, in the survivability simulations for each design candidate, the float and the spar were locked together as it is expected the system will go into survival mode in this situation. Two simulations of independent phase realizations and durations of 20 minutes each were used to extract peak loads that then were fitted into a cumulative Weibull distribution with a 90% confidence interval. The following figure illustrates how the peaks where selected.

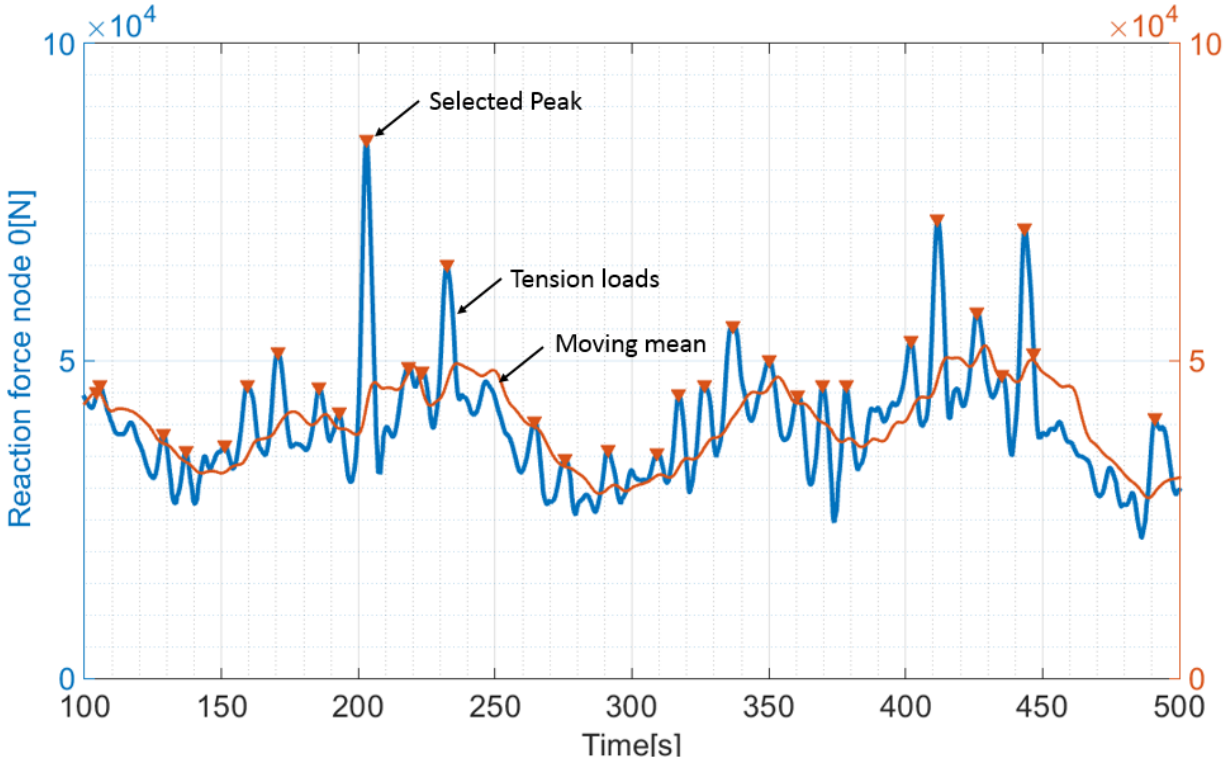

Figure 3-6: Line tension.
The peaks where defined as the maximum value between two crossing points between the moving mean and the tension signal.

The Weibull distribution was then used to forecast the maximum expected load in the mooring lines during the 50 year condition. To ensure that the automated Weibull fitting procedure did not produce spurious results during the optimization run and derail the optimization, a sensitivity study was completed that examined the stability of the Weibull fit with respects to the histogram structure used to approximate the probability distribution of the peak tension values (i.e. how the bin widths used in the histogram impact the extrapolation of a maximum tension). The sensitivity study was based on the following configuration.

Table 3-2: Sensitivity study configuration for selecting number of bins.

Parameter	
Number of Lines	1
Float Mass (Percentage of total line weight)	0
Line Slope (b/a according to Figure 3-2)	1:3
Connection Point on the Spar (distance e according to Figure 3-2)	14.9 m
Line Diameter chain	110mm
Float location (distance along line from spar to anchor)	2%
Slack in line (Percentage b according to Figure 3-2)	5%

Once the peak tension database was built, it was classified using different bin sizes and fit to a Weibull distribution, as it is illustrated in the following figure.

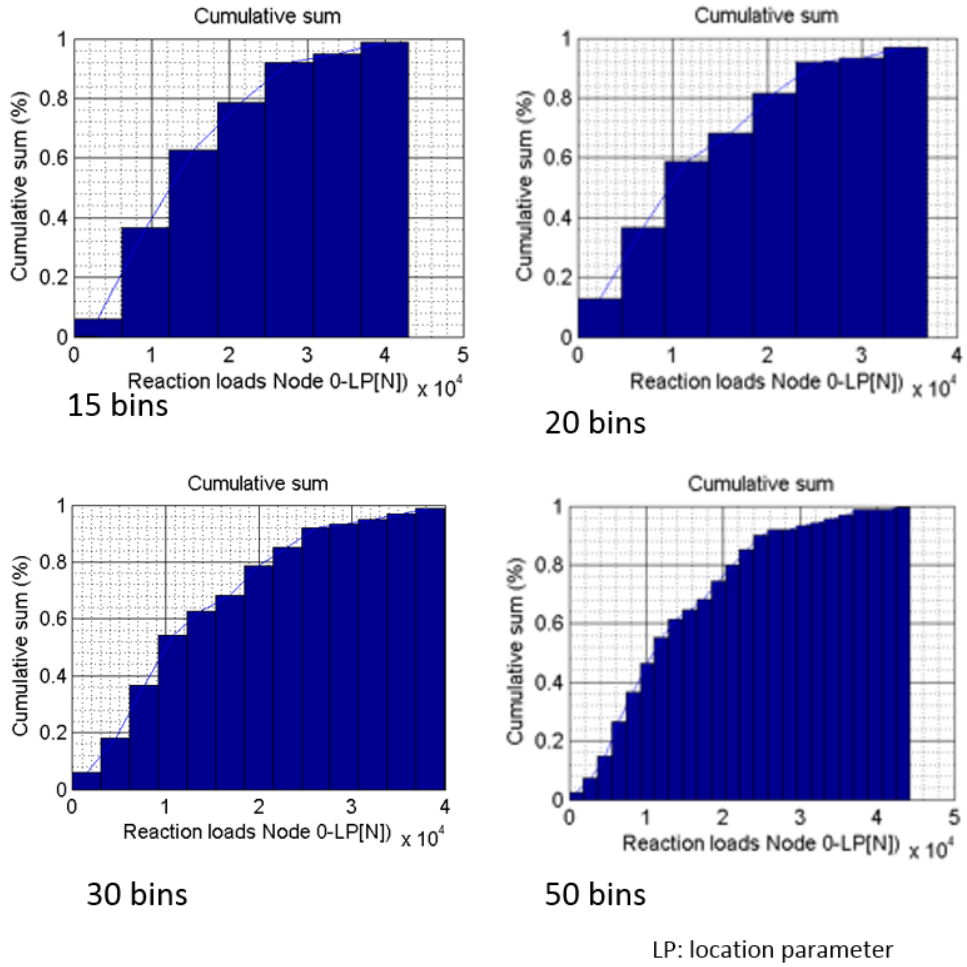

Figure 3-7: Weibull distribution.
3 different Weibull fit are show using different bin sizes.

The distributions were assessed in terms of fit quality. The fit quantity was defined as the norm of the error between the predicted values from the Weibull distribution and the tension database extracted from the simulations, normalized by the number of bins.

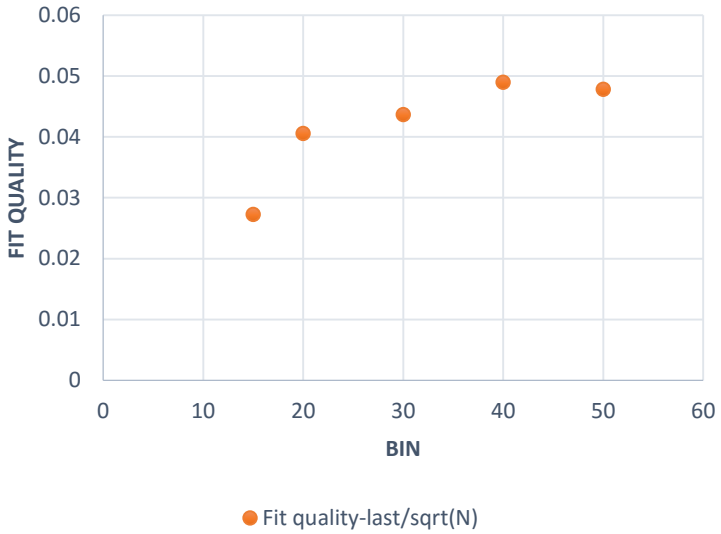

Figure 3-8: Bin size independence study
The quality of the fit is normalized from the square root of the number of data points.

Figure 3-8 shows the independence study used to define the minimum number of bins required for properly representing the Weibull distribution. A good trade-off between the division of the data and stability of the quality of the fit is desired. When the fit quality become stable the results of the Weibull distribution are not dependent any more of the division of the data. On the other hand it is desirable to minimize the number of bins that are being used, as a large number of bins could lead to empty bins that could damage the quality of the Weibull fit. Order to keep a good balance between these two parameters 20 bins will be used in the rest of the work presented.

3.2 Numerical Optimization

In this chapter, we present how a full hydrodynamic time domain simulation can be utilized within a Metamodel-Based Optimization to improve the design of the mooring system of a SRPA WEC. The section begins by introducing the objective function that will be used in the optimization routine. It continues by explaining the theory required to understand the Metamodel-Based Optimization.

3.2.1 OBJECTIVE FUNCTION

The objective function for the optimization routine is defined by the average power in operating conditions for the SRPA WEC. Since the SRPA WEC functional requirements react to the waves in order to extract power, the mooring system will have a dynamic response to waves which not only should be considered in the design of the mooring lines but also in the power production of the system[9]. Since the SRPA WEC and the mooring act as a coupled system, a time domain simulation is required to properly assess the average power. The following figure illustrates the how the objective function was obtained.

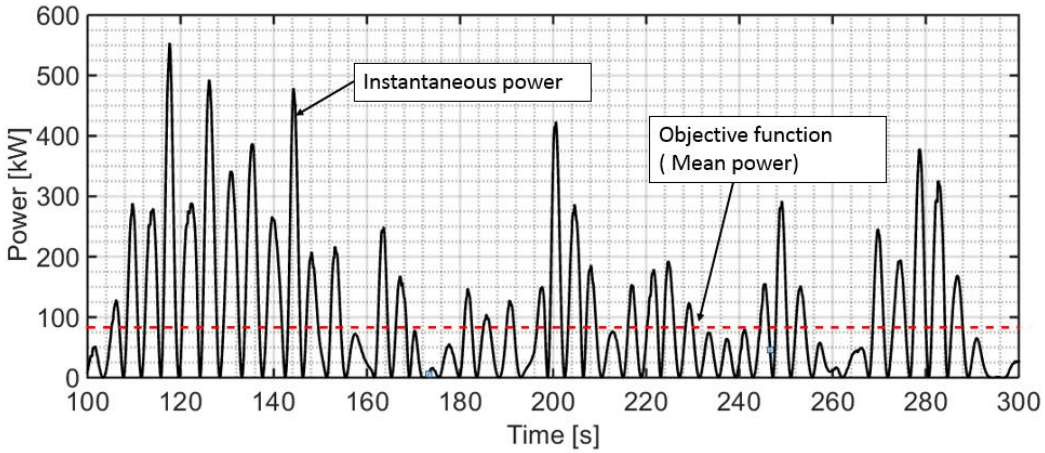

Figure 3-9: Objective function.
The instantaneus power and the objetive funtion
are show in this figure.

These simulations are very computationally expensive. It has been estimated a complete simulation takes around 72hr, which makes reliance solely on this kind of model infeasible. In order to mitigate the long run times required by the non-linear dynamics simulator, the WEC mooring DS is explored by using a Metamodel-Based Optimization routine.

3.2.2 METAMODEL-BASED OPTIMIZATION

An Metamodel-Based Optimization is a technique devised to study the DS associated with computationally-expensive objective function where a Meta-Model is constructed using specific points evaluated on the high fidelity simulators which are then fitted in a hypersurface. The Meta-Model can be used as the objective function to optimize the system with a lower computational cost, as the high fidelity model only needs to be evaluated a limited number of times [47].

As shown in Figure 3-10, the first step of the mooring optimization process consists of gaining knowledge of the objective function's shape across the DS by evaluating the objective function over a

sparse set of sampling points. The first sampling points are determined by applying a Design of Experiment strategy; then, using this initial population a Meta-Model is constructed that can then be used to estimate the objective function at any point in the DS. Using the Meta-Model the next points to be evaluated are selected considering their possible impact on the model. The idea is to pick the points with the highest information contribution to the Meta-Model, so they can be used to validate the model and improve its accuracy by incorporating them into the data pool and recalculating the Meta-Model coefficients. Finally, the collective set of generated observations are used to explore the DS and find the minimum of the objective function. If the termination criteria is met, the optimization is terminated. If it is not, the process is repeated, until one of the stopping criterion is met [48]. The Metamodel-Based Optimization was implemented using the Matlab toolbox MATSuMoTo [49].

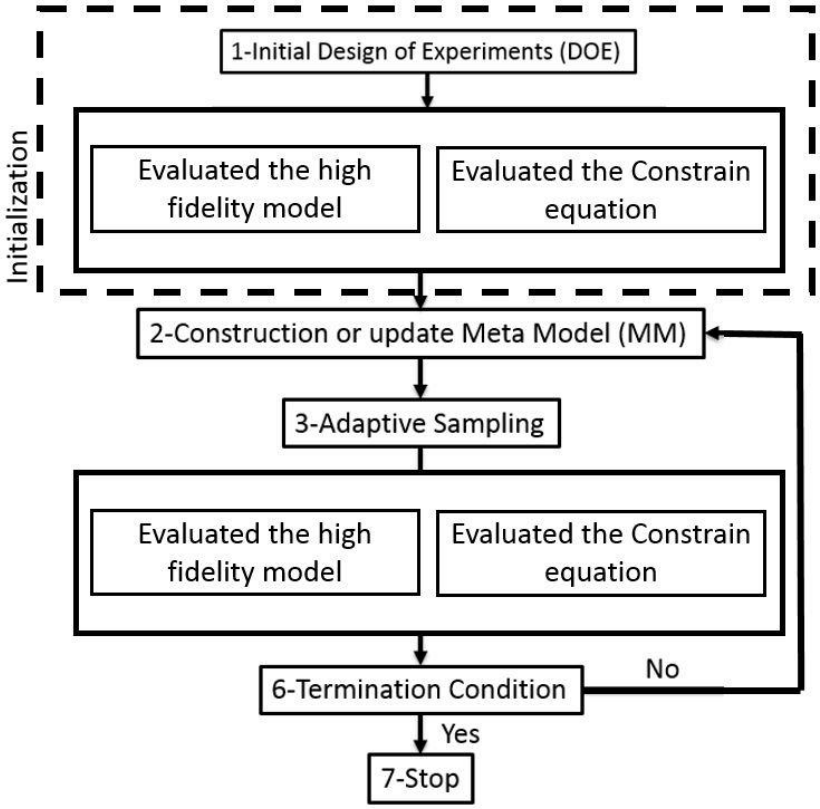

Figure 3-10: Metamodel optimization

If the problem needs to be constrained, the Meta-Model can be alternated by using the same approach. As will be explained at the end of this section, a penalty approach will be adopted in this study. In this approach, if any of the evaluated points violate any constraint, the objective function value used to construct the Meta-Model is altered by a penalty coefficient to impose the limit. Then the new Meta-Model is used in the optimization process.

Design of Experiments

At the beginning of the optimization process, a Design of Experiment is used to strategically select sample points in the DS. Several techniques have been developed for executing a Design of Experiment. These include Factorial Full, Factorial Central Composite, Latin Hypercube, etc. [47]. In this work, a Latin Hypercube is used. This method generates samples over the DS by dividing it into subspaces and then selecting plausible configurations on the multidimensional DS, in such a way that each sample point is the only one in each aligned hyper plane [47]. 48 points in the nine dimensional DS were used for the Design of Experiment – these spanned the intervals defined in § 3.1.2. Figure 3-11 shows the sampled points over the DS.

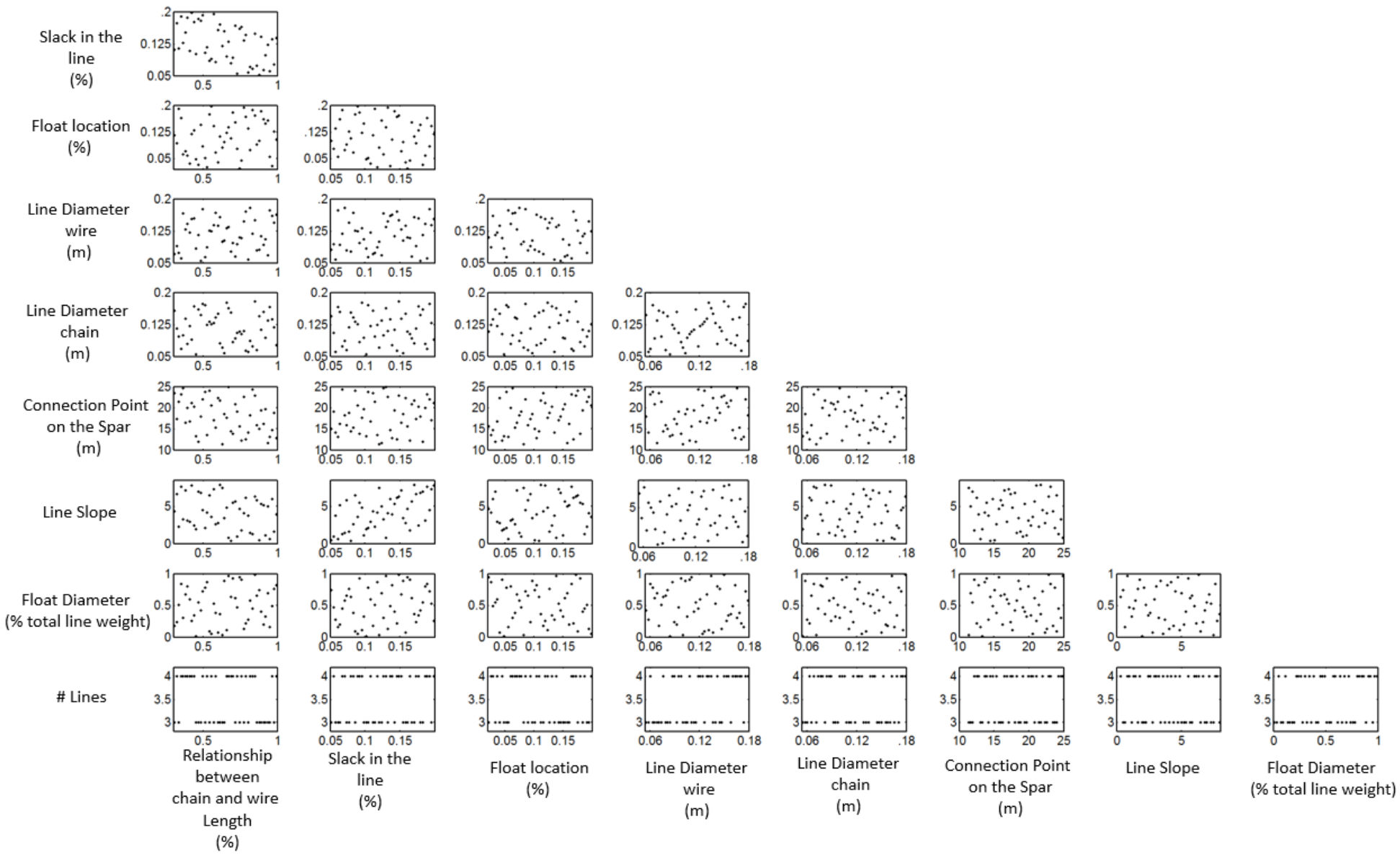

Figure 3-11: Selected Design of Experiment points

Each window represents a planar projection of the hyper dimensional design space. As only two values are possible for the parameter "# Lines", it is represented by two lines. The other parameters are considered continuous over the DS; therefore their distribution is broader.

Meta Model

Results gathered by the Design of Experiment are used to create a response surface (Meta-Model). An Meta-Model consists of a mathematical representation of a more complex system, where coefficients are fit in order to approximate the DS. Even though this model will not yield to the exact solution of the problem, it can be used to efficiently estimate the objective function and find the optimum design point. This makes it a powerful tool when the objective function must be calculated with a computationally expensive simulation. For this technique to work, the Meta-Model form needs to be selected carefully in order to accurately describe the DS. The large number of mathematical models that exist make this selection a challenging decision, as normally little information about the system is known before starting the optimization process. In this paper, a weighted combination approach is used, according to Mueller & Piche [50].The basic idea consists of using different Meta-Models that are added together using a weighted sum model. The predicted model $\hat{f}(x)$ of the mixed Meta-Model can be generalized as:

$$\hat{f}(x) = \sum_{i=1}^{N} w_i \hat{f}_i(x) \qquad \sum_{i=1}^{N} w_i = 1 \tag{0.18}$$

where x is a vector that contains the design parameters, $\hat{f}_i(x)$ represents the predicted value of each model, w_i the corresponding weight and N the number of models. The weights are calculated according to the Dempster-Shafer theory which allows the used of information from different sources, even when it seems contradictory, in order to build a degree of belief. The idea consists of combining the Meta-Models according to how well they describe the real DS, represented by the sample points. Each Meta-Model is evaluated according to its normalized correlation coefficients, root mean square errors , maximal absolute error and median absolute deviation (see Appendix 2 for details on normalization). A good DS representation has a high correlation coefficient and low root mean squared errors and median absolute deviation. Sometimes these coefficients can present contradictory information; Dempster-Shafer theory can be applied to find the probability for each representation and to assign a weight to each Meta-Model.

In this paper, a combination between a Kriging model and Multivariate Adaptive Regression Splines (MARS) is considered. Kriging is a regression Gaussian process which uses a weighted average of known values to predict a point in the same neighborhood. Mathematically, it is defined as:

$$\hat{f}(x) = f(x) + \mathrm{Z}(x) \tag{0.19}$$

where f(x) represents the global model and Z(x) the local deviation, defined as a stochastic process realization with mean zero and non-zero covariance. As the DS is globally approximated by f(x), Z(x) adds local deviations, in order to interpolate the sample points using a defined function to predict the correlation function for the stochastic processes. For this paper, first order polynomials were used to approximate the global space, and a spherical correlation function to interpolate the local deviations. This model was implemented using Matlab toolbox DACE [51].

The MARS algorithm considers a non-parametric weighted sum regression technique [52]:

$$\hat{f}(x) = \sum c_i B_i(x)$$
$$\hat{f}(x) = c_1 \max(0, x - a_1) + c_2 \max(0, x - a_2) + c_3 \max(0, x - a_3) \max(0, x - a_4) + \ldots \tag{0.20}$$

where c_i are constant coefficients related to the best fit of the data, $B_i(x)$ are the basic functions defined by combinations of the hinge equation, and a_i (referred to as “Knot”) are constants in the hinge equation. As part of the range of a hinge function is zero, it can be used to partition the data into disjointed regions, which can be treated independently.

The Meta-Model is built through a two phase iterative approach. The first step consists of building a model using a forward strategy, in which a new equation is added after each iteration, beginning with the intercept and then continuing with a pair of equations based on the hinge function. In each step, the required coefficients are fitted, by reducing the mean square error of the residuals. The process stops when the residual error is too small or when the number of iterations, defined by the user, is reached. In the second part of the process, terms are removed from the model, one by one, until the best representation is found. The performance of the different subsets of the model are compared using a cross validation scheme, where at least one of the training points is not included in the fitting process, so it can be used to calculate the error of the model.

Adaptive Sampling

In order to keep the evaluations of the high fidelity model to a minimum, it is important to define a strategy to select the candidate points that contribute the most information and lead to a converged

solution as quickly as possible. The strategy selection will be linked to the end purposes of the model: if only a local exploration is required, new samples should be selected so as to improve the accuracy of the overall model in the neighborhood of the optimum points predicted by the Meta-Model. On the other hand, if a complete DS exploration is required, the infill strategy should be such that general accuracy is enhanced by selecting the samples on the less explored areas [53]. A third strategy is to combine both approaches by increasing the resolution of the model near feasible points, but also exploring less populated areas that could lead to a better solution.

For this work, the algorithm considered is based on this idea [53]. It contemplates 4 different regions where candidate samples are picked. The first group of candidates is generated by keeping the discrete variables near the most feasible point constant and perturbing the continuous variables, by randomly adding and subtracting small, medium and large perturbations. The second group is prepared in the opposite way: the discrete variables are perturbed and the continuous variables are kept constant. The third group is generated by perturbing both the discrete and the continuous variables near the most feasible point, by randomly adding and subtracting small, medium and large perturbations. The last group is constructed by randomly sampling the DS in order to ensure that every point has a positive probability of being picked. From this pool of promising mooring configurations, the best candidates are then determined using two scoring criteria. The first criterion calculates the score using the objective function value predicted by the Meta-Model; the difference between the predicted mean global optima and the possible sample is calculated and normalized by the difference between the predicted maximum and minimum points.

$$V_R = \frac{\hat{f}(x_i) - \hat{f}(x_i)_{\min}}{\hat{f}(x_i)_{\max} - \hat{f}(x_i)_{\min}} \tag{0.21}$$

The second criterion is derived from the distance between the candidate point and the already sampled points. For each candidate, the Euclidean distance to the already evaluated points are calculated and the maximum and minimum distance for all the possible candidates are defined. Then the score is defined by the difference between the minimum distance calculated of a particular candidate and the maximum distance calculated for all possible candidates and normalized by the difference between the maximum and minimum differences for all possible candidates.

$$V_D(x_i) = \frac{\Delta_{max} - \Delta_{min}(x_i)}{\Delta_{max} - \Delta_{min}} \tag{0.22}$$

where Δ_{max} and Δ_{min} are the maximum and minimum distances for all possible candidates and $\Delta_{min}(x_i)$ is the minimum distance for a particular candidate.

Finally, a weighted sum is used to determine the final score for each candidate. In order to prevent instabilities in the model, the weights are adjusted in a cyclical manner, beginning with high weight for the distance score and low weight for the prediction score. In this way, the search at the beginning is more global than local. As the optimization process continues this relation changes in order to focus more on the located minimum. Then when a cycle has ended the roles are inverted for the process to begin again.

Constrained Optimization

When constraints are considered in an optimization problem the level of difficulty increases as new equation evaluations are required. In this way, whenever possible, the problem should be solved such that the constraint functions (CFs) are embedded in the objective function and not considered as independent considerations.

Two different constraints were applied to the optimization scheme. First, the DS was constrained by imposing hard limits for the design variables as shown in Table 3-1. Also, a penalty function approach was used to constrain the stress on the mooring lines, which was evaluated using 2 time domain simulations as explained in section 3.1.4.

This approach works by applying a penalty to the objective function whenever it breaks one or more constraints. The penalty function can take different forms depending on the complexity of the constraints that is going to be applied. One of the simplest approaches is called “one pass extreme function”. This method adds a large constant (P) to the objective function value of a design candidate if the constraint is violated.

For this, the CF is evaluated for each of the points as shown in Figure 3-10, by considering the limit state defined in § 3.1.4. In this thesis the stress is limited by as Safety Factor (SF) of 2.5 which was defined according to [9] as the ration between the maximum tension and the allowable stress on the line. The CF is implemented as:

:

$$f(x) = \begin{cases} if \\ CF \geq S.F \Rightarrow f_p(x) = f(x) + P \\ else \\ f_p(x) = f(x) \end{cases} \quad (0.23)$$

where S.F is the safety factor, f'(x) the unalternated objective function value and f(x) the modified value for objective function. The penalty coefficients P is calculated as

$$P = 40000 \quad (0.24)$$

This approach is very simple to implement but as the shape of the Meta-Model is deliberately changed the optimization process can fail at locating minimums close to the limits, as the slope in this area has changed (infinite) and the function becomes discontinuous.

.

Termination Condition

As explained by Muller et al.[50], the algorithm is asymptotically complete, which means that if it is run long enough, it will converge to a global minimum; for practical reasons, the termination condition was defined by maximum number of allowed iterations. A limit of 40 samples on each adaptive sampling stage was imposed and an overall limit of 200 simulations in total was set. Considering an approximate simulation time of 72 hours, the total maximum simulation time was approximately 15 days if it is run in parallel in 40 processors.

Chapter 4

Results

The optimization scheme described in §3.2 was executed to determine a recommended mooring line configuration for the SRPA that will be described in §4.1 3.1 . As described in section 3.1.2, the objective function was the average power extracted by the SRPA over 300 s of operation in the energy weighted average sea-state at Amphitrite Bank off the coast of Ucluelet at Vancouver Island BC, Canada. While the operational performance is the primary factor in the objective function, survivability was implemented as a constraint on the design space. The tensions in the lines were constrained by considering the ULS as described in §3.1.4.

In this chapter, the population of 200 design candidates considered by the optimization are compared on the basis of performance (what was the average power produced by the different candidates) and survivability (how many candidates in the population met the survivability, or safety factor, constraint). In addition, four of the design candidates generated in the Metamodel-Based Optimization execution are examined in greater detail. These are:

- NM: No Mooring configuration; used as baseline for the analysis. NM is defined as the configuration where the SRPA WEC is floating freely but still extracts power. The PTO for a SRPA WEC relies on the relative movement between bodies and not directly on the reaction with the mooring lines, so this configuration implies the WEC drifts freely but still extracts power.

- OC: the Optimum mooring Configuration found through the Metamodel-Based Optimization execution. The OC improves on the power extraction of the baseline NM SRPA by 15% in the specific environmental condition considered in the optimization and demonstrates a safety factor of 8.4 – well above the threshold of 2.5.

- H3: the configurations that extract more energy with three lines. H3 improves on the power extraction of the baseline NM SRPA by 10% in the specific environmental condition; but when it is compared with the OC it extracts 7% less energy. It demonstrates a safety factor of 5.9 – well above the threshold of 2.5. This configuration is not the final result of the Metamodel-Based Optimization but a sample that was picked from the configurations that were assessed on the adaptive samples phase.

- L4: Is the four line mooring line configuration that extracted around 7.6% less energy when compared with the NM configuration and around 24% when compared with the OC configuration. This is the configuration that extracted less energy in the complete DS. As with H3, this configuration is not the final result of the Metamodel-Based Optimization but a sample that was picked from assessed configurations.

- L3: Is the three line mooring line configuration that extracted around 5.5% less energy when compared with the NM configuration and around 19% when compared with the OC configuration. As with H3 and L4, this configuration is not the final result of the Metamodel-Based Optimization but a sample that was picked from the assessed configurations.

This Chapter is organized as follows: Section 4.1 provides an overview of the population of design candidates from the perspective of performance – how the candidates converted energy from the wave spectrum considered in the optimization study. Section 4.2 illustrates progress made by the optimization algorithm in adjusting the designs to adhere to the safety factor constraints. Section 4.3 presents contour plots extracted from the hyper-dimensional design space that illustrates where the OC design sits in the design space and the sensitivity of the objective function to changes in the design variables in the region surrounding the OC location. Section 4.4 shows the differences in the power conversion time series for the 5 particular cases mentioned above, and also provides Sankey diagrams that illustrate how the different moorings create changes in the energy flow from the waves into the viscous power-take-off.

4.1 Optimization Results – Energy Conversion

To find the optimization configuration the algorithm was allowed to iterate until the full 200 Proteus simulation limit was reached. This process was executed in different data sets evaluations. First, to assess the DS a Design of Experiment was executed using 40 different cases. The Design of Experiment objective is to define a broad range of candidates in order to give a good enough representation of DS to begin the optimization. Then, for the adaptive sample phase, 5 different data sets were evaluated. The sample evaluations of the data set was limited to 40 for each iteration and each sample was selected from a pool of 500 possible candidates that were generated and evaluated using the Meta-Model. They are picked according to the scoring system presented in §3.2.2 . In this section, the discussion is centered on the 200 ProteusDS simulation runs.

In Figure 4-1 below, the mean extracted power for the design candidates has been plotted in an ordered stack – the curve is constantly increasing left to right. The horizontal axis has been normalized against the total number of design candidates considered (the horizontal axis ranges from 0% to 100%). The different populations of design candidates generated in each of the 5 iterations of the adaptive sampling phase are individually marked to illustrate how the evolution of the optimization process correlated with SRPA performance improvements.

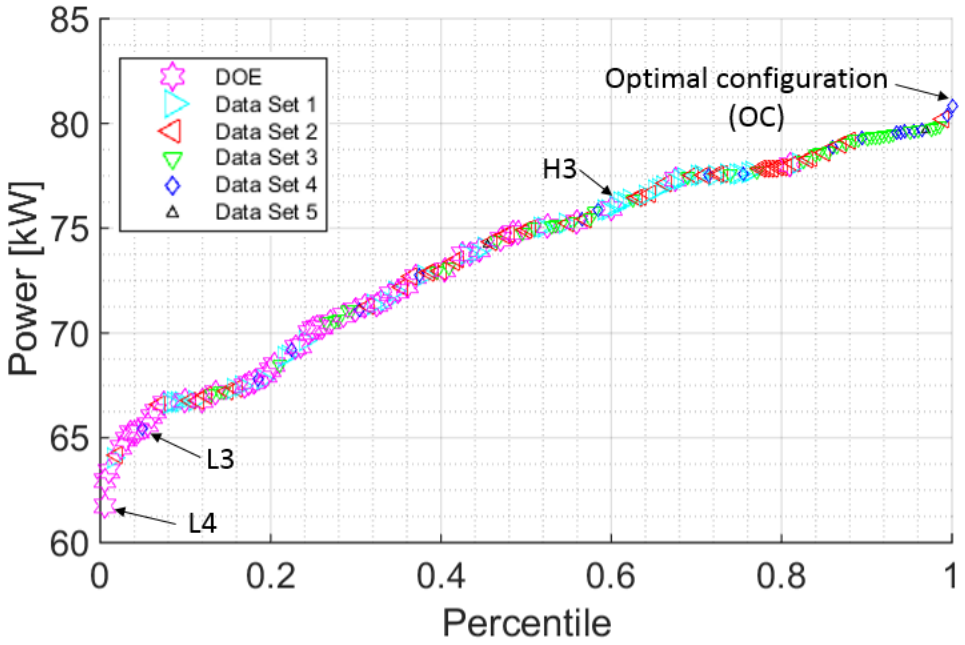

Figure 4-1: Power [kW] vs Population Percentile
This figure shows 4 specific mooring configurations that are going to be considered in this chapter: L3, L4, H3 and OC

Figure 4-1 shows that the design candidates generated in the Design of Experiment stage, the first step of the Metamodel-Based Optimization, works well for covering the DS, as the Design of Experiment generated candidates spanned performances between 62 kW and 77 kW which is a majority of the performance range uncovered by the complete Metamodel-Based Optimization execution. However, several more adaptive sampling iterations were required to locate the OC. Figure 4-1 also shows how the adaptive sampling stages approached to optimum configuration while still continuing to explore other locations of DS to assure that the global maximum was found. The evidence of these competing mandates of the Metamodel-Based Optimization is seen in Figure 4-1, it shows that when the algorithm was approaching the optimal, samples were still been generated at low energy locations to ensure that the complete DS had been covered. In the fourth data set evaluation, the optimal configuration (OC) was found, and the physical parameters (or design variables) for the OC are summarized in Table 4-1. That the fifth adaptive sampling stage could not produce any candidates with further performance improvement indicates that the 200 simulation limit was adequate – there is no evidence that further progress could be made.

By using the assessed points, the design candidates that extract the least energy for the design condition was used for the analysis (shown in orange in Table 4-1 and referred to hereafter as candidate *L4*). Both of configurations *OC* and *L4* are four line configurations; the best and worst of the three line design candidates in the full population were also identified for comparison studies. These will be referred as *H3* (best 3 line candidate) and *L3* (worst three line candidate), respectively. Finally, the power extracted by the device without moorings was also computed and presented in Table 4-1.

Table 4-1: Optimization results

	# of lines	% weight float	Slope	Connection height location (m)	Chain diameter (m)	Wire diameter (m)	Float location	Slack of line (%)	Relationship between chain and wire length
OC	4	0.21	6.08	12.52	0.08	0.18	0.20	0.14	0.77
L4		0.99	6.30	22.84	0.18	0.15	0.17	0.15	0.85
H3	3	0.21	6.08	12.45	0.08	0.18	0.20	0.14	0.81
L3		0.95	4.69	15.65	0.11	0.11	0.02	0.16	0.74
NM	-	-	-	-	-	-	-	-	-

	Mean Power (kW)	Mean Power (Normalized by the best configuration	Number of examples *
OC	80.82	1.00	152
L4	61.68	0.76	
H3	76.30	0.94	48
L3	65.31	0.81	
NM	68.94	0.85	-

*Number of examples refres to the number of simulation that where done using a particular number of lines.

As shown, the difference in performance between the *OC* configuration and *L4* is around 24% for the design condition, which points to the importance of selecting the right design variables for the design of the lines. In Chapter 5, it will be shown that this affirmation holds for other sea states and in general for the overall power production.

4.2 Optimization Results - Survivability

The following figure presents a scatter diagram with all the evaluated mooring design candidates. The allowable safety factor is shown as a dashed red line. It can be seen that the majority of the evaluated points are above the safety factor. This is due to how the tension constraint was applied to the model, by changing the objective function and directing the optimization algorithm far from unsuitable points.

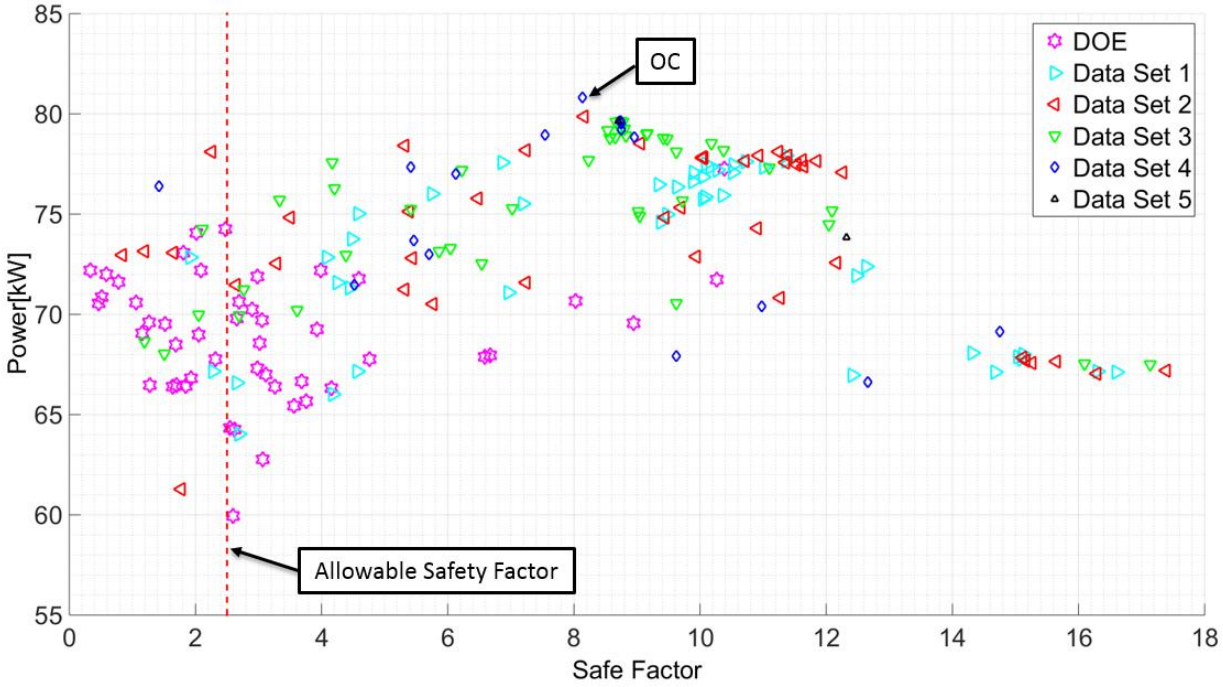

Figure 4-2: Power vs. Safety factor [W].
The figure shows that the automated search is key to establishing a "safe" design, since in the points of the first stages are close to the allowable safety factor, but when the optimization algorim approaches to the optimal configuration the selected points are farther from the allowable safety factor.

Figure 4-7 shows that the optimization algorithm is driven by the power and not by the tension constraint. As it can be seen, near the allowable safety factor, the average power seems to be less compared to the design candidates near the optimal point, where the tension loads are far from the limit. This suggests further opportunities for design improvement, as it appears the weight properties of the lines is more important than their strength, suggesting lower cost and strength but higher weight lines could be employed.

As it will show in the next section, for the mooring lines to have a positive impact in the system, they should reduce the leak of energy on unwanted degrees of freedom. This makes the device move less and in consequence reduces the peak loads in the line.

4.3 Contour Plots

In order to continue the analysis of the influence of the design variables on the power production, a contour plot for each of the L3, H3, L4, and OC design candidates is presented. The contour plots show the normalized average power that was calculated using the final MetaModel, against two of the optimization design variables. The power is normalized by the maximum average power found. Each

subplot is built by keeping six of the eight design variables constant and equal to the optimum value, while the other two design variables were varied through the entire DS. The two design variables that were varied correspond to the labels provided to the left and beneath each figure. For example, in the top left plot of Figure 4-3, the % of slack in each mooring line, and the ratio of chain and wire lengths in each line were the properties varied. In each of the subplots of Figure 4-3 to Figure 4-6, the number of mooring lines is constant as only two options (three lines or four lines) were considered in the optimization routine. The number of lines considered in each figure is defined in the figure captions.

From Figure 4-3 to Figure 4-6 it is important to understand the coupled behavior of the WEC and the mooring system, as the relationship between design variables can be inferred by understanding each subplot. It is required to study these figures as a whole to have a better understanding of the complete DS. For example, on the cross-sections of Figure 4-3 and Figure 4-6 it can be seen that the candidates are at or near a local optimum in the section cuts. Even though this is not a complete picture of how the objective function is changing, since variables are being held constant in each section cut, this is a positive indication that there was no further improvement to find. In the same way, in Figure 4-4 it can be seen that in the vicinity of the L4 candidate, the objective function is close to a local minimum. In Figure 4-6, the L3 device isn't located at a local minimum, indicating that the device is an intermediate result that the optimization traversed on its way to OC.

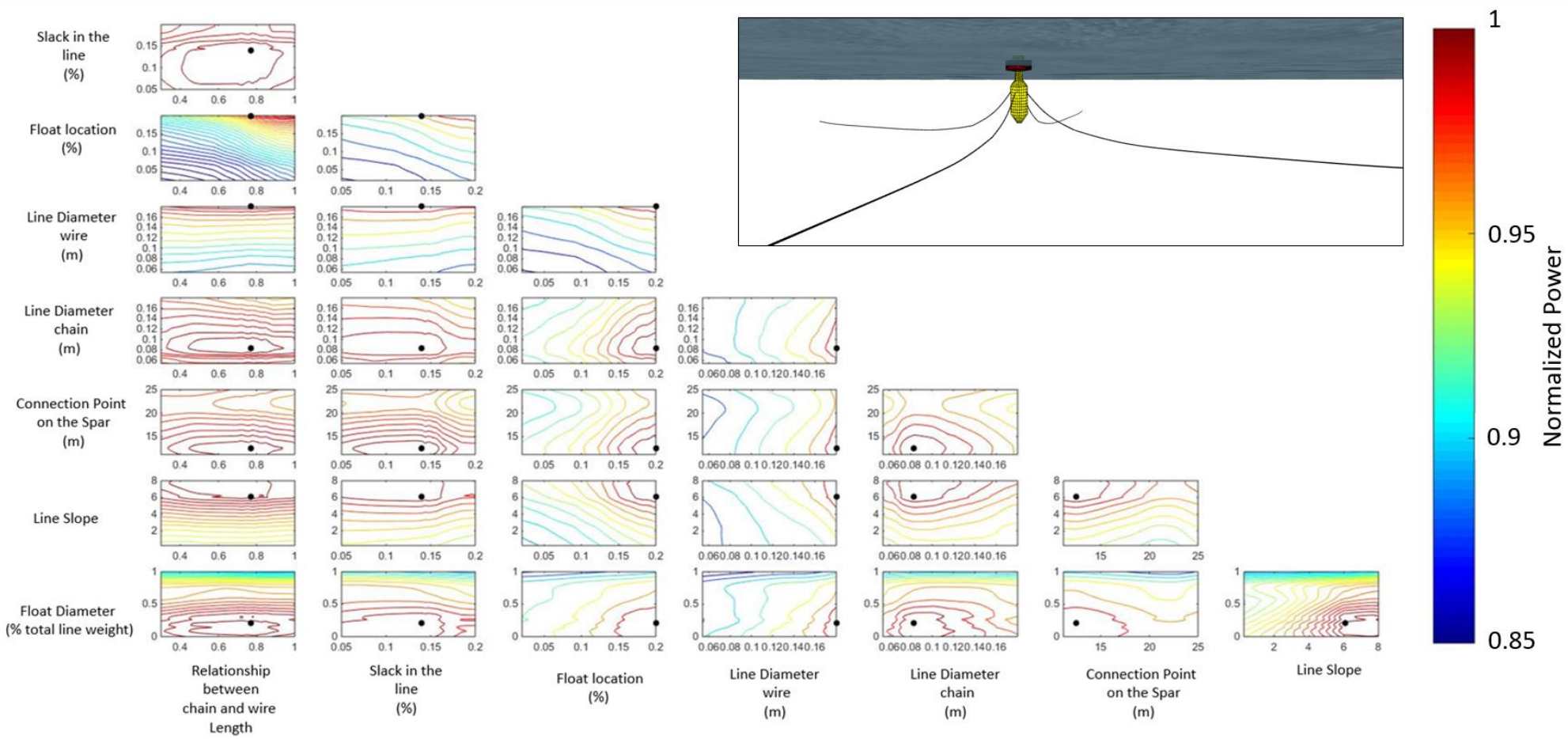

Figure 4-3: Contour plots OC

These plot was constructed by consider a 4 mooring line configuration.
The OC configuration is represented by a black dot.

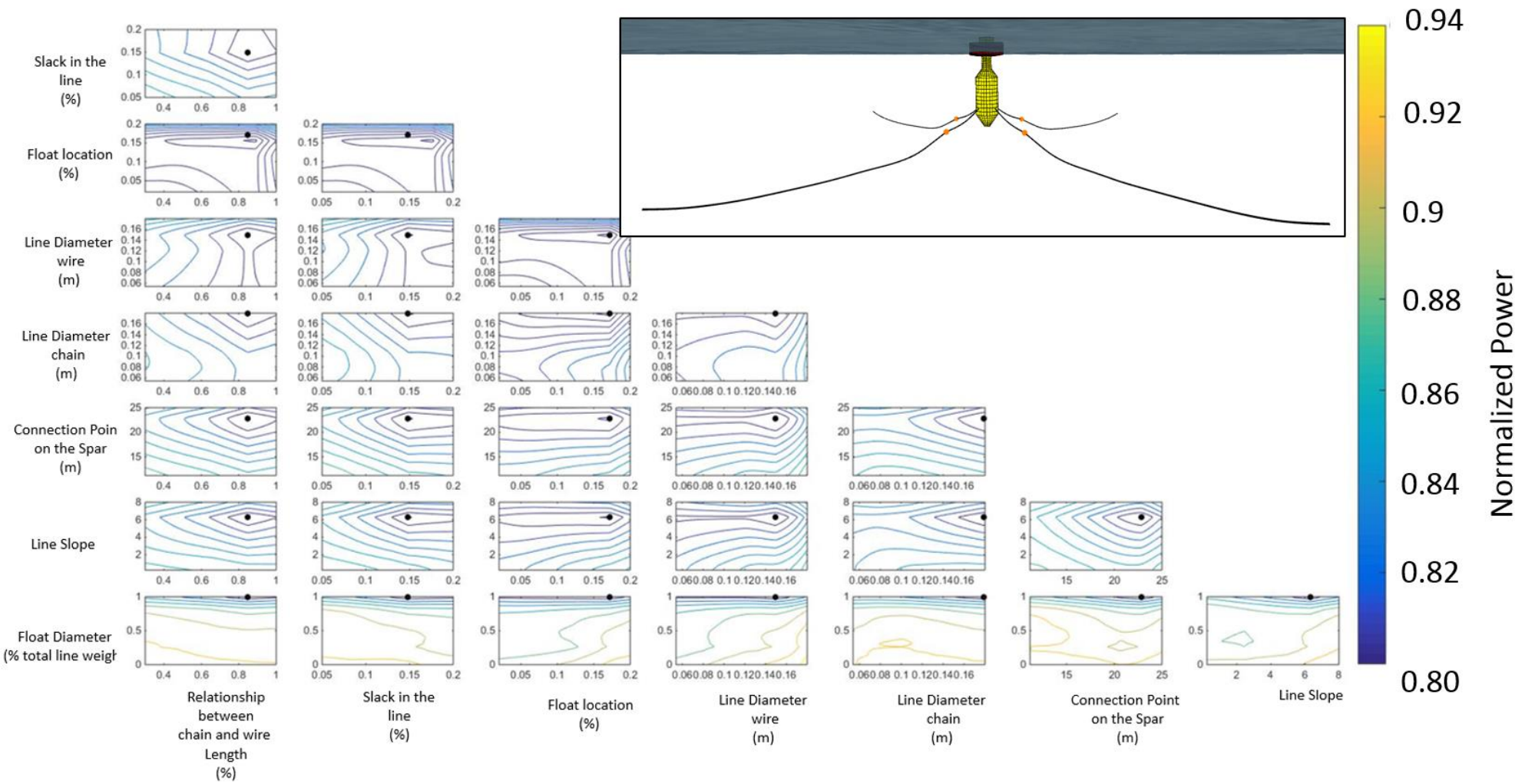

Figure 4-4: Contour plots L4

These plot was constructed by considering a 4 mooring lines configuration.
The configuration is represented by a black dot.

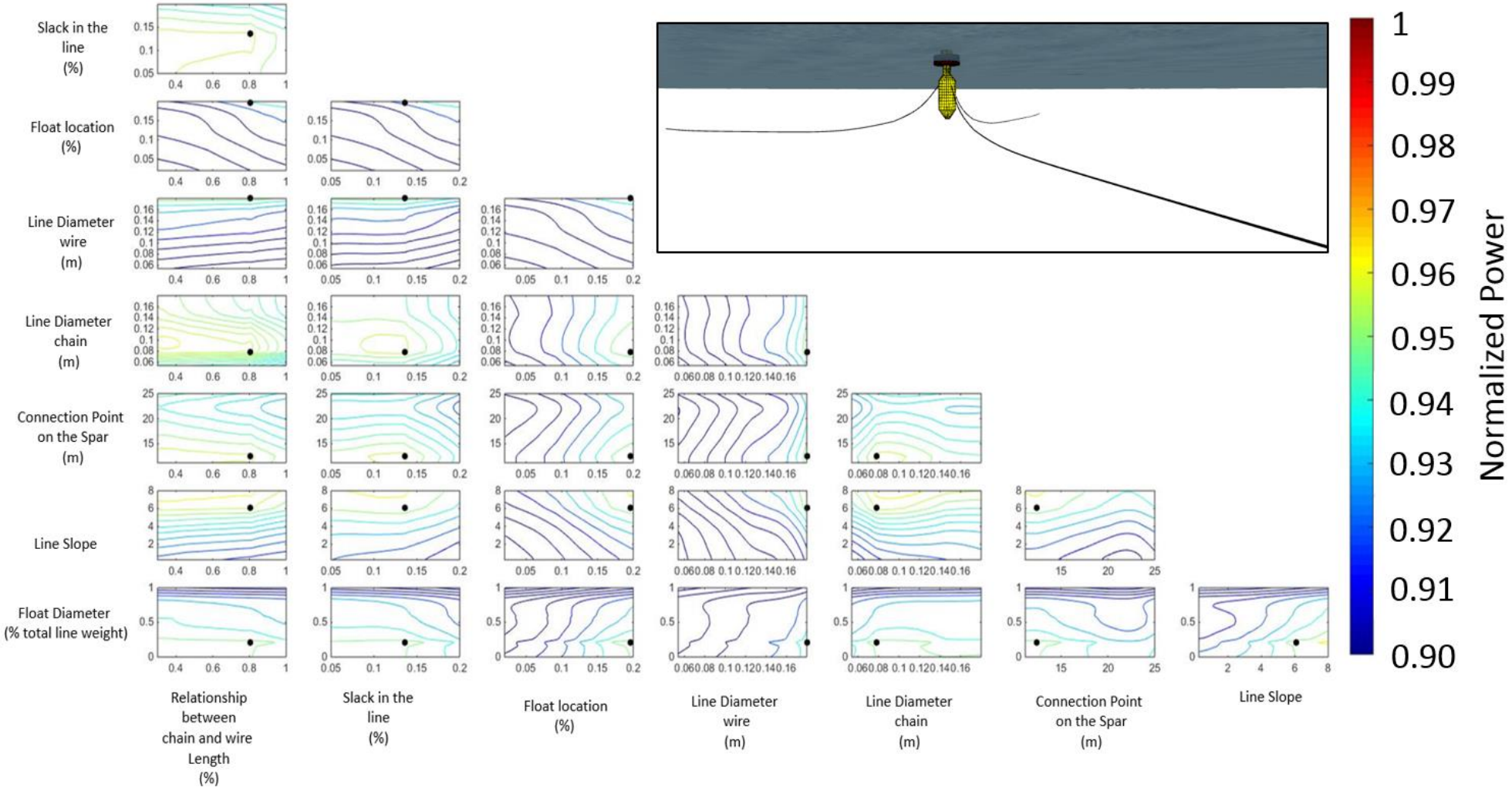

Figure 4-5: Contour plots H3

These plot was constructed by considering a 3 mooring lines configuration.
The configuration is represented by a black dot.

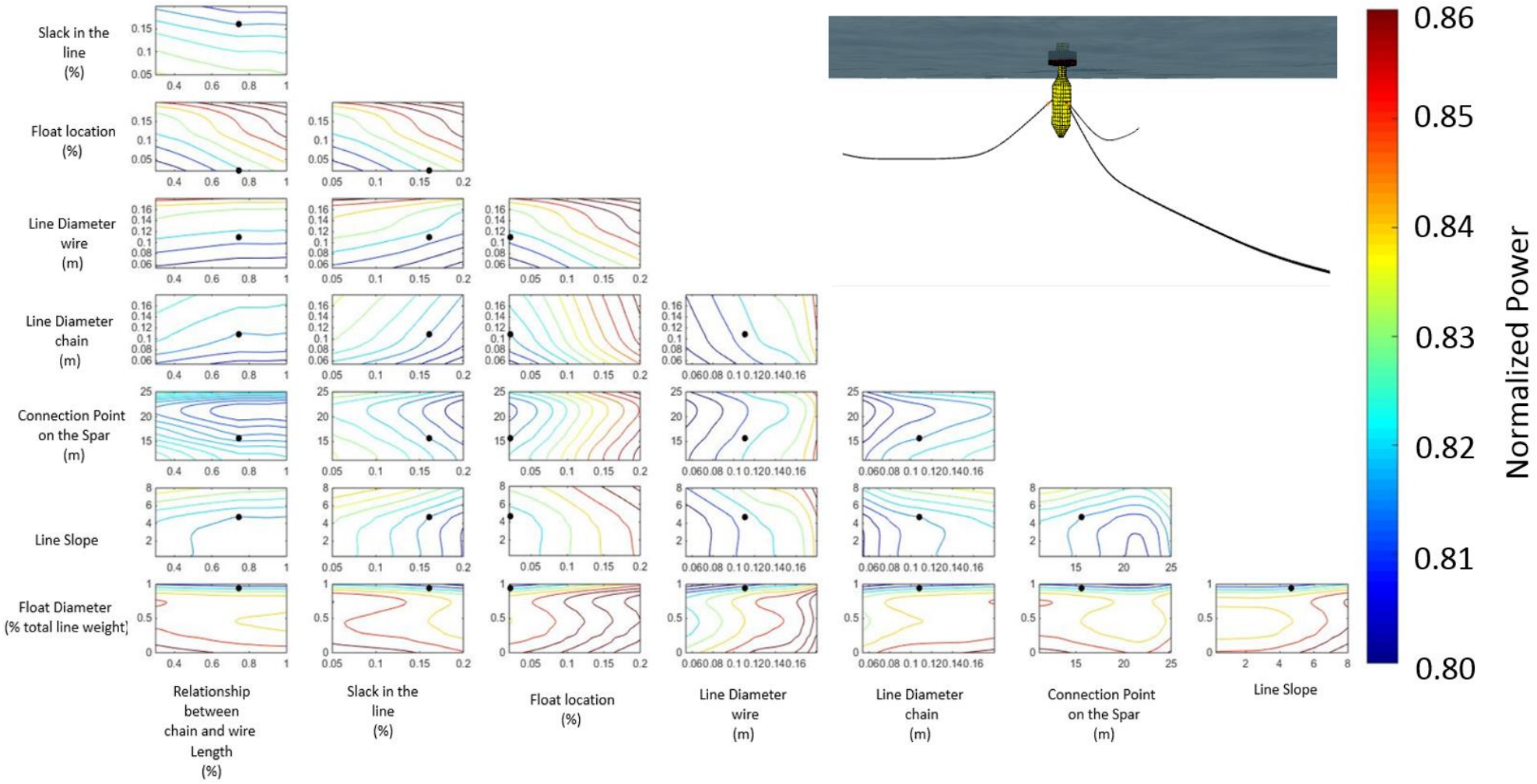

Figure 4-6: Contour plots L3

These plot was constructed by considering a 3 mooring lines configuration.
The configuration is represented by a black dot.

Figure 4-7 illustrates the effects of the tension in the lines and the imposed constrains, due to the limit state described in § 3.1.4. Figure 4-7 represents the safety factor of the mooring lines in an extreme sea state with a return period of 50 years. The figure's construction used the same approach as in the previous figures regarding the extracted power; i.e. the contour plots show the safety factor of the mooring lines over variations in two of the optimization design variables using the optimal configuration.

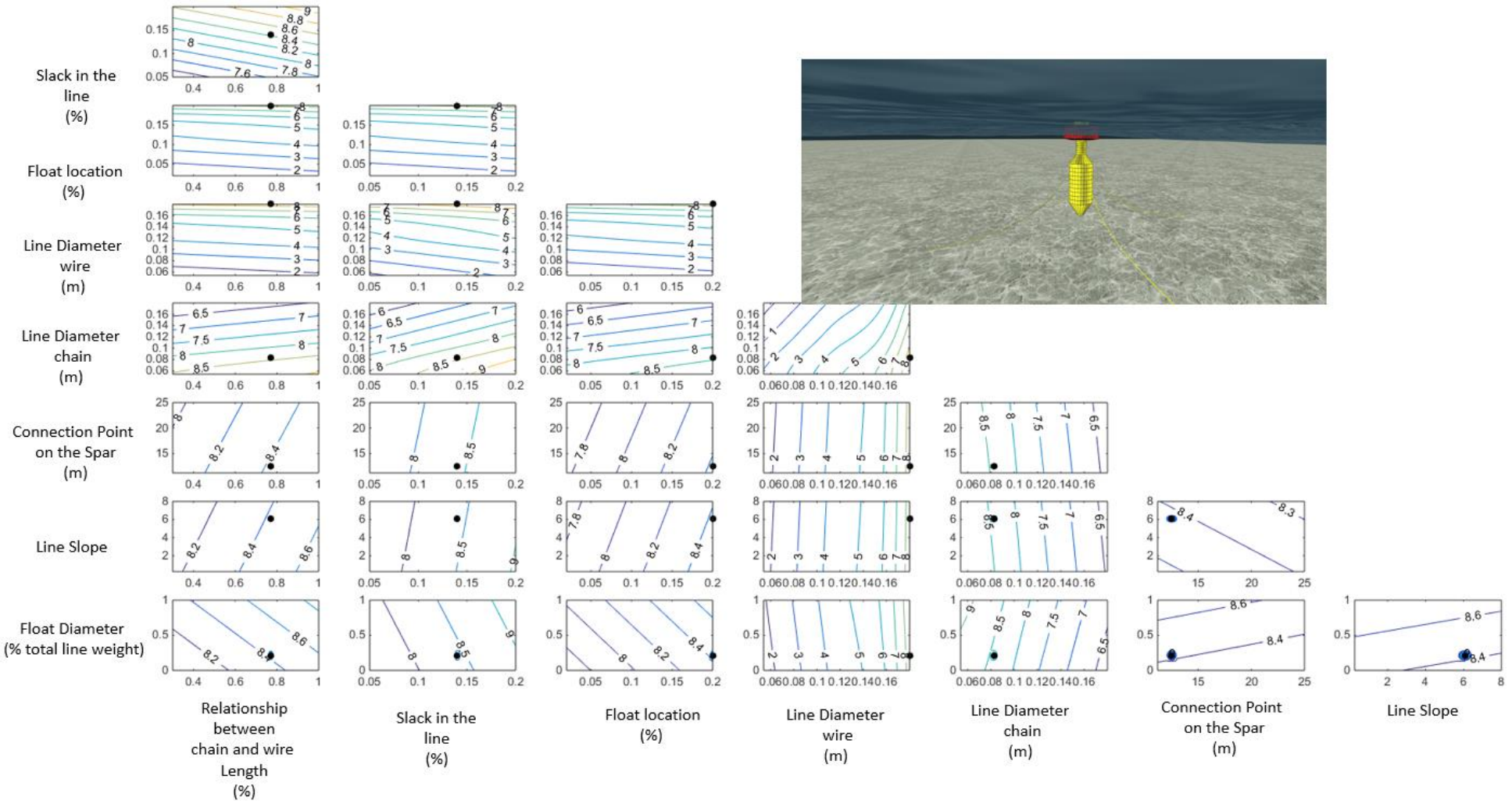

Figure 4-7: Safety factor.
The optimal configutation shown as a black dot.

4.3.1 MOORING SYSTEM GEOMETRY

In this section, the optimal geometry for the mooring system is studied by analyzing the optimization design variables. As was shown before, the optimal configuration found consists of four mooring lines. By studying Table 4-1, it can be seen that some of the design variables for both configurations are very similar with the exception of the *Relationship between chain and wire length* and the *Connection height location*, all the other design variables are the same. These three design variables are related to the dynamics of the system; the *Relationship between chain and wire length* controls the distribution of the weight on the lines, while the *Connection height location* affects the center of rotation of the system and the number of lines how the loads are transmitted to the body from the mooring lines. Even though the difference between the normalized power between these two configurations is only 6% , the improvement in the power on the OC configuration could be caused by a changed in how the SRPA reacts to the incoming waves and as will be explained in 4.4 a change in the energy entering the system

The other important parameter for defining the mooring system geometry is the *Line Slope*. The optimization results of the *Line Slope* parameter seem to be contradictory, as the *L4* and OC configurations have similar values: 6.08 and 6.30, respectively. This can be explained by acknowledging that each of the configurations is a point in the multidimensional space, and each parameter needs to be understood as dependent to the other design variables. The DS cannot be understood by observing only a three dimensional space, as shown in each of the contour windows, even though the contour subplots are a powerful tool for inferring tendencies. For example, the *Line Slope* parameter seems to have a big rate of change, as all the different relationships shown in the different windows have large slopes. This can be interpreted as this parameter having an important impact on the power production, so it should be selected carefully in the design phase.

By studying the third row of contours plots, *connection point to the spar*, it can be observed that the device has a better performance when the moorings are connected near the top of the device, 12.52 m below the water line. This SRPA is particularly sensitive to this parameter, as small changes in the connection height have a large influence on the power captured. This could be due to a change in the momentum of the device, depending on where the mooring is connected, as this can prevent the device from rolling and pitching, which adversely affect its performance. This idea will be studied in more depth in §5.2 . The relationships between the *connection point to the spar* and *float location, wire diameter* and *chain diameter* present the sharpest gradients in the OF, as it can be seen in the contour plots. This should

be taken into account in the design of the mooring system of a SPRA WEC. Also, the *float location* and the *wire diameter* for the optimized configuration matches the upper limit of the design space, which may indicate that the design can be improved by increasing the design space limits.

4.3.2 LINE CONSTRUCTION

In this section, the results of the optimization algorithm related to the line construction are presented. The mooring lines considered in this analysis consist of two sections. The top section is made of a spiral strand steel wire, as it has a good resistance to tension loads and fatigue. The bottom part, in contact with the sea floor, is made up of chain, which has a better resistance to abrasion. By studying the contours subplot that shows the relation between *chain and wire diameter*, it can be appreciated that for this particular sea state, the WEC has better performance with thick lines in the wire section, which are limited by the predefined design space, as the optimized result matches the upper limit diameter (180 mm). The chain section thickness does not seem to be limited by the DS bounds, as the optimizing algorithm defined a diameter of 80 mm. This indicates that the weight distribution of the line plays an important role in the power extraction. This result is reflected in the relationship between the line diameters and the *Relation between chain and wire length, the line slope* and *slack in the line,* design variables that are related to the length of the line and, therefore, its weight. For example, if the *Relation between chain and wire Length* is compared to the *wire diameter*, it can be seen that, for a constant *Relation between chain and wire length,* the power extraction results drastically change as the wire diameter is changed (see Figure 4-3). Similar findings occur when the *slack* is compared with the *wire diameter*. According to Figure 4-3, if the *slack* is kept constant and the *wire diameter* is varied, the power extraction increases as the diameter increases. The same behavior is seen for the relation between the *line slope* and *wire diameter* and the *connection location* and the *wire diameter*. These design variables also play an important role in the weight distribution of the line.

On the other hand, the relation between the *Relation between chain and wire length* against the *chain diameter* is optimal near the center of the subplot, without reaching the defined limits. It can also be observed that the power increases along both axes which could indicate that both design variables have similar importance. This same behavior is also present in the relation between *slack* in the line and *chain diameter, line slope* with the *chain diameter* and the *connection location* with the *chain diameter*.

The other important component of the mooring line design is the line float. According to Table 4-1, the lines' float volume, which is defined by the percentage of the weight of the line that the float is required

to lift, is optimal at 21%, for both the four and three mooring line configurations. The similarity between the results suggests that the line float has an important role in the power production and needs to be dimensioned carefully. When comparing the first row of Figure 4-3 to Figure 4-6 it seems that a big float has a negative impact on the power extraction, while a small float can be beneficial.

4.4 POWER EXTRACTION

For a better of understanding of the effects of the mooring system on the power extraction, a comparative study was completed considering the OC, NM and L4 cases defined in § 4.1 . In this way, the instantaneous relative position, velocity, and PTO force were plotted in Figure 4-8 for part of the time series to study how the power conversion rates reported in Table 4-1 manifest in the time domain.

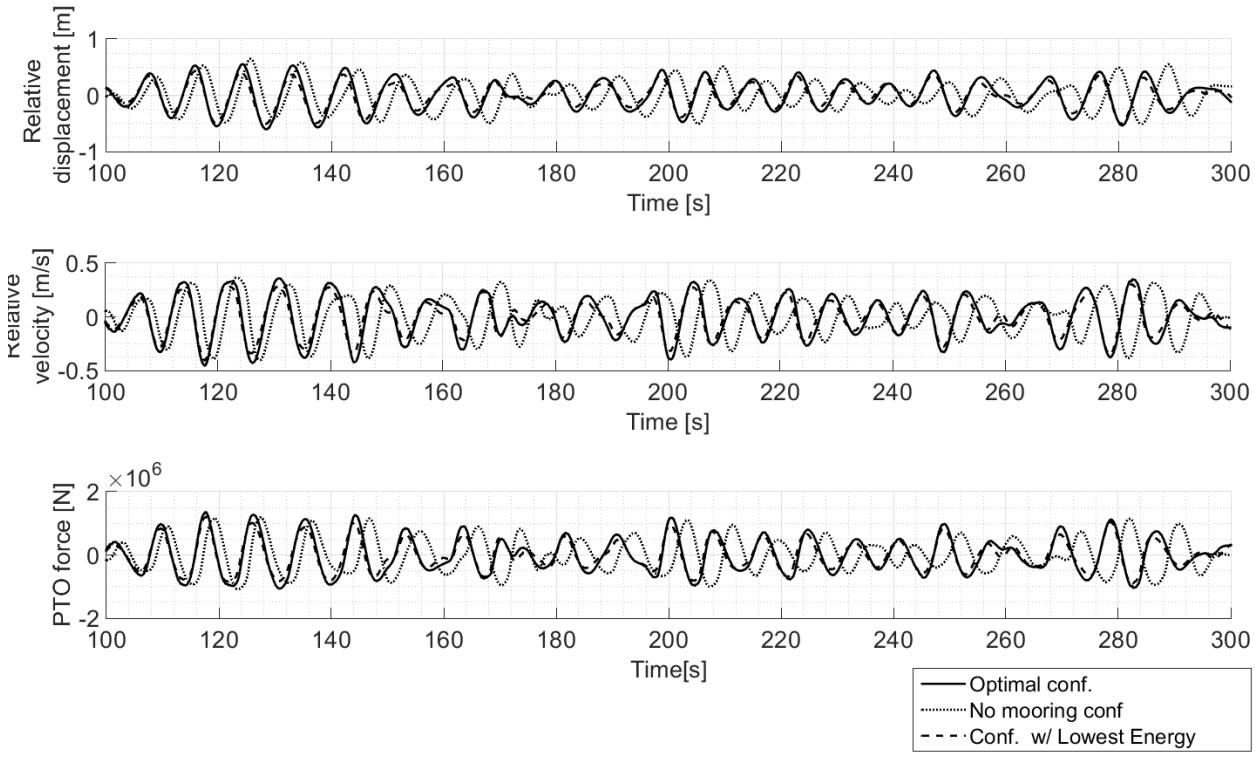

Figure 4-8: Relative displacement, velocity and PTO force.

As expected, there are notable differences in the behaviour of the OC and L4 configurations compared to the NM, but not so much between OC and L4. In this way, understanding the differences in power absorption between the two candidates (L4 and OC) is important to examine them on the basis of accumulated energy conversion.

The following figures present the energy balance for the three configurations. It was calculated by integrating the power over time for all the forces that act on the WEC. The power is calculated by multiplying the reaction forces by the relative velocity between the body and the element with the body it reacts (e.g. the mooring lines, water). The results are presented in two figures for each of the studied configurations; the cumulative power is plotted over time to show the interaction between sources and sinks of energy, and a Sankey diagram is used to quantify the impact of each forces.

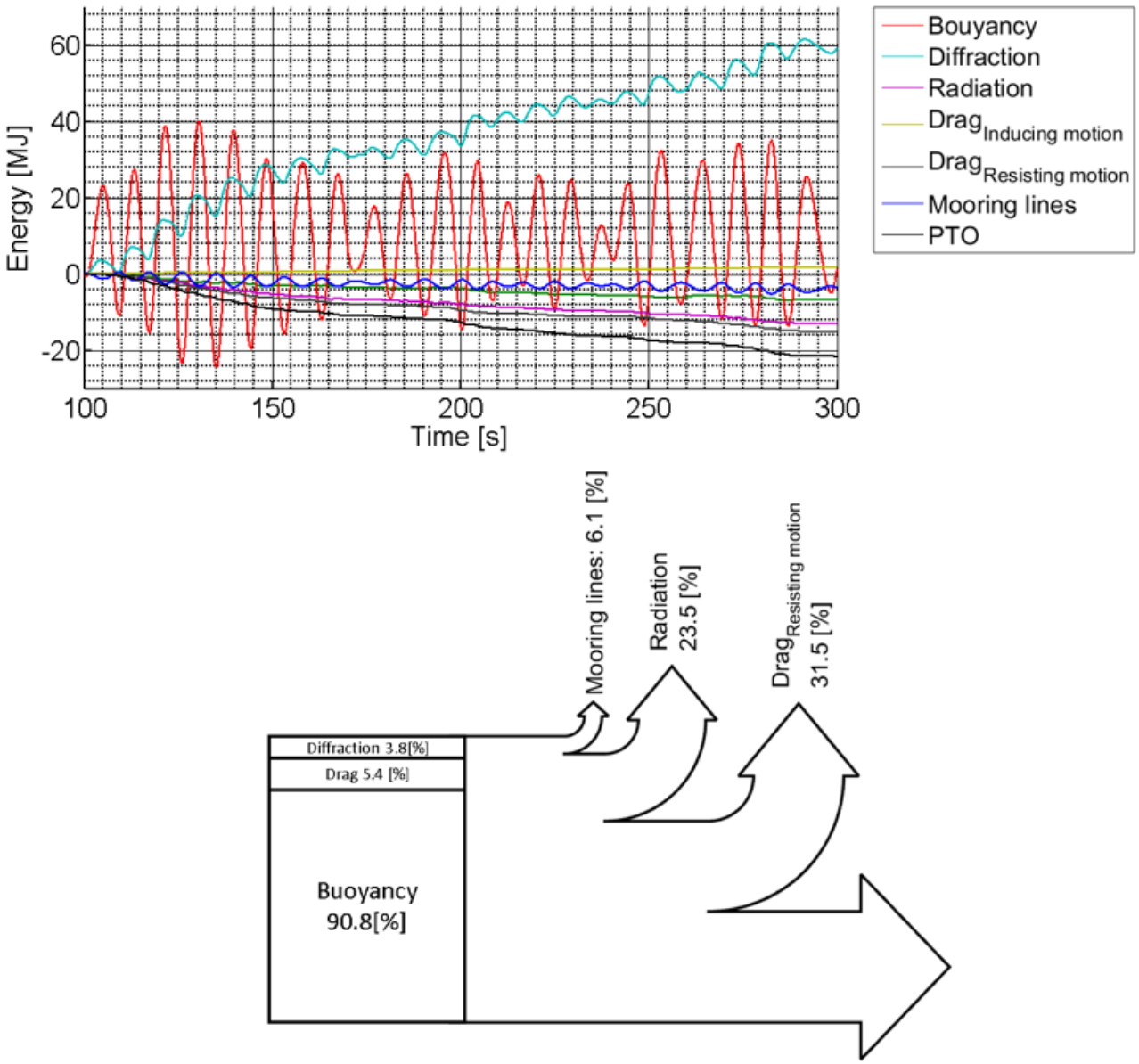

Figure 4-9: Energy vs time/ Sankey diagram OC configuration.

The Sankey diagram was constructed using 1100 sec.

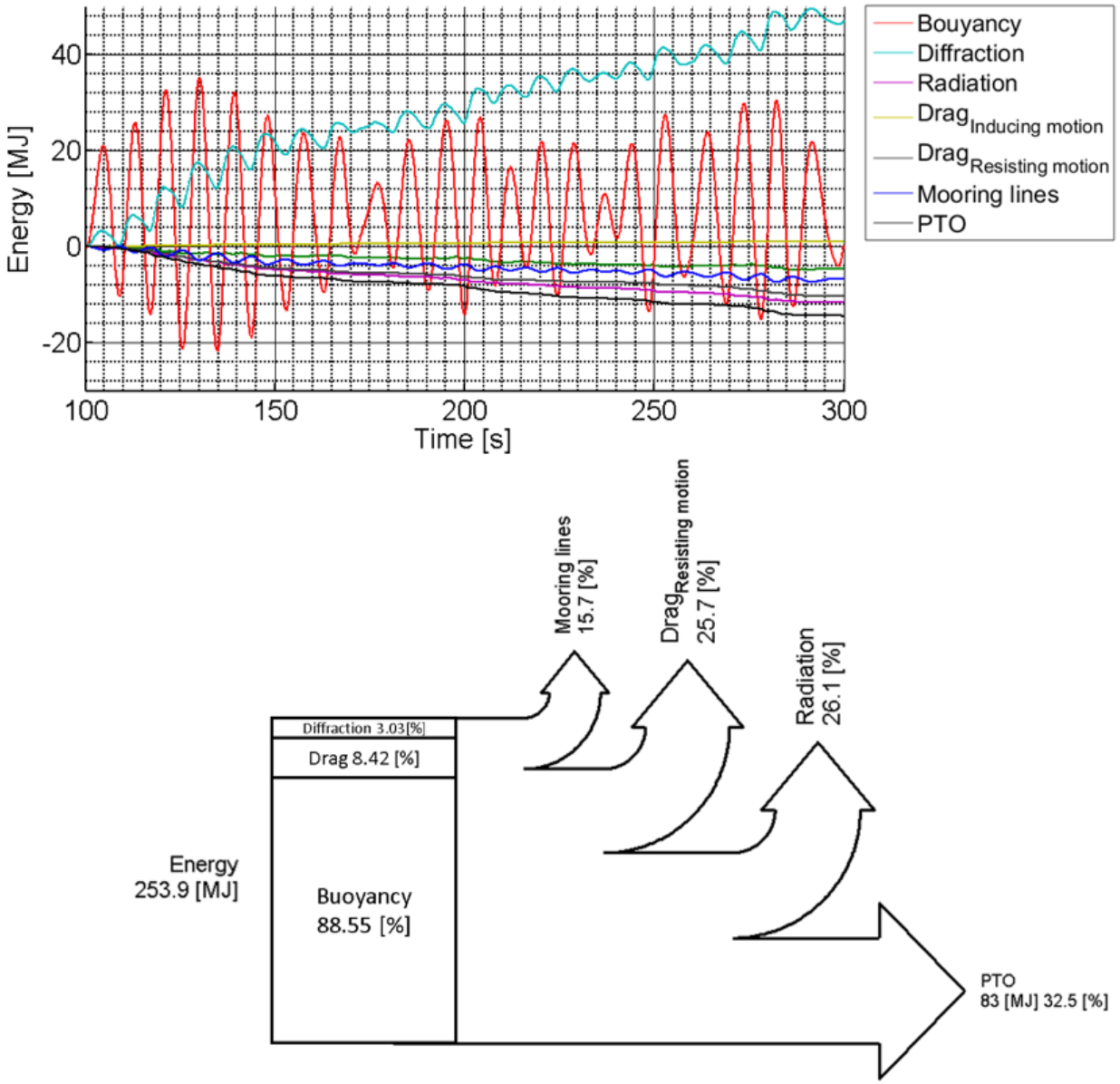

Figure 4-10: Energy vs time/ Sankey diagram L4 configuration.
The Sankey diagram was constructed using 1100 sec.

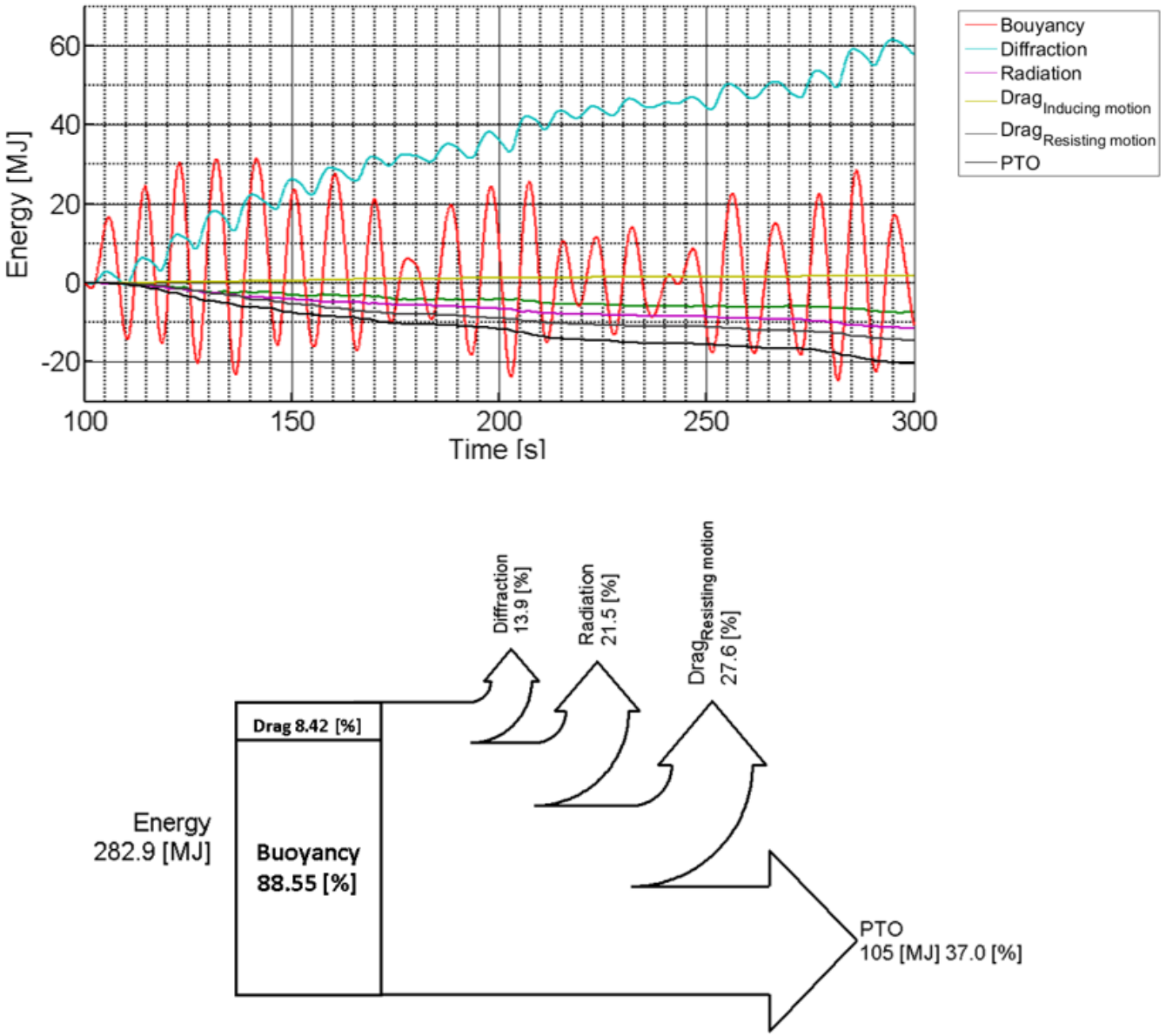

Figure 4-11: Energy vs time/ Sankey diagram NM configuration.

The Sankey diagram was constructed using 1100 sec.

It can be seen from Figure 4-9, Figure 4-10 and Figure 4-11 that the overall energy input is being provided primarily by the buoyancy force on the float. This constituent excitation force provides between 88- 90% of the total input energy. In the other hand, the biggest sink of energy is the PTO that extracts around 32 to 38 % of the available energy. It seems that the mooring lines have an impact in the wave – WEC interaction, increasing, for the OC configuration, the energy input by 7% when it compared to the NM configuration and 20% when compared with L4. By comparing OC and L4, it can be seen that the mooring lines extract less energy for the optimal configuration. The following figure shows the relationship between wave height, instantaneous power and the energy.

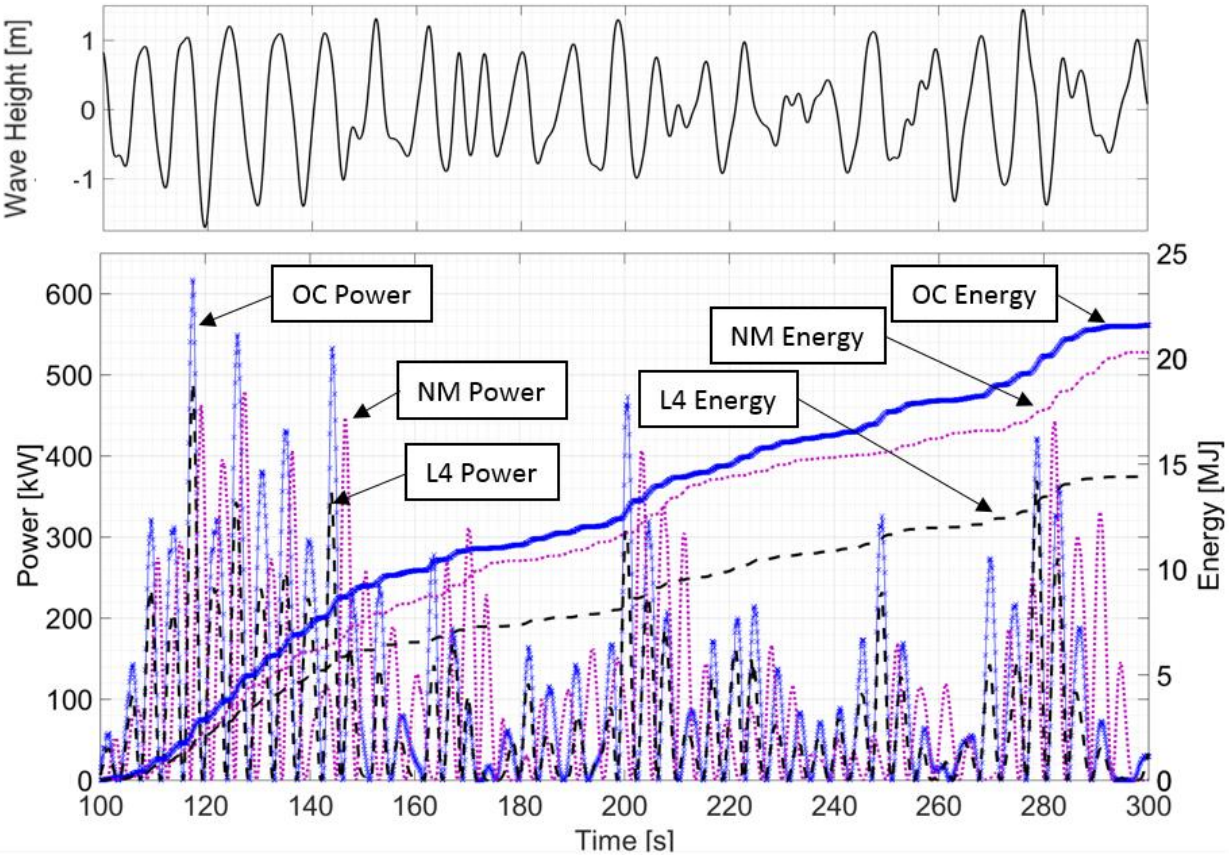

Figure 4-12: Power [kW], Energy [MJ], Wave Height [m].

Figure 4-12 shows that for the same wave crest each configuration reacts differently. Sometime the OC configuration will produce more power sometimes the NM, but when the power is integrated a clear trend of the OC configuration extracting more energy can be observed.

This is also illustrated in Figure 4-13 where the response amplitude operator (RAO) of the relative displacement between the two bodies is presented. The RAOs were calculated using a fast Fourier transform (FFT) over the relative displacement of the SRPA on the irregular sea state considered for the optimization. The FFT converts a signal from the time domain to a representation in the frequency domain by recognizing that any irregular wave is composed of a number of regular waves with different phase and amplitude that are sum in the time domain. The FFT decomposed wave signal is smoothed using multiple overlapped sections of the full time history and a hamming window.

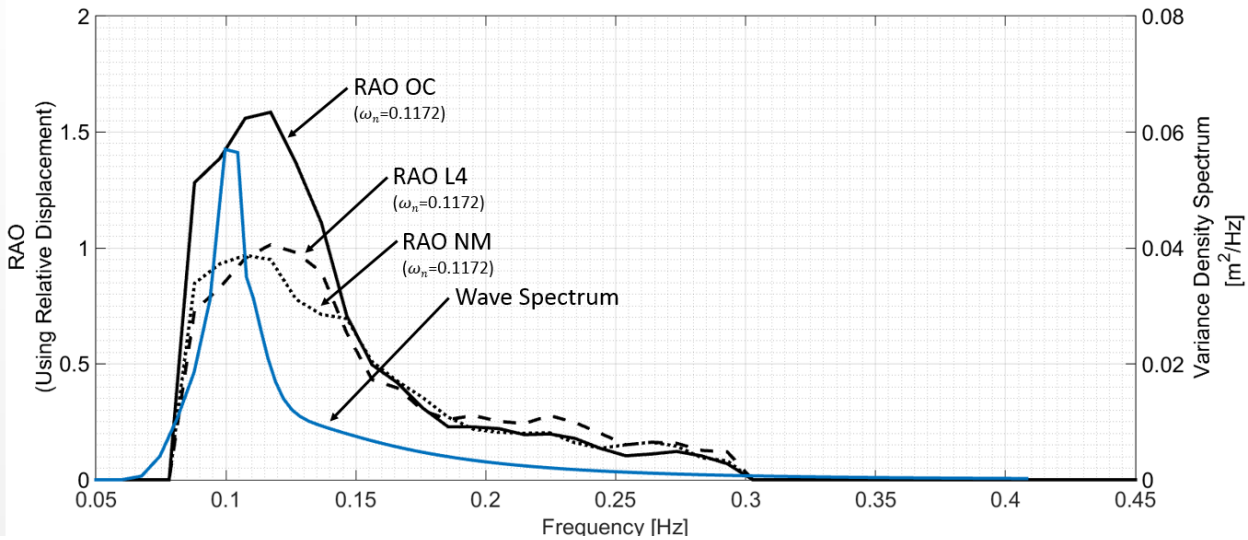

Figure 4-13: RAO (Relative displacement)
This figure shows the transfer function of the effect of the sea state upon relative response of a floating device. For this device, the relative response is linked with higher energy extraction.

As can be appreciated, the OC experiences higher relative displacement and a small shift in the natural frequency. The natural frequency (ω_n) is defined as $\omega_n = \sqrt{k/m}$, where k is the inertial stiffness and m the mass. Both the inertial stiffness and the mass change, as a slack moored system incorporates both a resistive and a restorative force. Also, as will be shown in the next section, the mooring lines can have an impact on the movement of the WEC. The connection point and the structure of the line can decrease or increase unwanted movements in the system, which can prejudice the energy harnessing.

Chapter 5

Operational Ramifications

In this chapter, the focus is on the behaviour of the Optimal Configuration (OC) for environmental conditions outside the specific wave spectrum that was considered in the optimization study introduced in Chapter 3 and discussed Chapter 4. This investigation occurs in three stages. First, the influence of wave directionality on performance is examined by changing the angle of incidence of the wave spectrum (the optimization considers the waves to arrive in a unidirectional manner aligned with the first mooring line). Second, the ability of the OC mooring to mitigate parametrically excited pitch and roll oscillations of the SRPA is examined for a series of regular wave tests. It has been proposed that such parasitic motions have tremendous negative impact on power production and so it is of interest to see if the OC mooring can prevent such motions. Lastly, performance matrices for the OC and NM SRPA cases are calculated using the ProteusDS simulator, and then applied to estimate the annual yield of the two SRPAs if deployed at Amphitrite Bank. This last section draws upon the complete set of resource data for Amphitrite Bank that was first presented in §2.2.2.

5.1 Sensitivity to Wave Heading

As explained in section 3.1.3 the Metamodel-Based Optimization was executed considering a unidirectional sea state which was aligned with one of the mooring lines at zero degrees (configuration 1, according to Figure 5-1). Even though the selected WEC is axisymmetric, the mooring configurations are not and this could affect the performance of the device. Additionally, different asymmetries can be

developed for 3 and 4 leg mooring configurations and the performance of the mooring may not degrade at the same rate with wave heading changes for the 3 and 4 leg cases. To quantify the impact of the 3- and 4-leg asymmetries on the power extraction, a sensitivity study considering different wave headings was used. The same sea state used for the optimization was considered (constituent wave heights and frequencies were maintained) and five different wave headings were evaluated as shown in Figure 5-1 below.

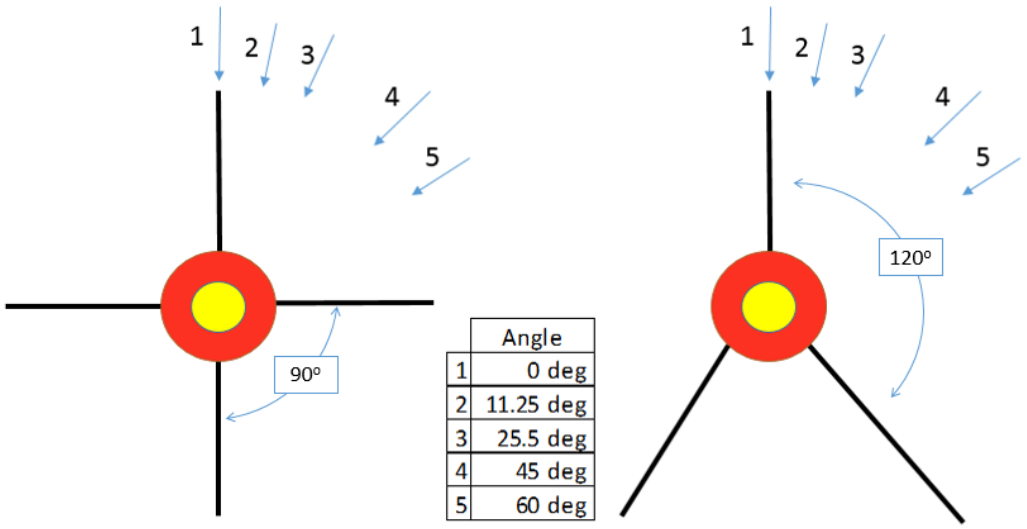

Figure 5-1: Wave headings considered in the wave direction sensitivity study.
Five different headings were selected to assess the impact of the wave heading on the WEC.

The five wave headings were picked in order to cover a wide range of possible headings. For the study, the OC and H3 configurations were used. The following table presents the normalized power for this study. The power was normalized against the OC configuration with a zero degree wave heading – case 1 in Figure 5-1.

Table 5-1: Power average power for different wave headings.

	0 deg.		11.25 deg		22.5 deg		45 deg.		60 deg.	
Configuration	Power [kW]	Normilized w/ optimal	Power [kW]	Normilized w/ optimal	Power [kW]	Normilized w/ optimal	Power [kW]	Normilized w/ optimal	Power [kW]	Normilized w/ optimal
OC	80.82	1.00	80.96	1.00	80.96	1.00	80.95	1.00	80.96	1.00
H3	76.30	0.944	76.29	0.944	76.31	0.944	76.32	0.944	76.31	0.944

Properly designed catenary mooring lines do not become taut during operations; the mooring line self-weight should provide a restoring force that prevents the SRPA from traveling to the full extent of the line, and thus prevent significant reaction loads from developing at the sea bed (e.g. the anchor point). Consequently, within the spectrum of operating conditions the wave incident direction should not

drastically affect the WEC power extraction. This can be seen in Table 5-1, where the OC and H3 configurations do not show any influence from the wave headings.

5.2 MITIGATING PARASITIC PITCH AND ROLL

As explained in section 1.2.3 , SRPAs, can become unstable if excited by waves arriving at approximately twice the pitch natural frequency. This phenomenon is referred to as 'parametric excitation' since the resulting motions are excited by changes in the buoyant stiffness parameters as the wave passes by. Previous works have suggested, that this phenomenon can have negative impact on the power production of WEC especially when the wave frequency is near to the Mathieu frequency - the Mathieu frequency being defined as twice the SRPA pitch natural frequency [23]. In this section, the potential to mitigate parametric excitation with the OC mooring is studied.

For this study, pitch/roll RAO of the NM configuration was calculated for the spar by a frequency domain analysis, as it was consider that the movement of the spar is dominant for the degree of freedom. As shown in the following figure, the pitch/roll natural frequency for the spar is around 0.44 rad/s, so the expected Mathieu frequency should be around 0.88 rad/s.

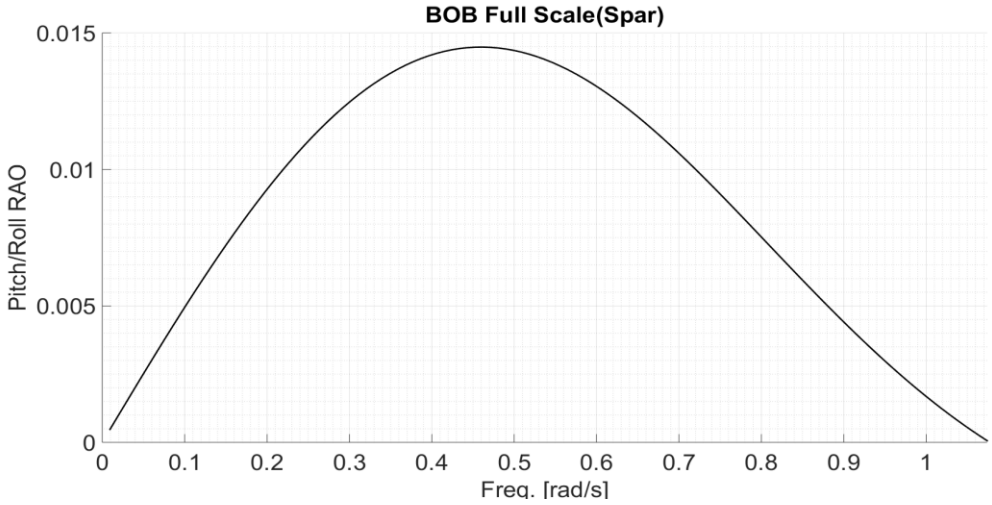

Figure.5-2: Pitch/Roll RAO NM
Mathieu frequency is around 0.88 [rad/s]

As an irregular sea state, such as the operational condition used in the optimization, is constructed by the superposition of many regular waves, it is hard to identify and isolate a parametrically excited motion in corresponding time domain simulation data. As such, a sensitivity study was conducted that considered a series of distinct monochromatic unidirectional waves separately so as to reveal the onset of parametric

excitation for the NM case. The same PTO damping constant used in Chapter 3 (see eq. ((0.16))) was considered for all the monochromatic wave trials.

Table 5-2 Regular waves. Constant PTO damping constant

Configurations	Frequency	Wave height	C PTO	Results					
				Power		Pitch(Θ) [deg]		Roll(Φ) [deg]	
	rad/s	[m]	[N s/m]	[kW]	Difference* (%)	Max.	Standard deviation	Max.	Standard deviation
OC	0.88	1.50	2.97E+06	99.5	50%	5.90	1.84	0.46	0.13
NM				50.2		8.88	3.99	9.29	5.08
OC	0.80			130.7	43%	7.44	1.89	0.15	0.02
NM				74.0		11.06	3.99	9.42	4.92
OC	0.74			103.7	7%	8.801	2.15	0.15	0.02
NM				96.6		7.96	1.91	0.87	0.27
OC	0.64			52.7	1%	9.22	3.04	0.17	0.03
NM				52.3		8.46	2.44	0.84	0.28
OC	0.41			4.0	-46%	6.37	3.70	0.17	3.70
NM				7.5		8.06	5.48	0.30	5.48

* Percentage differences are measured relative to the NM case

As can be seen in Table 5-2, the efficiency of the OC mooring system compared with the NM configuration varied widely. However, by comparing the reported power and roll standard deviation values, it seems that there is a relation between excessive roll motions and the efficiency of the SRPA energy conversion. As shown in Table 5-2 and in Figure 5-3 , when the magnitude of the roll motion is close to that of the pitch motion for the NM configuration, the addition of the OC mooring has a significant positive impact on performance. This is the case for the frequencies of 0.88 rad/s, 0.8 rad/s and 0.74 rad/s. On the other hand, when the excessive roll motions are not present in the NM case, the addition of the OC mooring produced mixed results with the NM configuration actually having better performance at omega=0.41 rad/s.

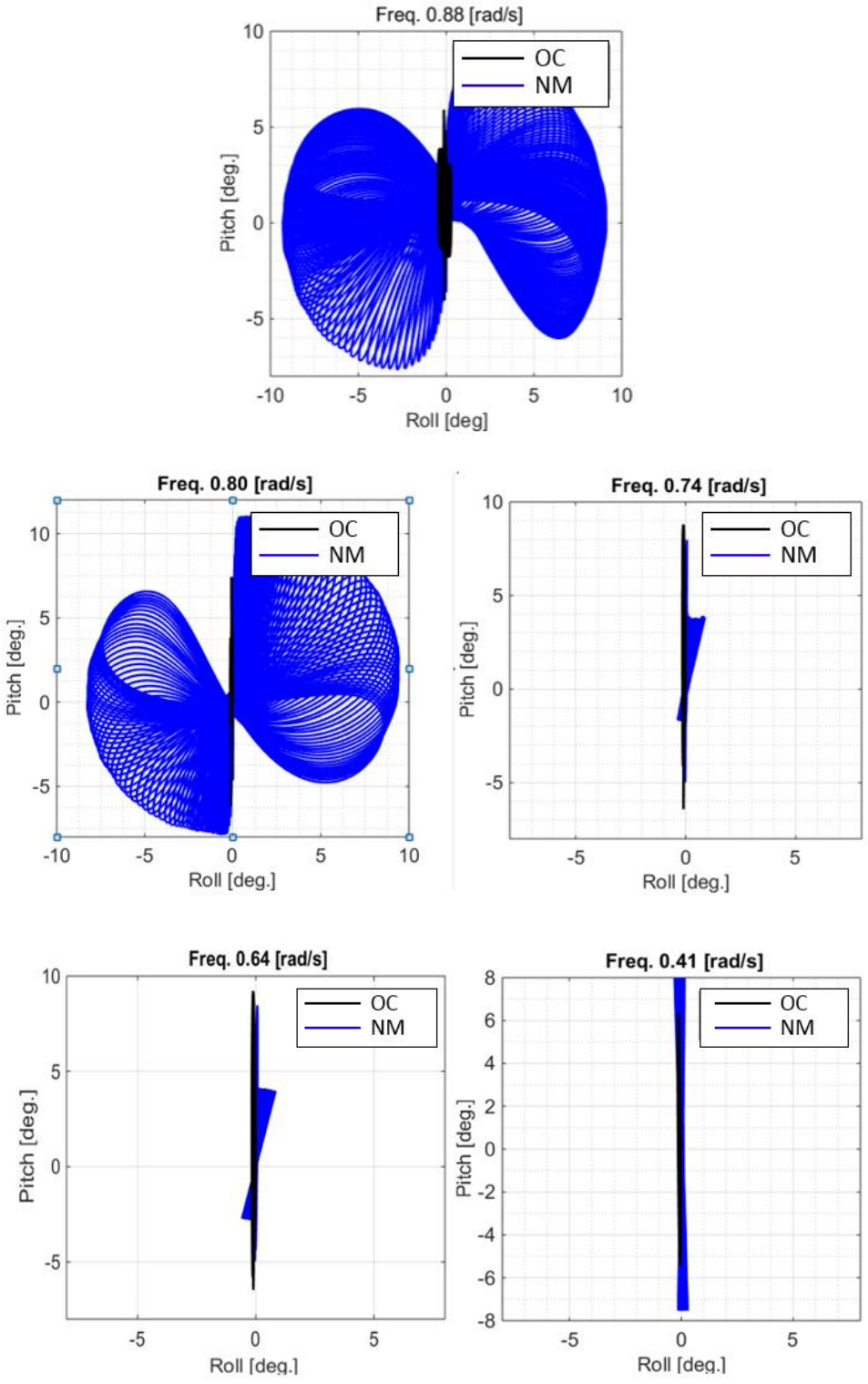

Figure 5-3: A locus of the SRPA Roll angle vs Pitch angle during regular wave trials

This phenomenon occurs when two degrees of freedom get coupled and the device begin to roll over the wave crests as a rigid body to destroying any travel at the PTO.

The same experiment presented in Table 5-3 was repeated considering the different damping coefficients for each sea state. The damping coefficients for each wave frequency were calculated according to the procedure presented in Appendix 2.

Table 5-3 Regular waves. Variable PTO damping coefficient.

Configurations	Frequency rad/s	Wave height [m]	C PTO [N s/m]	Results					
				Power		Pitch(ω_P) [deg]		Roll(ω_R) [deg]	
				[W]	Difference* (%)	Max.	Standard deviation	Max.	Standard deviation
OC	0.88	1.50	2.25E+06	103.22	51%	22.45	1.36	0.19	0.04
NM				50.20		8.88	3.99	9.29	5.08
OC	0.80		2.97E+06	130.73	43%	7.44	1.89	0.15	0.02
NM				74.02		11.06	3.99	9.42	4.92
OC	0.74		2.50E+06	119.27	11%	8.36	2.02	0.14	0.03
NM				106.37		7.81	8.70	0.23	0.19
OC	0.64		1.50E+06	65.39	9%	8.79	3.07	0.15	0.02
NM				59.36		7.76	2.50	0.61	0.25
OC	0.41		3.86E+05	13.60	-26%	7.19	4.30	0.17	0.02
NM				18.27		9.39	6.32	0.72	0.37

* Difference between OC and NM for the same sea state.

As expected, the power improved at each frequency when a damping constant specific to that frequency was used. However, the same general observation holds: the OC mooring can drastically improve power production when the NM configuration is plagued by large coupled roll and pitch motions.

Table 5-4 shows the mean power extracted, as well as the maximum pitch and roll motions for both configurations in the operational condition considered in the optimization study. Based on the statistics shown, even though the OC case exhibited a better average power (around 17% more), this improvement cannot be conclusively attributed to reduction in the parametrically excited roll – the reduction in maximum roll angle and the standard deviation of the roll angle signal is not overwhelming.

Table 5-4: Parametric roll results irregular waves.

		Pitch(ω_P) [deg]		Roll(ω_R) [deg]	
Configurations	Power	Max.	Standard deviation	Max.	Standard deviation
OC	80.82	16.45	4.01	6.96	1.70
NM	68.94	18.83	4.46	11.46	2.96
% difference	17%				

However, if the time histories of power conversion, roll and pitch are compared for both the NM and OC configurations, some periods of time can be identified where the roll reduction attributed to the OC mooring is significant and there is observably better power capture in these periods compared to the NM configuration, as it can be seen in the interval between 100 sec. and 140 sec. show in Figure 5-4 . However, there are also time intervals where the NM configuration extracts more power; an example is between 260 sec. and 300 sec. Interestingly, the roll motions were lower for the NM configuration in this period which, based on the monochromatic test results, indicates that there was little potential for power conversion improvements through the addition of the OC mooring.

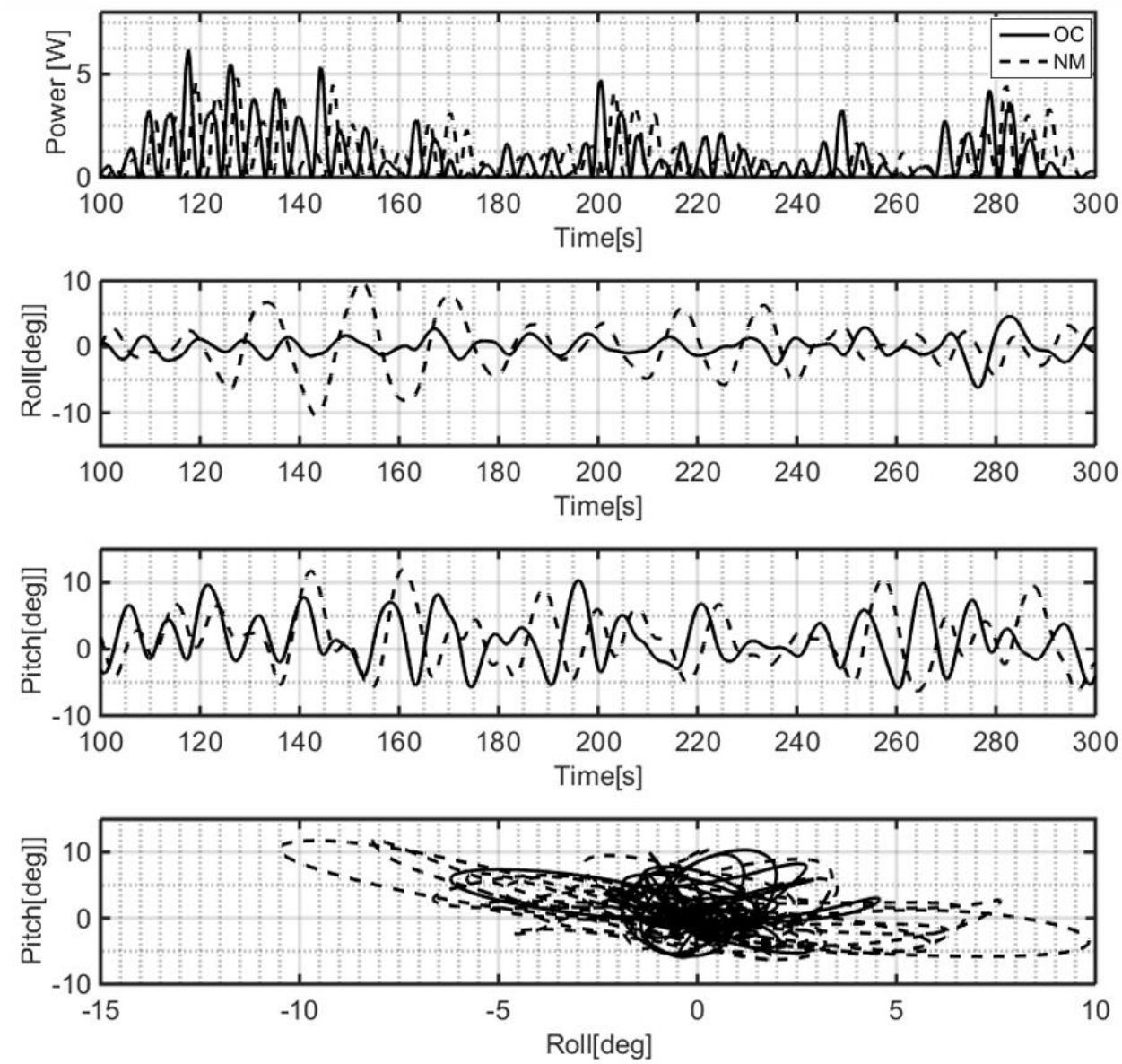

Figure 5-4: Irregular wave SRPA reaction.
The power of the SRPA

5.3 ANNUAL ENERGY YIELD

In order to translate the performance improvements achieved through the mooring design optimization study for the single operational condition into real-world economic performance metrics, the total potential annual energy extraction was calculated for each configuration. Following the emerging international standard for WEC performance assessment [54], this calculation consists of multiplying a histogram of wave heights and periods, which describe the changing sea state at the specified location at hourly resolution, over a representative power matrix of a device. A power matrix is a tabular representation of the average power conversion rate delivered by a WEC for given wave conditions. The power matrix is indexed against a finite set of wave statistics and the current international standard is to use the significant wave height and the peak period as the two delimiters. For this study an operational condition was determined for Amphitrite bank using the procedure described in §2.2 . The wave sea states were recorder every hour and then classify in 51 bins affording to its significant wave height and the peak period as shown in Figure 2-7.

The SRPA WEC was then simulated using each of this sea states and the mean power extraction was quantify for 1200sec. of operation. To approximate the sea state within ProteusDs a JONSWAP spectrum was consider as shown in Figure 2-4, with random phase seed for each simulation. Approximately, each simulation lasted 24 hours, and the complete power matrix was concluded in 8 days by running 8 simulation in parallel. The following figures present the average instantaneous power captured for three moorings configurations: the OC, NM and L4 moorings. In these figures, the axis labels indicate the range of wave heights and peak periods. For example, the top left cell of each matrix defines the average power output of the SRPA for wave spectrum with a peak period between 4.0 and 4.5 s and significant wave heights between 0.5 and 0.75 m. The entries in the cells are the average power conversion attributed to all conditions falling within that cell.

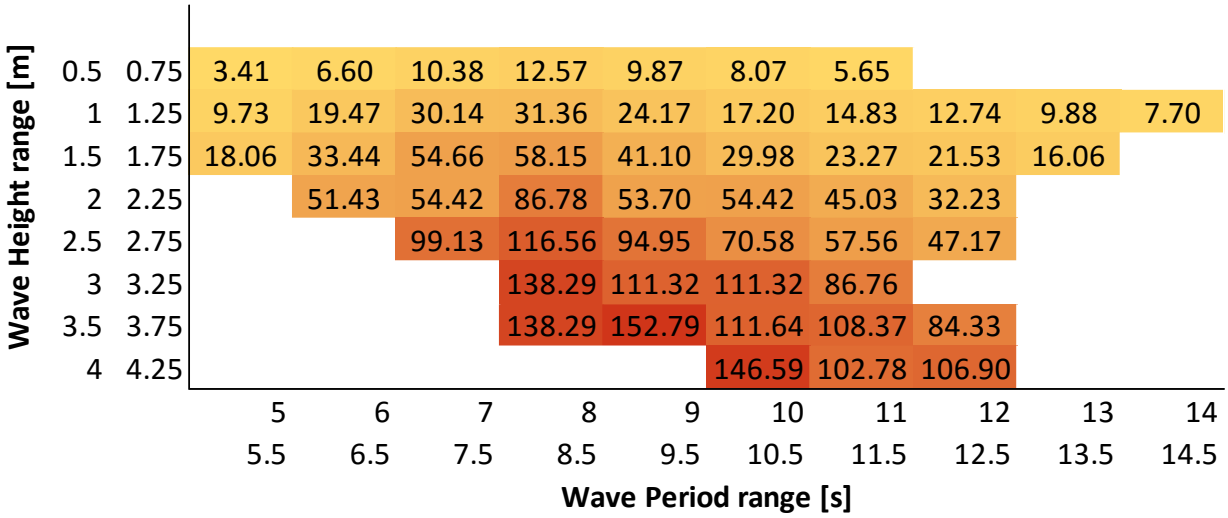

Figure 5-5: OC configuration/ Averaged Instantaneous Power Captured [kW]

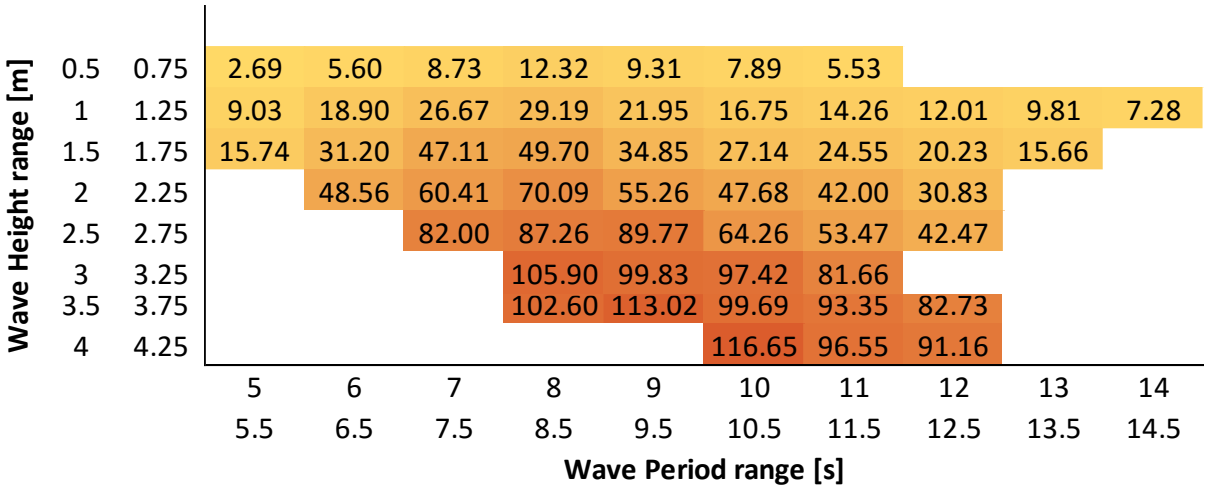

Figure 5-6 : NM configuration /Averaged Instantaneous Power Captured [kW]

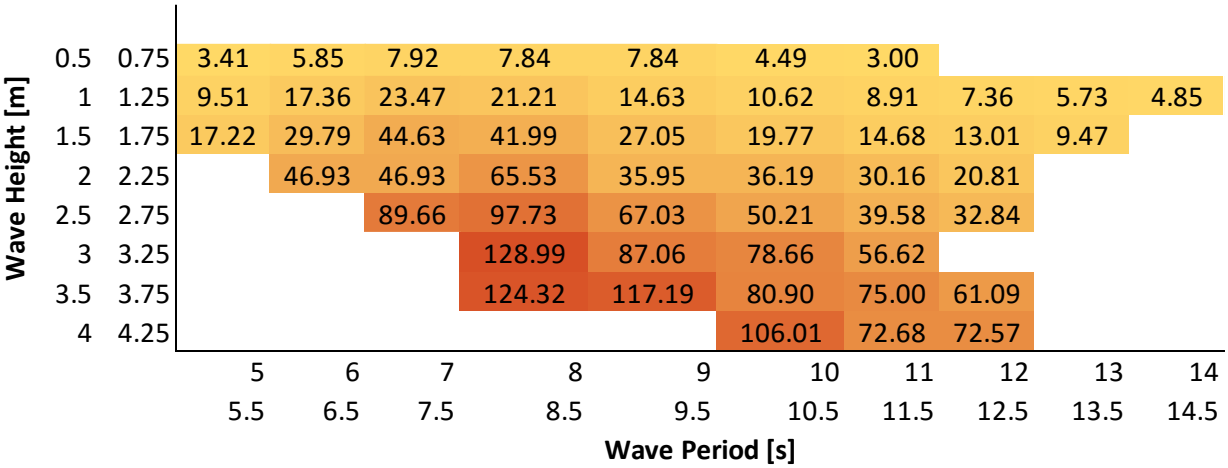

Figure 5-7: L4 configuration /Averaged Instantaneous Power Captured [kW]

This particular SRPA WEC seems to react better to wave periods between 7 and 10.5 sec and wave height below 2.3m, which is close to the most energetic sea state for this location. In general the OC configuration has a higher average instantaneous power than the other configurations while, the NM configuration performed better the L4 for almost of the sea states. L4 performed better than NM only for the area between the periods 6.5 sec. and 9 sec. and below 2.3m

While maximum output is one indicator of performance, it is also necessary to determine the annual yield, the total converted energy that is produced from wave conditions within each cell of the performance matrix. The annual yield for each cell is calculated by multiplying the average power for the cell by the hours of occurrence for that condition. Figure 5-8 to Figure 5-10 show the annual yield of the OC, L4 and NM configurations in different sea states.

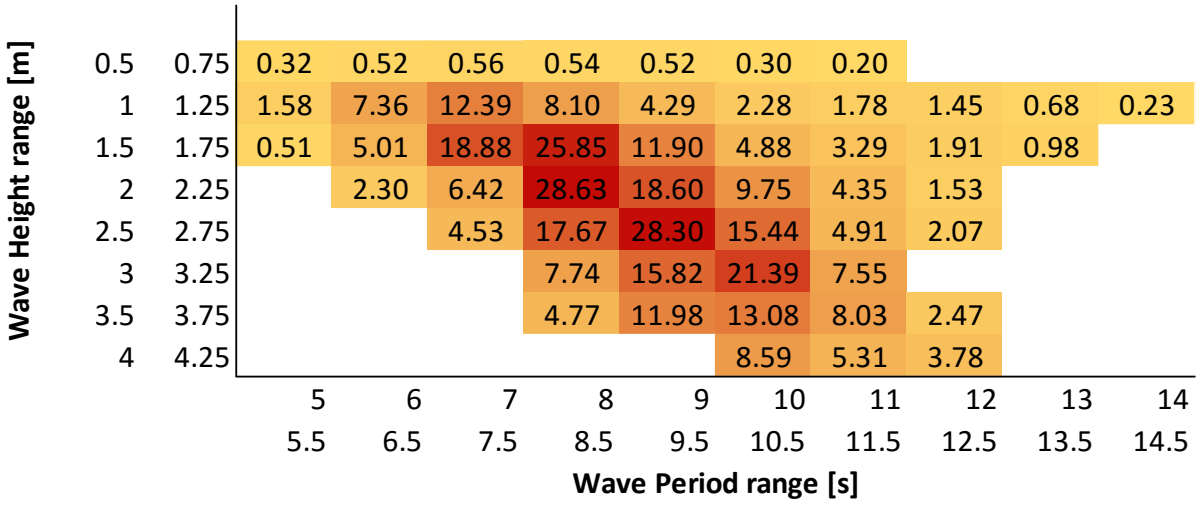

Figure 5-8 : OC configuration/ Annual Power Production [MW-hr]

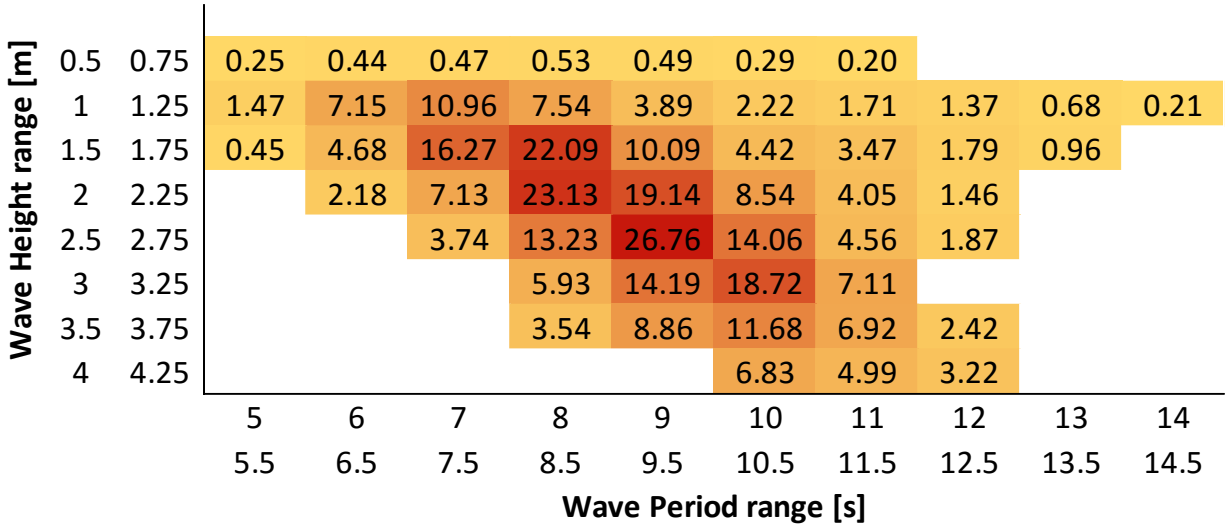

Figure 5-9: NM configuration / Annual Power Production [MW-hr]

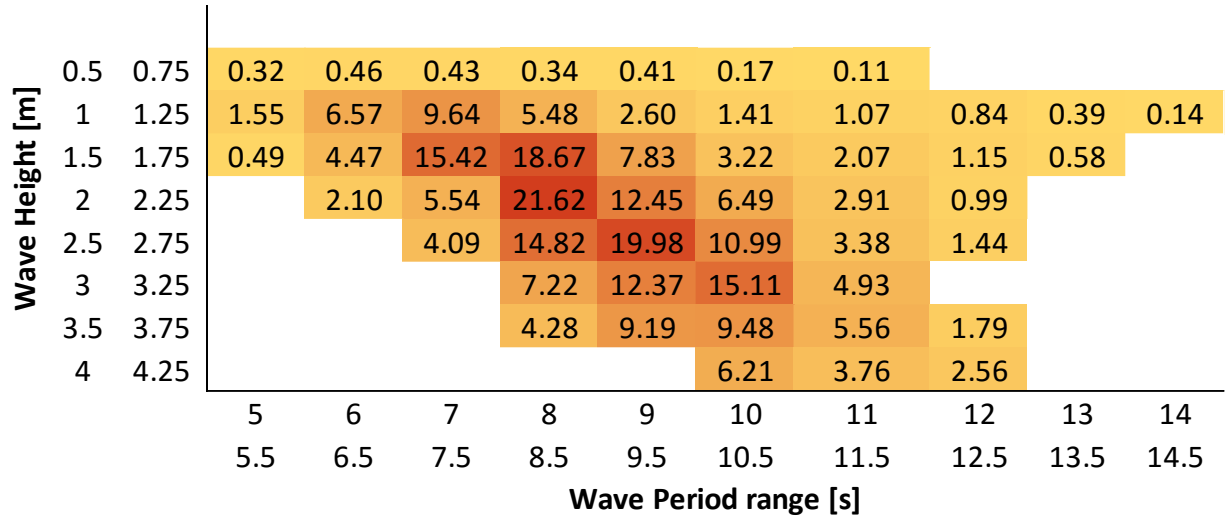

Figure 5-10: L4 configuration/Annual Power Production [MW-hr]

In general, the OC configuration has a higher yield in each cell than the other two configurations while the NM configuration has a higher yield for all cells than that of L4. It can be seen in Table 5-5 , that in a one year period, the OC configuration extracts around 12% more energy than the NM configuration and 26% more than the L4 configuration. These results confirm the importance of properly selecting the mooring line system, as they have a significant impact on the annual energy extraction.

Table 5-5: Annual Power extraction results.

Configuration	Total Annual Energy Production [MW h]	Year Energy Production normalized by the optimal Configuration	Average Power Capture [kW]	Average Power Capture normalized by the optimal Configuration
OC	371	1.00	42.3	1.00
NM	328	0.88	37.5	0.89
L4	275	0.74	31.4	0.74

Chapter 6

Conclusions and Future Work

This thesis presents a study of the complete DS for the conceptual design of mooring lines for a SRPA WEC. It is not intended to be the final design of the system, but to show general guidelines for this kind of converter. In this process, different configurations were compared and conclusions were drawn.

6.1 CONTRIBUTIONS

The research contributions made in the course of this research are summarized in this section. This section is organize in order that each of the sections of the chapter address one of the questions that were defined § 1.3 .

What are the effects of the mooring lines on power production for a SRPA WEC?

The mooring lines have a measurable impact on the power performance of the SRPA WEC. It has been show that when the OC configuration is compared with the L4 configuration, there is a difference of 25 % in the power that can be extracted for a particular sea state. When the OC configuration is compared to the NM configuration, the difference is 15%. When the overall power production was calculated for a particular location, it was shown that the optimal configuration performed better that the other configurations by as much as 12%, when compared to the NM configurations and 26% in comparison with the L4 configuration.

The increase in the power extraction is result of the way in which the mooring configuration were defined. For OC, the mooring connection is located higher than the center of gravity of the WEC and the lines are heavy, these reduces the movement on the degrees of freedom where power is not being extracted, making the configuration more efficient compared with NM and L4.

Is it important to study the whole design space in order to design a mooring system of a SRPA WEC?

SRPA WECs rely on their movement for power extraction, and it has been shown that they are sensitive to the mooring design. It was also shown that the difference in power between the mooring line configuration that behaves best and the one that extracts the least power is around 25%. In this way, a study of the design space is recommended to confirm that the optimal configuration has been chosen for the particular design and not only one that has been conceived by old assumptions, from other technologies.

How can the mooring system help to minimize the parametric excitation problems that SRPA WECs tend to present?

In §5.2 a sensitivity study was done to quantify the parametric roll by comparing the OC and NM configurations. As it can be seen in Table 5-2 and Table 5-3, the OC configuration reduces the roll movement by changing how the WEC reacted to the incident waves, this improves the power extraction for monochromatic sea states near Mathieu's frequency by over a 50% when a suboptimal damping coefficient is used and 56% when an optimal coefficient is considered. Far from Mathieu's frequency, the NM configuration harnesses more power that the OC configuration, around 46% with a suboptimal PTO and around 26% with an optimal PTO. This indicated that the moorings can indeed mitigate parasitic pitch and roll improving efficiency near Mathieu's frequency but when the Mathieu's frequency is not relevant the NM design performs better.

What is a "good" mooring system for a SRPA WEC?

For this particular SRPA WEC, it seems that the best mooring is the one that allows the WEC to move and react with the waves in the degrees of freedom where the energy is extracted, but reduces the undesired movement in those degrees of freedom that reduce the power extraction capability. As shown in section 4.4 the mooring lines affected the interaction between the SRPA WEC and the waves and can increase the energy that is extracted from the systems as well as the energy entering the system. This can be verify by comparing Figure 4-9 to Figure 4-11 where the energy balance for three different configurations are represented on a Sankey diagram. It is shown that the energy input for the OC configuration was 19% higher than the L4 and 7% higher than the NM showing that indeed that moorings are changing the way the WEC reacted to the incident waves and the energy enter the system. As well it can be seen that the mooring lines had less impact on the energy output for the OC configuration as it only extracted a 6% of the overall output energy while the L4 configuration they extracted 15%.

6.2 FUTURE WORK

The methodology used to optimize the mooring configuration system was successful in finding a mooring system that increases the power extracted by the system when compared with other configurations, but still there are areas in this subject that require further research:

- *Environmental conditions*: Only one sea state was used for the operating conditions of the optimization study. As the power extraction is sensitive to environmental conditions, the next logical step would be to optimize for a complete sea climate at a specific location. Studies of this kind can represents a challenge, due the computational time required to evaluate the model and may require a different strategy for calculating the power extraction. This also applies to the limit state study, since, due to the restrictions in computational time, a simplified approach was implemented. Further research may be needed in order to improve the proposed approach and fulfill the DNV standard.

- *Geometry:* The seakeeping design for any floating WEC is a challenge, as it requires allowing movement in certain degrees of freedom, for the WEC to harness power, as well as to constrain it from drifting. In this thesis, a specific geometry was used to study the interaction between the mooring system and the WEC. Any other floating WEC behaves differently, and therefore, further research is required in this field.

- *PTO:* It is known that the efficiency of a WEC is related with the strategy used to extract the power thru the PTO. There are different studies that show how to improve the performance of the WEC by optimizing the PTO. In this work, for simplification and consistency reasons, a viscous PTO was used with a single damping value. It may be of interest to study how the system behaves when the mooring system and the PTO are optimized concurrently.

- *Second order effects:* For floating structures, the natural period of the mooring system may coincide with the period of the second order wave effects, and this could cause large displacements and hence large mooring line tensions as the entire system resonates. This phenomenon has been widely studied for the offshore industry but not to the same extent for WECs. Moored WECs have significantly different dynamic characteristics compared to conventional moored offshore structures, as they are designed to move in reaction to the waves, not remain stationary. Since that motion drives an energy conversion process, a WEC that tends toward resonance in its power producing modes of motion will tend to convert more

wave energy. As was explained in § 2.3.4 second order wave effects were only partially considered for this analysis and further research is required to fully understand the effects on WECs.

- *Economical study:* This study was only based on performance of the device and economical aspects have not yet been included. Further research may be required in order to study the impacts of including an economical constraint on the analysis.

- *Directionality:* As explained in section 2.2.2 the optimization study was done considering an average wave direction aligned with one of the mooring lines. In section 5.1 a sensitivity study was used to analyze the effect of different average headings on the performance of H3 and OC. This study could be expanded to include other mooring configurations; it could also be interesting to study the effect of a wider sea spectrum and other seas states on the optimization of the device.

Bibliography

[1] S. Johnstone and J. Mazo, “Global Warming and the Arab Spring,” *Survival (Lond).*, vol. 53, no. 2, pp. 11–17, Apr. 2011.

[2] G. Melillo, JM, Richmont, T, Yohe, “Climate change impacts in the United States,” *Clim. Chang. Impacts 12 United States Third Natl. Clim. Assessment.*, 2014.

[3] J. A. Patz, D. Campbell-Lendrum, T. Holloway, and J. A. Foley, “Impact of regional climate change on human health.,” *Nature*, vol. 438, no. 7066, pp. 310–7, Nov. 2005.

[4] J. Cruz, *Ocean Wave Energy: Current Status and Future Prespectives*. Springer Science & Business Media, 2007.

[5] B. R. D. Robertson, C. E. Hiles, and B. J. Buckham, “Characterizing the near shore wave energy resource on the west coast of Vancouver Island, Canada,” *Renew. Energy*, vol. 71, pp. 665–678, Nov. 2014.

[6] G. Reikard, B. Robertson, and J.-R. Bidlot, “Combining wave energy with wind and solar: Short-term forecasting,” *Renew. Energy*, vol. 81, pp. 442–456, Sep. 2015.

[7] S. C. Parkinson, K. Dragoon, G. Reikard, G. García-Medina, H. T. Özkan-Haller, and T. K. A. Brekken, “Integrating ocean wave energy at large-scales: A study of the US Pacific Northwest,” *Renew. Energy*, vol. 76, pp. 551–559, Apr. 2015.

[8] J. Falnes and J. Løvseth, “Ocean wave energy,” *Energy Policy*, vol. 19, no. 8, pp. 768–775, Oct. 1991.

[9] L. Johanning, G. Smith, and J. Wolfram, “Mooring design approach for wave energy converters,” *Proc. Inst. Mech. Eng. Part M J. Eng. Marit. Environ.*, vol. 220, no. 4, pp. 159–174, Jan. 2006.

[10] A. C. Hansen and C. P. Butterfield, “Aerodynamics of Horizontal-Axis Wind Turbines,” *Annu. Rev. Fluid Mech.*, vol. 25, no. 1, pp. 115–149, Jan. 1993.

[11] P. Mccullen, A. Cle, A. Fiorentino, F. Gardner, K. Hammarlund, G. Lemonis, T. Lewis, K. Nielsen, H. Christian, and T. Thorpe, “Wave energy in Europe : current status and perspectives,” vol. 6, pp. 405–431, 2002.

[12] B. Drew, A. . Plummer, and M. . Sahinkaya, “A review of wave energy converter technology,” 2009.

[13] I. López, J. Andreu, S. Ceballos, I. Martínez de Alegría, and I. Kortabarria, “Review of wave energy technologies and the necessary power-equipment,” *Renew. Sustain. Energy Rev.*, vol. 27, pp. 413–434, Nov. 2013.

[14] a. P. McCabe, a. Bradshaw, J. a C. Meadowcroft, and G. Aggidis, “Developments in the design of

the PS Frog Mk 5 wave energy converter," *Renew. Energy*, vol. 31, no. 2, pp. 141–151, Feb. 2006.

[15] A. F. D. O. Falcão, "Wave energy utilization: A review of the technologies," *Renew. Sustain. Energy Rev.*, vol. 14, no. 3, pp. 899–918, Apr. 2010.

[16] C. Retzler, "Measurements of the slow drift dynamics of a model Pelamis wave energy converter," *Renew. Energy*, vol. 31, no. 2, pp. 257–269, Feb. 2006.

[17] M. Faltinsen, O, "Sea Loads on ships and offshore structures." Cambridge University Press, Cambridge, 2007.

[18] Y. Drobyshevski, "Hydrodynamic coefficients of a floating, truncated vertical cylinder in shallow water," *Ocean Eng.*, vol. 31, no. 3–4, pp. 269–304, Feb. 2004.

[19] G. Clauss, E. Lehmann, and C. Östergaard, *Offshore Structures: Volume I: Conceptual Design and Hydromechanics*. Springer, 2014.

[20] J. Falnes, "Wave-Energy Conversion Through Relative Motion Between Two Single-Mode Oscillating Bodies," *J. Offshore Mech. Arct. Eng.*, vol. 121, no. 1, p. 32, Feb. 1999.

[21] S. J. Beatty, A. Roy, K. Bubbar, J. Ortiz, B. J. Buckham, P. Wild, D. Stienke, and R. Nicoll, "Experimental and Numerical Simulations of Moored Self-Reacting Point Absorber Wave Energy Converters," *The Twenty-fifth International Offshore and Polar Engineering Conference*. International Society of Offshore and Polar Engineers, 27-Jul-2015.

[22] K. Tarrant and C. Meskell, "Investigation on parametrically excited motions of point absorbers in regular waves," *Ocean Eng.*, vol. 111, pp. 67–81, Jan. 2016.

[23] C. Villegas and H. Van Der Schaaf, "Implementation of a Pitch Stability Control for a Wave Energy Converter."

[24] B. J. Koo, M. H. Kim, and R. E. Randall, "Mathieu instability of a spar platform with mooring and risers," *Ocean Eng.*, vol. 31, no. 17–18, pp. 2175–2208, Dec. 2004.

[25] N. Fonseca, R. Pascoal, J. Marinho, and T. Morais, "Analysis of Wave Drift Forces on a Floating Wave Energy Converter," *Vol. 6 Nick Newman Symp. Mar. Hydrodyn. Yoshida Maeda Spec. Symp. Ocean Sp. Util. Spec. Symp. Offshore Renew. Energy*, no. 2003, pp. 831–839, 2008.

[26] S. J. Beatty, A. R. Roy, K. Bubbar, J. Ortiz, B. J. Buckham, P. Wild, D. Steinke, and R. Nicoll, "Experimental and Numerical Simulations of Moored Self-Reacting Point Absorber Wave Energy Converters," in *Proceedings of the 25th International Ocean and Polar Engineering Conference*, 2015.

[27] J. Fitzgerald and L. Bergdahl, "Considering mooring cables for offshore wave energy converters," *Proc 7th Eur. Wave Tidal Energy Conf, Porto*, 2007.

[28] M. J. Muliawan, Z. Gao, T. Moan, and A. Babarit, “Analysis of a Two-Body Floating Wave Energy Converter With Particular Focus on the Effects of Power Take-Off and Mooring Systems on Energy Capture,” *J. Offshore Mech. Arct. Eng.*, 2013.

[29] F. Cerveira, N. Fonseca, and R. Pascoal, “Mooring system influence on the efficiency of wave energy converters,” *Int. J. Mar. Energy*, vol. 3–4, pp. 65–81, Dec. 2013.

[30] P. Vicente and P. Justino, “Slack-chain mooring configuration analysis of a floating wave energy converter,” *iwwwfb.org*.

[31] S. J. Beatty, M. Hall, B. J. Buckham, P. Wild, and B. Bocking, “Experimental and numerical comparisons of self-reacting point absorber wave energy converters in regular waves,” *Ocean Eng.*, vol. 104, pp. 370–386, Aug. 2015.

[32] J. P. Ortiz, H. Bailey, B. J. Buckham, and C. Crawford, “Surrogate Based Design of a Mooring System for a Self-reacting Point Absorber,” in *The Twenty-fifth International Offshore and Polar Engineering Conference*, 2015.

[33] H. Bailey, J. P. Ortiz, B. Robertson, B. J. Buckhamn, and R. S. Nicoll, “A Methodology for Wave-to-Wire WEC Simulations,” in *2nd Marine Energy Technology Symposium*, 2014.

[34] L. H. Holthuijsen, *Wave in oceanic and costal water*, Cambridge. Cambridge: Cambridge University Press, 2007.

[35] D. N. DNVVeritas, “DNV-RP-C205 Environmental conditions and environmental loads,” *Dnv*, no. October, pp. 9–123, 2010.

[36] A. A. E. Price, C. J. Dent, and A. R. Wallace, “Frequency domain techniques for numerical and experimental modelling of wave energy converters.”

[37] D. Veritas, “DNV-OS-E301: Offshore standard-position mooring,” 2010.

[38] S. J. Beatty, “Self-Reacting Point Absorber Wave Energy Converters.” 2015.

[39] D. C. Hong, S. Y. Hong, and S. W. Hong, “Numerical study on the reverse drift force of floating BBDB wave energy absorbers,” *Ocean Eng.*, vol. 31, no. 10, pp. 1257–1294, Jul. 2004.

[40] W. C. Koo, S. J. Kim, and M. H. Kim, “Numerical Analysis of Hydrodynamic Performance of Backward Bent Duct Buoy (BBDB),” in *Volume 4: Offshore Geotechnics; Ronald W. Yeung Honoring Symposium on Offshore and Ship Hydrodynamics*, 2012, p. 669.

[41] N. Fonseca, “Analysis of wave drift forces on a floating wave energy converter,” *ASME 2008 …*, 2008.

[42] J. Pinkster, “Low frequency second order wave exciting forces on floating structures,” 1980.

[43] B. Buckham, “Dynamics modelling of low-tension tethers for submerged remotely operated vehicles,” 2003.

[44] R. E. Randall, *Elements of ocean engineering*. The Society of Naval Architects and Marine Engineers, 1997.

[45] L. Johanning, G. Smith, and J. Wolfram, “Mooring design approach for wave energy converters,” *Proc. Inst. …*, 2006.

[46] D. Veritas, “DNV-OS-J101 offshore standard,” *Des. Offshore Wind Turbine Struct.*, 2010.

[47] M. Cavazzuti, *Optimization Methods: From Theory to Design Scientific and Technological Aspects in Mechanics*. Springer Science & Business Media, 2012.

[48] A. I. J. Forrester, A. Sóbester, and A. J. Keane, *Engineering Design via*. 2008.

[49] J. Muller, “MATSuMoTo.” Cornell University, New York, 2014.

[50] J. Müller and R. Piché, “Mixture surrogate models based on Dempster-Shafer theory for global optimization problems,” *J. Glob. Optim.*, vol. 51, no. 1, pp. 79–104, Oct. 2010.

[51] S. Lophaven, H. B. Nielsen, and J. Søndergaard, “DACE:A MATLAB Kriging Toolbox.” Lyngby,Denmark, 2002.

[52] & Aresl. Gints , J., “Regression Splines toolbox for Matlab/Octave.” 2011.

[53] J. Müller, C. A. Shoemaker, and R. Piché, “SO-I: a surrogate model algorithm for expensive nonlinear integer programming problems including global optimization applications,” *J. Glob. Optim.*, vol. 59, no. 4, pp. 865–889, Sep. 2013.

[54] TC-114, “IEC/TS 62600-Wave energy converter power performance assessment at a second location using measured assessment data,” 2016.

APPENDIX 1. Metamodel Normalized performance error coefficients.

Normalized coefficients for quantify the goodness of the Meta-Model[50].

Coefficient	Normalization
Correlation coefficients (CC)	$m_i^{CC} = \frac{CC_i}{\sum_j^N CC_j}$
Root mean square errors(RMSE)	$m_i^{RMSE} = \frac{1/RMSE_i}{\sum_j^N 1/RMSE_j}$
Maximal absolute error (MAE)	$m_i^{MAE} = \frac{1/MAE_i}{\sum_j^N 1/MAE_j}$
Median absolute deviation (MAD)	$m_i^{MAD} = \frac{1/MAD_i}{\sum_j^N 1/MAD_j}$

APPENDIX 2. Sensitivity Study Damping

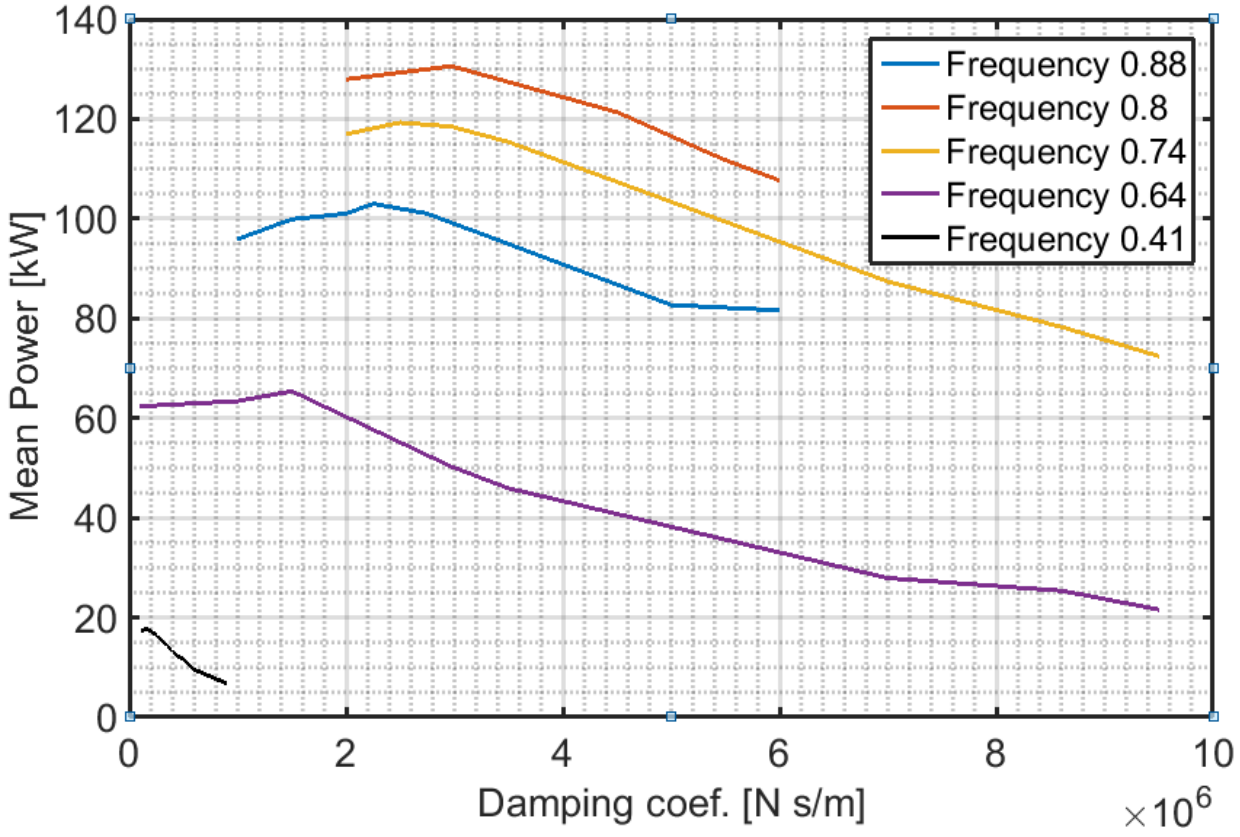

Figure A. 1: Sensitivity Study Damping

In Table 5-3 the impacted of the mooring lines in the mitigating of the parasitic pitch and roll was accede by comparing the performances of OC and NM in regular waves with optimal PTO damping coefficient. As shown in Figure A. 1, the optimal damping coefficient was found, by a sensitivity study of the mean power of the NM configuration when the damping coefficient was varied.